FACULTY OF HEALTH AND MEDICAL SCIENCES
UNIVERSITY OF COPENHAGEN

PhD thesis

Milad Rouhi Khorasani

Department of Pharmacy

Near-infrared (NIR) spectroscopy and NIR chemical imaging as process monitoring solutions in production of solid dosage forms

Academic advisor: Jukka Rantanen

Submitted: May 12th, 2015

Name of department:	Department of Pharmacy
Author:	Milad Rouhi Khorasani
Title:	Near-infrared (NIR) spectroscopy and NIR chemical imaging as process monitoring solutions in production of solid dosage forms
Academic advisor:	Jukka Rantanen
Submitted:	May 12th, 2015

SUPERVISORS

Professor Jukka Rantanen (Principal supervisor)
Faculty of Health and Medical Sciences
University of Copenhagen, Denmark

Ph.D. Poul Bertelsen (Primary co-supervisor)
CMC center Europe
Takeda Pharmaceutical Company GmbH, Singen Germany

Associate Professor José Manuel Amigo Rubio (Co-supervisor)
Faculty of Science
University of Copenhagen, Denmark

EVALUTATION COMMITTEE

Associate Professor Mingshi Yang
Faculty of Health and Medical Sciences
University of Copenhagen, Denmark

Ph.D. Morten Allesø
Research & Development
H. Lundbeck A/S, Valby, Denmark

Professor Jarkko Ketolainen
Drug Research & Development Centre, Pharmaceutical Technology
University of Eastern Finland, Kuopio, Finland

PREFACE

The thesis entitled “Near-infrared (NIR) spectroscopy and NIR chemical imaging as process monitoring solutions in production of solid dosage forms” was submitted to the Faculty of Health and Medical Sciences, University of Copenhagen, Denmark as part of the requirements to obtain the degree of Philosophiae Doctor (Ph.D.). The majority of the experimental work was performed at CMC Center Europe, Takeda Pharmaceutical A/S, Roskilde, Denmark, and partly at the Faculty of Science and Faculty of Health and Medical Science both at University of Copenhagen.

The thesis is based on the work presented in the paper (I-III) listed on page III.

The reader is encouraged to read those papers for a more detailed description of the methods and results before reading this thesis. The papers are available in the appendices I-III.

The thesis is comprises of seven chapters including; introduction, literature review, aims, material and methods, results and discussion, conclusions and perspectives.

ACKNOWLEDGEMENTS

The Drug Research Academy, the Danish Agency for Science, Technology and Innovation, and Takeda Pharmaceutical A/S are acknowledged for funding the Ph.D. project.
I wish to thank my supervisors Professor Jukka Rantanen, Principal Scientist & Honorary Professor Poul Bertelsen and Associate Professor José Manuel Amigo Rubio for your excellent guidance throughout the past three years. Your enthusiasm and support have been highly appreciated.

I would like to express my appreciation to Associate Professor Frans van den Berg, Associate Professor Jørn Sonnergaard, Associate Professor Changquan Calvin Sun and Ph.D. candidate Guilherme Alexandrino for pleasant collaboration.

At Takeda Pharmaceutical A/S, I would thank technician Majbritt Kvintel for technical support in the laboratory and Pharmaceutical Scientist Peder Mohr Olsen for scientific discussion.

At the Department of Pharmacy and Department of Food Science both at the University of Copenhagen, I wish to thank all my colleagues for scientific input, collaborations and for a friendly work environment.

Associate Professor Mingshi Yang (University of Copenhagen), QbD & PAT specialist Morten Allesø (H. Lundbeck A/S) and Professor Jarkko Ketolainen (University of Eastern Finland) are acknowledged for evaluating the present work.

Last but not least I would thank my family and friends for support. I would like to express my deepest gratitude to my dear fiancée Emilie Christensen for always being so supportive.

Østerbro, May 2015

Milad Rouhi Khorasani

LIST OF PUBLICATIONS

The thesis is based on Paper I-III listed below. Copies of these Papers are available in the appendices. The Papers were reprinted with permission from the publishers.

I. **M. Khorasani**, J.M. Amigo, P. Bertelsen, F. van den Berg, J. Rantanen. Detecting blending end-point using mean squares successive difference test and near-infrared spectroscopy. Journal of Pharmaceutical Sciences, **(2015).**

II. **M. Khorasani**, J.M. Amigo, J. Sonnergaard, P. Olsen, P. Bertelsen, J. Rantanen. Visualization and prediction of porosity in roller compacted ribbons with near-infrared chemical imaging (NIR-CI). Journal of Pharmaceutical and Biomedical analysis, 109 (**2015**) 11-17.

III. **M. Khorasani**, J.M. Amigo, Changquan Calvin Sun, P. Bertelsen, F. van den Berg, J. Rantanen. Near-infrared chemical imaging (NIR-CI) as a process monitoring solution for a production line of roll compaction and tableting. European Journal of Pharmaceutics and Biopharmaceutics, 93 (**2015**) 293-302.

List of Paper by the author, not included in the thesis

IV. G. L. Alexandrino, **M. Khorasani**, J. M. Amigo, J. Rantanen, R.J. Poppi. Monitoring of multiple solid-state transformations at tablet surfaces using multi-series near-infrared hyperspectral imaging and multivariate curve resolution. European Journal of Pharmaceutics and Biopharmaceutics, 93 (**2015**) 224-230.

LIST OF SYMBOLS AND ABBREVIATIONS

API	Active Pharmaceutical Ingredient
ASA	Acetylsalicylic acid
b	Matrix of regression coefficients
BUE	Blend Uniformity end-point
CaCO3-A	Calcium carbonate angular shaped
CaCO3-E	Calcium carbonate equant shaped
cGMP	Current Good Manufacturing Practice
CM	Continuous Manufacturing
CMA	Critical Material Attribute
CPP	Critical Process Parameters
CQA	Critical Quality Attributes
CU	Content Uniformity
d0.1	10% of the volume distribution is below this value
d0.5	The diameter where 50% of the distribution is above and 50% is below
d0.9	90% of the volume distribution is below this value
DC	Direct compression
DoE	Design of Experiments
E	Matrix residuals
FDA	The US Food and Drug Administration
FSS	Feed Screw Speed
ICH	International Conference on Harmonization
LD	Laser Diffraction
LV	Latent Variable
MCC	Microcrystalline cellulose
MIM	Mercury Intrusion Method
MPa	Mega Pascal
MSSDT	Mean Square Successive Difference Test
MVDA	Multivariate Data Analysis
NIR-CI	Near-infrared Chemical Imaging
NIRS	Near-infrared Spectroscopy
OAM	Oil Absorption Method

P	Loading matrix
p	Loading vector
PAT	Process Analytical Technologies
PC	Principal Component
PCA	Principal Component Analysis
PLS-R	Partial Least Squares regression
Q2	An estimate of the predictive ability of the model, calculated by cross-validation
QbD	Quality by Design
QbT	Quality by Testing
QTTP	Quality Target Product Profile
R	Raw reflectance data
R&D	Research and Development
RA	Risk Assessment
RC	Roller Compaction
RH	Relative Humidity
RM	Risk Management
RMSE	Root Mean Square Error
RMSECV	Root Mean Square Error of Cross Validation
RMSEP	Root Mean Square Error of Prediction
RP	Roll Pressure
RPM	Revolutions per minute
RS	Roll Speed
SD	Standard Deviation
SEM	Scanning Electron Microscope
Sieve	Sieve analysis
SNV	Standard Normal Variate
T	Score Matrix
t	Score Vector
TPP	Target Product Profile
TTS	Tablet Tensile Strength
TW	Tablet Weight
X	Dataset

ABSTRACT

With the introduction of Quality by Design (QbD) and Process Analytical Technology (PAT) concepts the pharmaceutical industry is driving towards improved process understanding. The pharmaceutical industry focuses on implementation of new tools for real-time monitoring and control of various unit operations. Enhanced process understanding will lead to a robust process and eventually enable Quality by Design into the product. Implementation of these new approaches will enable the pharmaceutical industry to shift from current batch manufacturing to continuous manufacturing.

The purpose of the present work was to develop analytical methods based on PAT tools together with chemometric method for process monitoring and control of a production line consisting of three unit operations (blender, roller compactor and tablet machine) aiming for pharmaceutical product (tablets).

Initially, we studied a pilot-scale bin blender and investigated the application of Near-Infrared Spectroscopy (NIRS) together with a developed algorithm to monitor and determine the blending profile and blend uniformity end-point. Model formulations consisting of an active compound (acetylsalicylic acid), together with microcrystalline cellulose and two grades of calcium carbonate ($CaCO_3$) with dramatically different particle shapes were prepared. The formulation comprised of angular shaped calcium carbonate reached blending end-point slower when compared to the formulation comprised of equant shaped calcium carbonate. Utilizing the ring shear test this distinction in end-point could be related to the difference in flowability of the formulations. Based on the two model formulations a design of experiments was conducted to characterize the blending process by studying the effect of $CaCO_3$ grades and fill level of the bin on blending end-point. Calcium carbonate grades, fill level and their interaction were shown to have a significant impact on the blending process.

Next, we studied a pilot-scale roller compactor and investigated the application of Near-Infrared Chemical Imaging (NIR-CI) together with chemometric models to visualize and determine both the pixel distribution and mean values of active compound and excipients, as well the ribbon porosity. The porosity of roller compacted ribbon is recognized as an important critical quality attribute which has a huge impact on the final product quality. Using NIR-CI in combination with Principal Component Analysis (PCA) and Partial Least Squares Regression (PLS-R) it was possible to, respectively, visualize the ribbon porosity distribution and determine the mean porosity values.

Finally, we studied a pilot-scale roller compactor together with a tableting machine and applied NIR-CI supported by chemometric modeling for monitoring and assessing the roller compaction and

tableting processes. Based on preliminary risk-assessment the critical process parameters (roll pressure and roll speed) and critical quality attributes (ribbon porosity, granule size, amount of fines, tablet tensile strength) were identified and a design space was established. Experimental runs with different process settings were carried out which revealed intermediates (ribbons, granules) and final products (tablets) with different properties. PCA based model of NIR-CI was applied to map the ribbon porosity distribution. The ribbon porosity distribution gained from the PCA based NIR-CI was used to develop predictive models for granule size fractions. Predictive methods with acceptable R^2 values could be used to predict the granule particle size. PLS-R based model of the NIR-CI was used to map and predict the chemical distribution and content of active compound for both roller compacted ribbons and corresponding tablets. In order to select the optimal process, setting the standard deviation of tablet tensile strength and tablet weight for each tablet batch were considered.

The research presented in this thesis reveals new methods for monitoring and assessing critical quality attributes for a production line consisting of blending, roller compaction and tableting. The results demonstrated that the QbD concepts and PAT tools can be utilized for creating improved process understanding during pharmaceutical manufacturing for increasing product quality and reducing the volume of costly laboratory testing of product quality.

RESUMÉ

Ved indførelsen af Quality by Design (QbD) og Process Analytical Technology (PAT) konceptet er den farmaceutiske industri i en forbedret retning hvad angår procesforståelse. Den farmaceutiske industri er fokuseret på, at implementere nye værktøjer til at monitorere og kontrollere forskellige enhedsoperationer i realtid. En forbedret procesforståelse vil medføre en robust proces og dermed gøre det muligt at designe kvalitet ind i produktet. Implementeringen af disse nye fremgangsmåder vil gøre det muligt for den farmaceutiske industri at skifte fra batchproduktion til kontinuerlig produktion.

Formålet med det foreliggende arbejde var at udvikle analytiske metoder baseret på PAT-værktøjerne sammen med kemometriske metoder til procesmonitorering og -kontrol af fastdoseret lægemiddelproduktion.

Indledningsvis blev en pilot-skala bin-blander studeret, hvor nær infrarød spektroskopi sammen med en udviklet algoritme blev undersøgt til at monitorere og bestemme blandingsprofilen og sluttidspunktet for blandingsensartetheden. Der blev udarbejdet modelformuleringer bestående af det aktive stof (acetylsalicylsyre) sammen med mikrokrystallinsk cellulose og to kvaliteter af kalciumkarbonat ($CaCO_3$) med markant forskellige partikelformer. Formuleringer bestående af kantede kalciumkarbonater nåede blandingsensartethed langsommere sammenlignet med formuleringer bestående af kubiske kalciumkarbonater. Ved at anvende Ring Shear tester, kunne denne forskel i blandingsensartethed relateres til forskellen i flydeevne af formuleringerne. Ved at inddrage de to modelformuleringer blev der udført en statistiskforsøgsplanlægning for at karakterisere blandingsprocessen ved at studere effekten af $CaCO_3$ kvaliteter og fylde niveau/mængde på slut tidspunktet for blandingsensartethed. Det viste sig, at kalciumkarbonatkvaliteten og fyldemængde samt interaktionerne mellem disse havde en betydelig indvirkning på blandeprocessen.
Dernæst blev en pilot-skala-rullekomprimator studiet, hvor nær-infrarød kemisk billeddannelse sammen med kemometriske modeller blev undersøgt til at visualisere og bestemme ribbon-porøsitetsfordelingen samt den gennemsnitlige porøsitetsværdi. Porøsiteten af ribbon er kendt som en vigtig kritisk kvalitetsegenskab, som har en enorm indflydelse på den endelige produktkvalitet.
Ved brug af nær-infrarød kemisk billeddannelse sammen med Principal Component Analysis (PCA) og Partial Least Squares Regression (PLS-R) var det muligt, at henholdsvis visualisere ribbonporøsitet og bestemme den gennemsnitlige porøsitetsværdi.
Til sidst blev en pilot-skala rulle komprimator sammen med en tabletmaskine studeret, hvor nær-infrarød kemisk billeddannelse sammen med kemometriske modeller blev undersøgt til at monitorere og vurdere rulle kompakterings-og-tabletprocessen. Ved anvendelse af indledende risikovurdering var

det muligt at definere kritiske procesparameter (rulle-/valsetryk og rulle-/valsehastighed) samt kritiske kvalitetsegenskaber (ribbonporøsitet, granulatstørrelse, mængden af fines og tabletstyrke) hvorefter en statistiskforsøgsplanlægning blev udarbejdet. Eksperimentelle forsøg med forskellige procesindstillinger blev udført og resulterede i forskellige mellem- samt slutproduktegenskaber. En model baseret PCA og nær-infrarød billeddannelse blev anvendt til at kortlægge ribbon-porøsitetsfordelingen. Den opfangede ribbon-porøsitetsfordeling via PCA baseret nær-infrarød billededannelse blev brugt til at udvikle prædiktionsmodeller for granulatstørrelsesfraktioner. Acceptable R^2-værdier blev observeret for prædiktionsmodellerne og kan bruges til, at forudsige granulatstørrelsen. Modeller baseret på PLS-R og nær-infrarød billeddannelse blev anvendt til at kortlægge og bestemme kemiskfordeling og det aktive stofindhold i ribbons samt tabletter. For at vælge de optimale procesindstillinger blev standardafvigelsen for tabletstyrke og tabletvægt for hver enkel tabletbatch vurderet.

Forskningen, præsenteret i denne afhandling, viser nye metoder til, at monitorere og vurdere de kritiske kvalitetsegenskaber under en produktionslinje bestående af blanding, rulle-kompaktering og tablettering. Resultaterne viste, at QbD konceptet samt PAT-værktøjerne kan anvendes til at skabe en forbedret procesforståelse for den farmaceutiske fremstilling og dermed øge produktkvaliteten samt reducere omfanget af dyre laboratorietest, relateret til vurdering af produktkvalitet.

TABLE OF CONTENTS

PREFACE ..... **I**
ACKNOWLEDGEMENTS ..... **II**
LIST OF PUBLICATIONS ..... **III**
LIST OF SYMBOLS AND ABBREVIATIONS ..... **IV**
ABSTRACT ..... **VI**
RESUMÉ ..... **VIII**
TABLE OF CONTENTS ..... **X**
1. INTRODUCTION **1**
2. LITERATURE REVIEW **5**
2.1 Pharmaceutical Manufacturing 5
2.1.1 Batch Manufacturing 5
2.1.2 Continuous Manufacturing 6
2.1.3 Quality by Design 6
2.1.4 Process Analytical Technologies 8
2.1.5 Pre-processing and multivariate data analysis - Chemometrics 13
2.2 Blending 15
2.3 Roller compaction 17
2.3.1 Roller compaction equipment 18
2.3.2 The use of roller compaction in pharmaceutical manufacturing 18
2.3.3 Roll compaction advantages and limitations 19
2.4 Tablet compression 21
3. AIMS OF THE STUDY **23**
4. MATERIALS AND METHODS **24**
4.1.1 Raw materials, formulations and flowability 24
4.1.2 Algorithm for blending end-point detection 24
4.1.3 Design of Experiments for blending study 24
4.2.1 Materials and Roller Compaction settings 25
4.2.2 Ribbon porosity measurements 25

4.2.3 Ribbon porosity mapping based on NIR-CI and PCA 25
4.2.4 Ribbon porosity prediction based on NIR-CI and PLS-R 25
4.3.1 Roller compaction and Design of Experiments 26
4.3.2 Granule characterization 26
4.3.3 Tablet compression 26
4.3.4 Tablet characterization 26
4.3.5 Instrumentation and data acquisition 26
4.3.6 Spectral data processing 27
4.3.7 Chemometric models 27
5. RESULTS AND DISCUSSION 28
5.1.1 Monitoring of blending process and detection of end-point for initial formulations using NIRS and blending algorithm 29
5.1.2 Flowability of pure $CaCO_3$ grades and powder formulations 30
5.1.3 Design of Experiments for blending study 31
5.2.1 Ribbon porosity measurements 33
5.2.2 Ribbon porosity mapping based on NIR-CI and PCA 33
5.2.3 Ribbon porosity prediction based on NIR-CI and PLS-R 36
5.3.1 Roller compaction and Design of Experiments 38
5.3.2 Ribbon characteristic 39
5.3.3 Granule characteristics 39
5.3.4 Ribbon porosity map based on NIR-CI and PCA 40
5.3.5 Ribbon chemical map based on NIR-CI and PLS-R 41
5.3.6 Relationship between ribbon NIR-CI porosity distribution and granule size distribution 42
5.3.7 Tablet characteristics 44
5.3.8 Tablet chemical map based on NIR-CI and PLS-R 45
6. CONCLUSIONS 47
7. PERSPECTIVES 49
8. REFECENCES 52
9. LIST OF APPENDICES 60

1. INTRODUCTION

During the past decade the pharmaceutical industry has faced challenges with productivity, tighter regulation and more difficult market conditions [1]. The pharmaceutical industries have experienced a slight decrease in scientific productivity in terms of new drug products reaching the market. Even though the number of new drug products reaching the market peaked in 2011, the pharmaceutical industries annual output has effectively flat lined for the past 10 years [2]. One main factor in this scenario is the increasing expense of developing new drug products. In 2006, the Tufts Center for the Study of Drug Development estimated average cost per molecule at $1.24 to 1.32 billion [3]. Various commentators have since challenged these numbers, claiming that the real cost is anything from $75 million to $4 billion, while the majority of the commentator lean towards the higher end of the range [4, 5]. Additionally, the regulatory environment is concurrently getting more demanding [2]. As an example the European Medicines Agency (EMA) introduced a new, three-pronged approach to the management of adverse reactions. The Food and Drug Administration (FDA) is building a surveillance system to monitor the safety of all drug products on the US market. Regulatory agencies all over the world are starting to collaborate in order to have a global overview of the safety of all drug products [2]. The pharmaceutical industries also struggle with recalls of their products due to manufacturing and quality testing complications [6]. Between 2004 and 2011 there have been reported, on average, one recall per month in the United States, which can have implications for the patients and can be very expensive for the manufacturer to recall [7]. Besides the cost of the recall procedure, the company can also lose business due to a tarnished reputation.

Furthermore, pharmaceutical industries have already and will in the near future experience tougher challenges in the marketing and sales front. The ‘patent cliff’ is another major factor. Between 2012 and 2018, the pharmaceutical industries will have a decrease about $148 billion of their revenues due to sale of generic drug products [2]. Another challenge is the harsher price controls by the governments. For instance, Russia started applying mark-up limits on imported drug products in April 2010 [2]. India announced plans to control the prices of 400 important drug products in November 2011 [8]. Additionally, Turkey has increased the discount on treatments reimbursed through its social security system [9]. All these above mentioned challenges will lead to less capital and or resource to invest in the development of drug products [10].

For decades, the pharmaceutical industries have used pioneering science to discover active pharmaceutical ingredients but have manufactured them using techniques dating to the days of the

steam engine [11]. The current predominantly batch manufacturing has driven a slow-paced and inventory heavy processing model that is increasingly considered as inflexible and unstainable. Even with progressive improvements in production process control and consequent productivity, the pharmaceutical industry suffers from much lower operational performance levels (e.g. waste, inventory, and flexibility) when compared with other process industries [12].
The pharmaceutical industry is a highly regulated industry and is required by the authorities to obey strict quality levels at each manufacturing step in order to transfer from one step to another. Therefore, large amounts of resources are used on testing the products. As a result of this quality-by-testing (QbT) paradigm a huge of amount of intermediate product is detained at the manufacturing site. These delays increase the cycle times of pharmaceutical products and the cost of manufacturing these products [13].

For many years, the innovation in pharmaceutical manufacturing and quality assurance has been slowed down due to stringent regulatory restrictions, which allowed little room for improvements. The uncertainty of approval by the regulatory agencies is one of the important reasons why the pharmaceutical industries have not been motivated to optimising the manufacturing processes [14]. However, during the past decade the pharmaceutical industries and regulatory bodies have realised the importance and needs for innovation in pharmaceutical manufacturing and quality assurance in order to overcome current and future challenges.

In this context, regulatory bodies have developed documents for a paradigm shift in pharmaceutical development, manufacturing and regulatory thinking. These documents include; “Guideline on Real Time Release Testing” [15], “Pharmaceutical cGMP for the 21st century: A Risk-Based approach” [16], “PAT – A framework for innovative Pharmaceutical Manufacture and Quality Assurance ” [17], Process Validation: General Principles and Practices [18] and International Conference of Harmonization (ICH) published guidelines [19-22]. These documents form the basis of the so-called Quality by Design (QbD) approach to pharmaceutical development and manufacturing. The aim of QbD is to design quality into the product. Implementation of QbD concept to pharmaceutical development and manufacturing utilizes modern scientific and quality risk management principles and quality control strategies based on product and process understanding. Including QbD approaches such as risk-assessment and Design of Experiments (DoE) for a pharmaceutical manufacturing, it is possible to; identify the critical quality attributes of the product and the critical process parameter of the unit operation. Creating a design space it is possible to gain knowledge of the pharmaceutical processes, products, and their relationship to each other. Including Process Analytical Technology (PAT) enables real-time process control, real-time process variance

management and real-time assurance of product quality during manufacturing. Implementation of the QbD concept may thus lead to increased product quality, production efficiency, reduced laboratory testing requirements and process optimization. The consumer/patient may benefit from this since improved quality and reduced production costs of the products may lead to faster time-to-market. Similarly, the regulatory authorities may benefit from a simpler documentation system. Also, ensuring a high level of process understanding, regulatory authorities may consider the products with less risk to the public safety and hence reduce approval time. IBM reported that by implementing the appropriate QbD and PAT approach, a successful top-end pharmaceutical company could reach a level with less than 1 % failure. Thereby the top 30 pharmaceutical companies could save approximately US$10 billion per year [23].

Future competitiveness within the pharmaceutical industry is related to shift from batch processing to continuous or, at least semi-continuous processing or a more flexible batch processing joined with the QbD concept [24, 25]. Continuous manufacturing (CM) defined as a process without interruption over a sustained period of time. This means connecting the throughput of all unit operations into one production line in order to maximize total capacity, capital utilization, the yield and quality of the product while minimizing inventory and product time-to-market. Additionally, continuous process scale readily to a certain extent through increases in operating time, total flow rate, and hence reducing the need for scale-up studies throughout the development process [25-28]. Ideally, QbD and PAT tools have to be implemented during the process development for process understanding and later in the full scale production for process monitoring and control in order to ensure consistent product quality [17, 26, 29, 30] .

Adaption of CM in QbD context in the pharmaceutical industry requires interdisciplinary expertise and cross-functional collaboration in areas such as upper management, regulatory, supply-chain, drug formulation, analytical chemistry, chemometrics, process engineering, process automation and manufacturing. Recently, there have been published several white papers concerning the opportunities and challenges the different areas in pharmaceutical industry will face when CM is implemented [12, 30-37]. These white papers have been produced by several experts from academia, industry, regulatory agencies and equipment vendors. At this stage of time several pharmaceutical industries have already shifted from batch to CM manufacturing [10]. As an example, GSK has demonstrated significant reduction in scale-up time and cost during development by switching from batch to continuous granulation [38]. It is now generally accepted that the pharmaceutical industry has started moving away from the batch manufacturing to a more flexible CM.

The focus of the present thesis is to utilize QbD approaches mainly based on DoE and PAT tools (Near-Infrared spectroscopy and Near-Infrared Chemical Imaging) for creating process understanding of solid dosage forms and, especially, to develop methods for monitoring and controlling critical quality attributes during a production line consisting of three unit operations; blending, roller compaction and tableting.

2. LITERATURE REVIEW

2.1 Pharmaceutical Manufacturing

Pharmaceutical manufacturing can be divided into primary and secondary manufacturing. During primary manufacturing the active pharmaceutical ingredient (API) is produced via e.g. fermentation, chemical synthesis or extraction. To ensure the safety and efficiency of pharmaceutical products, the process for manufacturing the API must be carefully controlled ensuring consistent of purity and quality. Secondary Pharmaceutical Manufacturing refers to all the processing steps after the API, has been manufactured. The API is formulated with excipients and manufactured into a particular dosage form that is most suitable for the patient. Oral solid dosage form (e.g. tablet) is the most popular form due to ease of administration, compliance, low manufacturing costs, and improved chemical and microbiological stability, when compared to liquid dosage forms [13, 24]. Many steps are involved during pharmaceutical manufacturing. A simplified schematic overview is depicted in Figure 1.

Figure 1. Simplified diagram of Pharmaceutical Manufacturing steps. Blue and green arrows represent, respectively steps during primary and secondary manufacturing.

2.1.1 Batch Manufacturing

In many decades, the pharmaceutical industries have been applying batch processing during manufacturing of pharmaceutical products. Pharmaceutical products are manufactured in batches that can vary in size from kg-scale for special pharmaceutical products with very small market size, to ton-scale for blockbuster products. Batch processing is suitable for small batch sizes, however, for bigger batch sizes, the cost of batch manufacturing tends to be higher and inefficiency compared to continuous manufacturing [24, 28]. The development process of tablets can be divided into the following three stages. I) the drug is formulated in lab-scale, II) production of pilot and clinical batches and III) up-scaling from lab-scale to production scale. Optimization and validation is necessary at each scale level, since the settings according to process and formulation are not transferable from lab-scale to production-scale. Pharmaceutical products are stringently regulated and authorized to obey strict quality requirements. The pharmaceutical industry ensures quality by testing the product at various stages during manufacturing. As a result of this Quality by Testing (QbT) paradigm, a lot of work-in-

progress material is held in the manufacturing site, since product cannot proceed without passing the quality assessments conducted by the quality control laboratory. This leads to delays and increases the cycle times of pharmaceutical products and the cost of manufacturing these products. Another challenge that batch manufacturing face is the lack of in-depth process understanding [24, 26, 28, 29]. During batch manufacturing batch to batch variation often occur and not having in-depth process understating (e.g. in-line process monitoring) the root cause is not understood. The lack of process knowledge will then be of more concern to the regulatory agencies.

2.1.2 Continuous Manufacturing

Continuous manufacturing is defined as a process without interruption over a sustained period of time. This means connecting the throughput of all unit operations into one production line in order to maximize total capacity, capital utilization and the yield and quality of the product while minimizing inventory and product time-to-market [25-29].

The pharmaceutical industry is required by the regulatory agencies to constantly assess and assure the drug quality and safety at any time. The uncertainty of approval by the regulatory agencies is one of the important reasons why the pharmaceutical industries have not been motivated to take initiative to move from batch production to continuous production [14]. However, in recent years, continuous manufacturing has gained importance in the pharmaceutical industry. Also the regulatory bodies have shown an enormous interest in moving towards continuous processing in order to improve quality in pharmaceutical production [11, 27, 34].

The US Food and Drug Administration (FDA) and International Conference for Harmonization (ICH) have outlined guidelines [16, 17, 19-22] through which they try to encourage the pharmaceutical industry to implement state of art scientific approaches such as Quality by Design (QbD) and Process Analytical Technologies (PAT). Implementation of these approaches will improve and optimize pharmaceutical development, product quality and hence make it easier to shift from batch to continuous processing.

2.1.3 Quality by Design

Quality by Design is a systematic, scientific, risk based, holistic and proactive approach to pharmaceutical development that begins with predefine objectives and emphasizes product and process understanding [29, 39]. QbD follows the idea that quality cannot be tested into the product; it needs to be built into the product, as stated by the ICH Q8(R2) guideline [19] and FDA´s PAT

guideline to the industry [17]. This means that quality has to be considered already when the product is developed.

One QbD approach could be as follows: Initially, the target product profile (TPP) or by means the “user interface” of the product is identified. TPP includes defining the quality target product profile (QTPP) which is related to quality, safety and efficacy, route of the route of administration, dosage form, bioavailability, strength, and stability [19]. Once the TPP has been identified the next step is to identify, the relevant critical quality attributes (CQA). A CQA is defined as a physical, chemical, biological, or microbiological property or characteristic that should be within appropriate limits to ensure the desired product quality [19]. Future it is essential to identify the critical material attributes (CMA) and the critical process parameters (CPPs). CPPs are process inputs that have a direct and significant influence on CQAs when they are varied within regular operating range. It is important to understand the interaction between CPP and CQA in order to vary CPP to compensate for changes in raw material quality [29]. Risk assessment can be used to identify the most critical CMAs, CPPs and CQAs. Identification of CQAs, CMAs and CPPs are done through risk assessment as per the ICH guidance Q9 [20].

Risk management

According to ICH Q9 [20], “risk assessment consists of the identification of hazards and the analysis and evaluation of risks associated with exposure to those hazards”. Traditionally, risks to quality have been assessed and managed in several informal ways (empirical and/ or internal procedures) based on, for example, compilation of observations, trends and other information. Additionally, the pharmaceutical industry and regulators can assess and manage risk using recognized risk management tools and/ or internal procedures (e.g., standard operating procedures). Some examples of these tools are: Basic risk management facilitation methods (Ishikawa diagrams ,flowcharts, check sheets etc.), Failure Mode Effects Analysis (FMEA), Failure Mode, Effects and Criticality Analysis (FMECA), Hazard Analysis and Critical Control Points (HACCP), Hazard Operability Analysis (HAZOP), Risk ranking and filtering, Supporting statistical tools etc. Risk assessment is typically performed early during pharmaceutical development and may be repeated as more information and greater knowledge is obtained. Appropriate use of risk management does not hinder industry’s responsibility to comply with regulatory requirements. However, effective risk management can enable better and more informed decisions, can provide regulators with greater assurance of a pharmaceutical industry’s ability to deal with potential risks, and might affect the extent and level of

direct regulatory oversight. Applying risk management processes offers greater understanding of decision-making processes and builds confidence in quality risk management outcomes [20, 29, 40].

Design of Experiments

Utilizing Design of Experiments (DoE) the influences and interactions of CPPs on CQAs can be clarified and a design space can be established. The design space is defined as “the multidimensional combination and interaction of input variables (e.g. material attributes) and process parameters that have demonstrated to provide assurance of quality”. Inside the design space is the control space (or normal operating ranges), wherein the process should be run. The control space is usually defined with upper and lower limits for each input variable (raw material attributes and process parameters).

The next step is to establish risk-and-science-based control strategies. Control strategy is defines as “a planned set of controls” derived from current product and process understanding that assures process performance and product quality. One approach of process control is the implementation of Process Analytical Technology (PAT) tools for real-time monitoring. Having process monitoring implemented in a process, deviation from normality can be observed. In well-established processes any deviation from normality will trigger the system to apply changes so that the process is brought back on track [26, 29]. Finally, product lifecycle management and continuous improvement are also part of the QbD strategy and a quality system is recommended by ICH Q10 [21] and Q11 [22] .

2.1.4 Process Analytical Technologies

In QbD context, PAT plays a crucial role in the design, analysis and control of manufacturing processes based on timely in-line, on-line, at-line an off-line measurements of CQAs with the goal to ensure the final product quality. Implementation of PAT will enhance process understanding and knowledge. FDA promotes the use of QbD and PAT approaches, to ensure manufacturer’s ability to maintain consistent quality. It is encouraged to use PAT to monitor and control processes instead of just testing products. Therefore, the implementation of QbD and PAT in real-time industrial production setups is crucial before continuous manufacturing can become a reality in the pharmaceutical industry. In order to implement PAT, four main PAT tools have to be complied [17]:

- Multivariate tools for design, data acquisition and analysis
- Process analyzers
- Process control
- Continuous improvement and knowledge management tools

The most applied process analysers in the pharmaceutical context are Near-Infrared spectroscopy (NIRS) and Near-Infrared Chemical Imaging (NIR-CI) spectroscopy. Of the multivariate/chemometrics methods, principal component analysis (PCA) and partial least squares (PLS) regression are the most used [41-48].

In this thesis only process analysers: NIRS and NIR-CI and multivariate/chemometrics methods, PCA and PLS will be discussed.

Near-Infrared Spectroscopy

The discovery of near-infrared energy was ascribed to William Herschel in the 1800s [49]. The first industrial application began in 1950s. Prior 1950s the near infrared (NIR) region was not considered useful for spectroscopy because near infrared bands are severely overlapping and difficult to interpret. With the introduction of the first single-unit, stand-alone NIRS system in 1980s, light-fiber optics in mid 1980s, and the development of monochromator detector in 1990s NIRS became a more powerful tool for scientific research [46, 50]. The progresses within computational power and the use of multivariate data analysis/chemometrics have proven the effectiveness and use of NIRS in different fields as pharmaceutical [42], agriculture [51], chemical [52] and food industry [53].

The absorptions in the NIR region are primarily due to overtones and combinations of the fundamental molecular vibrations from the mid-infrared region between X-H bonds (X = O, N, C, S). NIRS covers the transition from the visible spectral range to the mid-infrared region in the area of (800–2500 nm, respectively 12821–4000 cm^{-1} [46]. NIR spectra can be obtained in three different modes: transmission, diffuse reflection or transflection. In this project only diffuse reflectance measurements have been conducted on solid samples and therefore a brief introduction is given.

In diffuse reflectance spectroscopy, the light source and detector are located on the same side of the sample. The detector measures the amount of light reflected from the sample surface, which contains a specular component and a diffuse component. The specular (speculum (lat.) = mirror) component is the light that is just reflected from the sample surface and not absorbed. The specular component has little or no information about the sample. The diffuse component is the light reflected after interaction with the sample. The diffuse reflected light contains information about the sample materials at various depths and locations in the sample. Therefore, only the diffuse component is of interest and not the specular component. The specular component is often minimised by performing appropriate pre-processing on the collected spectra [43, 54].

The depth of near-infrared radiation penetrates into a sample depends on the wavelength. Clark et al. [54] found an exponential relationship of NIR light penetration with wavenumber. The information depth, which is the depth of sample contributing to the measured reflected radiation, was found to increase exponentially with increasing from 1100 to 2500 nm the information depth varied from 777 µm to 109 µm. However, it was also determined that half of the contribution to any obtained reflectance spectrum will come from the top surface (from 180 µm to 25 µm for the spectral range from 1100 to 2500 nm) [54].

NIR spectroscopy is a fast and non-destructive PAT tool which in combination with chemometric models can be used for process monitoring/analysis [44, 47]. Process analysis can be defined as in-line, on-line, at-line and off-line. Figure 2 shows the different process analysis. In-line analysis is measured on the sample in the process stream, on-line analysis is performed by withdrawn the sample from the process stream via sampling loop, where the sample is measured and then returned to the process, at-line analysis is performed by removing the sample from the process stream and measured in near proximity of the process within the timescale of processing and off-line analysis is performed by removing sample from the process stream and measured in a laboratory and not necessarily at the same time as the production is running [55].

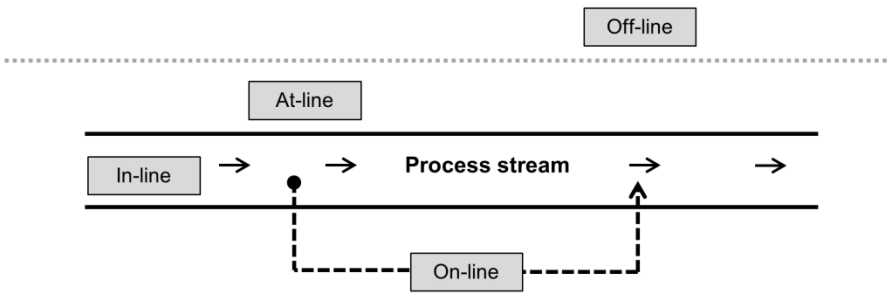

Figure 2. Illustration of different types of process analysis.

Near-Infrared Chemical Imaging

In conventional NIR spectroscopy a bulk NIR spectrum is measured that reflects an average composition of the measured sample. NIR-CI adds spatial information to the spectral information by combining conventional NIR spectroscopy with digital imaging, where the spectral and spatial information are simultaneously recorded and stored as three dimensional dataset or hyperspectral data cube. The **x** and **y** axis represent the spatial or pixel information and z is the wavelength axis in

the spectral measurement (Figure 3a). Prior data processing it is necessary to unfold the 3D hyperspectral data cube to two-dimensional (2D) data matrix in which each row is a spectrum (sample) related to one of the pixels (Figure 3b). The 2D data matrix is processed by the desire chemometric model (Figure 3c) and refolded to the 3D hyperspectral data cube, where the chemical or physical image can be obtained. The images provide distribution information from the sample surface (Figure 3d), [45, 56].

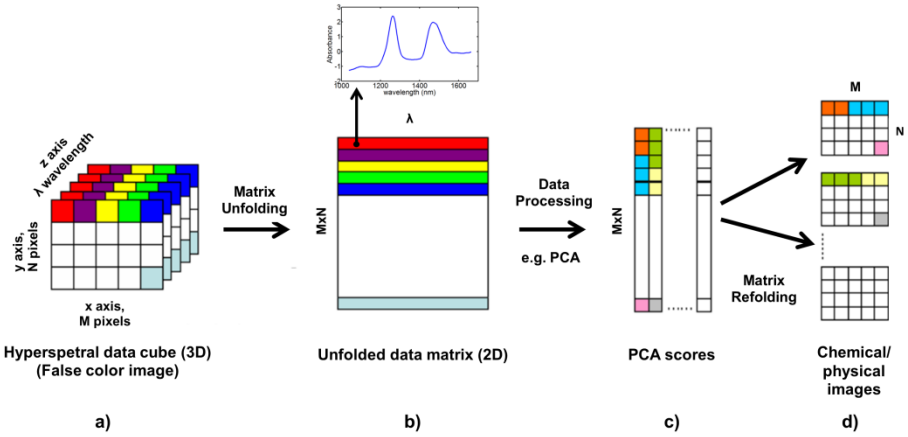

Figure 3. Schematic description of 3D hyperspectral data cube unfolding for data processing approaches (as example PCA) and subsequent matrix refolding.

There are two main types of NIR-CI systems; Line mapping or pushbroom system and global imaging system. During the present work only the line mapping system has been used and therefore this will be discussed. In line mapping systems the sample area and pixel resolutions are defined. This determines the number of recorded pixels. For each acquisition diffuse reflectance spectra are collected from a line of 320 pixels. With a very accurate moving sample stage the sample is moved and another line of spectra are recorded. In this way a grid of spectral information is built up from the lines of spectra until spectra from all pixels in the defined sample area are obtained to establish the hyperspectral data cube. Figure 4 represents a mechanical setup of the line mapping system used in this thesis.

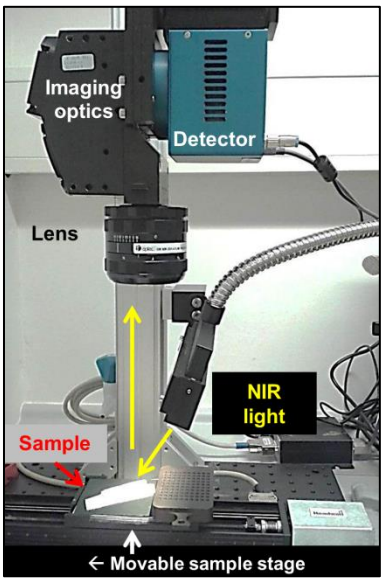

Figure 4. Mechanical setup of the hyperspectral camera system.

Spectral correction and transformation

The spectral responses obtained by both NIRS and NIR-CI measurements consist of information from both the sample and the instrument. Therefore, an initial background measurement is performed to correct for the instrument response. This is carried out by measuring the intensity of light ($\mathbf{I_b}$) which is diffusively reflected from a stable standard material with a high absolute reflectance. The intensity of light reflected from the sample is then measured ($\mathbf{I_s}$). The corrected NIR diffuse reflectance raw data (**R**) is archived by equation 1.

$$\mathbf{R} = \mathbf{I_s}/\mathbf{I_b} \qquad \text{(Eq. 1)}.$$

The raw reflectance data (**R**) archived for NIRS and NIR-CI are stored into, respectively, a matrix and a hypercube with three dimensions.

Prior to multivariate data analysis the raw reflectance data (**R**) are transformed into absorbance (**A**) using equation 2.

$$\mathbf{A} = -\log_{10}\mathbf{R} = \log_{10}(1/\mathbf{R}) \qquad \text{(Eq. 2)}.$$

Assuming the path length (**ℓ**) on average is constant for the NIR measurement and using the Beer Lamberts law a linear relationship between the absorbance (**A**) and analyt concentration (**c**) can be established, equation 3.

$$\mathbf{A} = \log_{10}(1/\mathbf{R}) = \boldsymbol{\varepsilon} \times \boldsymbol{\ell} \times \mathbf{c} \qquad \text{(Eq. 3)}.$$

where ε is the molar absorptivity that is specific to each analyte and a function of wavelength.

2.1.5 Pre-processing and multivariate data analysis - Chemometrics

Collected NIR spectra contain both chemical and physical information of the measured sample. In order to extract the desired information either chemical or physical proper pre-processing and multivariate data analysis or chemometrics is in practice a necessity. Some of the basic principles will be explained in this section.

Pre-processing of spectral data

Pre-processing of spectral data is generally used to improve the chemometric model [57].
It is often desired to decrease the influence of various signal sources that are not related to the chemical or physical information by the raw spectra [58]. The most used pre-processing techniques for NIR spectral data can be divided into two categories: scatter correction methods and spectral derivatives. As an example standard normal variate (SNV) is one of the most used scatter correction techniques. In SNV correction the variation in slope and offset are removed, for each wavelength, on an individual spectrum basis [59]. As an example of derivatives the second derivatives are often used to remove baseline and linear trend. However, prior application of derivatives to spectral data, smoothing and fitting into a low-order polynomial within a data window (e.g. Savitzky-Golay) is often advantageously processing methods. Since application of derivation should be done with care as this may add noise to the spectral data [60].

Principal Component Analysis

Principal component analysis (PCA) is one of the most applied qualitative methods for dimension reduction and pattern recognition in spectral data sets. The PCA model obtains the main variation in a dataset (**X**) and reduced the variables (spectral wavelengths) into fewer orthogonal variables, called principal components (PCs). Each PC is composed of two sets of data: the scores (**t**) and loadings (**p**)

with the scores referring to spectral variation and the loadings representing the spectral contribution to each PC. The first PC explains the majority of the variation in the dataset. The second PC describes the majority of the remaining variation and in the dataset and are orthogonal to the first PC. For the reaming PCs same procedure is applied. After calculating the PCs the difference between the explained variance and the original data is the residual (**E**) [61, 62]. The mathematical model for the PCA model is described below in equation 4:

$$\mathbf{X}=\mathbf{TP}' + \mathbf{E} \qquad \text{(Eq. 4)}$$

where, **X** contains the spectral dataset of *N* samples and *M* variables (wavelengths), **T** is an *N* by *A* matrix containing the scores on the *A* principal components, **P** is an *M* by *A* matrix containing the loadings on the *A* principal components, and **E** is an *N* by *M* matrix of residuals.

Partial Least Squares Regression

Partial Least Squares (PLS) regression is a quantitative multivariate data analysis method that is built and used to predict desire characteristics (**y**) from a measured spectrum (**X**). PLS is a two-block regression method based on estimated latent variables (LV) that needs an X-block and a y-data [63]. The mathematical model for the PLS regression model is described below in equation 4:

$$\mathbf{y}=\mathbf{X}\cdot\mathbf{b}+\mathbf{E} \qquad \text{(Eq. 4)}$$

where, **b** is the regression coefficient and **E** is the residual. It is desired to maximize the covariance between **y** and **X** and to lower the residual. In order to estimate the PLS-model capability the root-mean-square-error of cross validation (RMSECV) or cross-validation can be calculated by equation 5.

$$RMSECV = \sqrt{\frac{\sum_{i=1}^{N}(y_i-\hat{y}_i)^2}{N}} \qquad \text{(Eq. 5)}$$

where, $\mathbf{y_i}$ is the measured **y** (e.g. chemical reference method), $\hat{\mathbf{y}}_\mathbf{i}$ is the predicted value (e.g. spectral prediction), and N is the total number of samples. It is desired to minimize the complexity of the model and use as few LV as possible. Using the minimum point in the RMSECV curve it is possible to estimate the optimal number of LVs that should be used for a good PLS model. Including to many LVs

will results in modelling of noise and over-fitting of the model, this may lead to poor model performance [63, 64].

Another approach to validate the PLS model is to include independent samples or test-set validation, with known and y-values. These samples are then predicted by the PLS model and the predicted values are compared with the actual measured values. The set of parameters leading to the smallest root-mean-square of prediction (RMSEP) is selected for the PLS model. The RMSEP is calculated in the same way as for the RMSECV. Cross-validation is less labour demanding compared to test-set validation. Although, cross-validation has a slight tendency to suggest more LVs for the model building for optimal models compared to test-validation [63, 65].

2.2 Blending

One of the most critical unit operations during the manufacturing of solid dosage forms is the blending operation. Achieving a uniform mixture of the active pharmaceutical ingredient (API) and the needed excipients is particularly important. A blend, in the classical pharmaceutical sense, is considered to be homogeneous when the API content of the blend samples is within specification, while assuming that all excipients are also evenly distributed [66]. Most pharmaceutical powder mixtures consist of materials with different physical properties; particle size, particle shape, density, and surface area. Many variables, such as the blender type and design, scale and properties of the constituents as particle size distribution, particle shape, density, cohesion, and electrostatic charge, can influence the degree of blending [67-72]. Even though, powder blending is a routine operation, it is not always simple. As an example blending of particles with significant different particle size may lead to segregation and hence inadequate final product quality, such as content uniformity, disintegration time and/or dissolution behaviour [73]. All these performance parameters can directly impact the final dosage form efficacy, in-vivo performance, and ultimately patient safety. Therefore, optimum process settings are unique to every product [74].

Blending is a reshuffling process involving the random movement of individual (groups of) particles. Competing process with the powder blending process are segregation and/or demixing [71, 75]. Three main mechanisms are responsible for blending, namely diffusion, convention and shear.

- Diffusion blending is characterized by the small scale random motion of powder particles. The movement of blender increases the mobility of the individual particles and hence promotes diffusive blending. Bin blenders and v-blenders function by diffusion blending.
- Convection blending is characterized by the large scale random motion of powder particles. In convection blending groups of particles rapidly moved from one position to another due to the action of a rotating agitator or the presence of baffles. Bin blenders, ribbon blenders and paddle blenders function by convection blending.
- Shear blending is characterized by the change in configuration of ingredients through development of slip planes or shearing strains within a bed of material. Mechanical force is imparted to the powder material by the blender to induce shear blending. High shear blenders with chopper blades function by shear blending.

The degrees to which these mechanisms influence a blending process depend on the flow properties of the powders being blended, the specific equipment selected and the process parameters/settings [75, 76].

In industrial practice the homogeneity of a powder blend is determined by invasive thief sampling followed by a time-consuming off-line chemical of physical analysis of the sampled material [76]. The current blend sampling technology is not considered as the optimal approach, since thief probes may not provide consistent and representative blend samples. Furthermore, using the thief sampling method only single points (blend samples) of the powder blend can be measured for homogeneity. Blends can undergo segregation during additional handling steps (e.g. discharging the blender into containers, transporting containers on the manufacturing floor or dumping the contents of the container into the equipment hopper) [73, 77]. Therefore, an alternative approach is needed in order to overcome current challenges related to the sampling and time-consuming off-line analysis.
Near-Infrared spectroscopy (NIRS) has evolved as more robust, consistent, rapid, and noninvasive blend monitoring techniques compared to current method. In addition NIRS is a fast and easy method to interface with the process for in-line or on-line monitoring [66, 78, 79].

Several researchers have used NIRS and different classical statistic, univariate and multivariate approaches to develop qualitative [66, 78, 80-89] and quantitative [83, 90-94] methods for studying the blend homogeneity. The qualitative methods are typically simple to use, whereas the quantitative methods are more complex but provide information about the mixture composition. However, none of

the developed qualitative methods for blend homogeneity considered the process stability to detect the end-point but rather stability compared to a target spectrum. This hampers the method for real-time usage, because the method is strictly depending on knowing beforehand the spectral profile of the final blend. And this is not feasible in many occasions.

2.3 Roller compaction

Roller compaction (RC) is an agglomeration process where the feed powder is densified between two counter rotating rolls due to mechanical pressure. When pressure is applied the powder particles deform, fragment and bond together to form ribbons [95]. In 1965 Johanson [96] developed a simplified method where it was assumed that the space between the two rolls was divided into three different regions (Figure 5): slip, nip and release regions. The slip region is the zone close to the feeding of the powders. The powders slip along the roll surfaces where particle rearrangements occur and relative moderate pressure is exerted on the powder material. The nip region begins at a roll angle α, termed the *nip angle* when the wall velocity of the powder becomes equal to that of the rolls. In this zone, the powder is dragged to the smallest gap and compressed by the increasing pressure applied by the rolls. Powder densification primarily takes place in this region. The compacts then enter the release region after passing the smallest gap in which elastic recovery could take place [95, 97, 98].

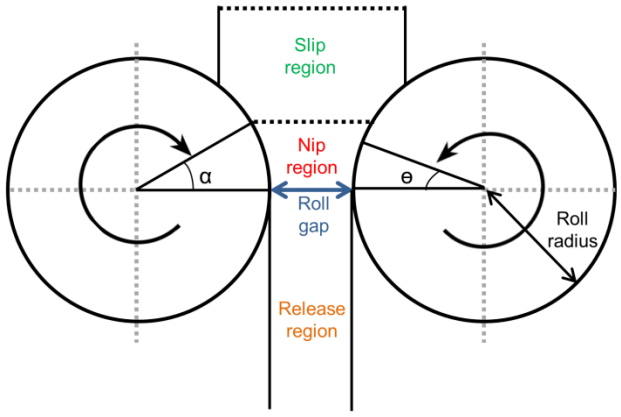

Figure 5. Schematic diagram of roll compaction showing the slip, nip and release regions defined by Johanson's theory (1965), where nip angle and roll angle are respectively α and ɵ.

2.3.1 Roller compaction equipment

In the pharmaceutical industries a wide range of roll compactors are used. The equipment's could be classified by roll assembly, sealing systems [99], feeding methods [100], roll layouts [101], roll surface conditions, and powder de-aeration method [102].

Generally, they may be classified by:

- Roll assembly: fixed rolls or movable rolls
- Sealing systems: side cheek plates or rim sealed rolls
- Feeding methods: gravity fed and force fed (with one or two screws)
- Roll layout: vertical, horizontal and inclined
- Roll surface: smooth, knurled or pocketed rolls
- Powder de-aeration system (for example, vacuum de-aeration in slip region)

2.3.2 The use of roller compaction in pharmaceutical manufacturing

In the pharmaceutical industries, roll compaction is adopted in secondary pharmaceutical manufacturing of tablets (Figure 6). The blended powder formulation containing the API and excipients are processed to tablets. During roll compaction ribbons are produced and subsequently milled into granules which are ready for tableting. Roll compaction is used to achieve the required increase in bulk density flowability and uniformity of particular formulations.

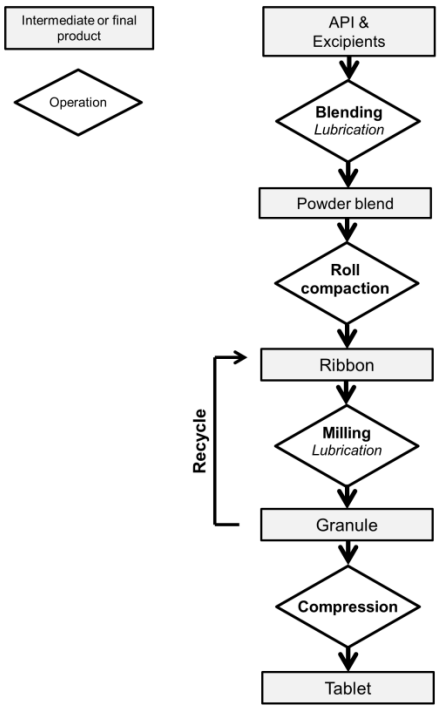

Figure 6. Flowchart diagram of the pharmaceutical secondary manufacturing of tablets using roll compaction.

2.3.3 Roll compaction advantages and limitations

Roller compaction (RC) as dry granulation process has been used in the pharmaceutical industries for more than 50 years. RC is a simple, continuous, environmentally friendly and relatively inexpensive process that is an attractive process for heat, moisture and solvent sensitive drugs. Specifically, in pharmaceutical applications, accessible process control, high mass throughput, and produced compacts with desired density and strength [103] make the roll compaction an outstanding option for dry granulation. RC has a significant advantage compared to wet granulation process as it excludes possible degradation of drugs caused by heat and moisture and therefore RC ensures better drug stability [95, 104-106]. RC has been used to improve the flow properties of cohesive powders for tableting and capsule filling [107]. However, the limitations of the technique cannot be ignored. Roller compaction possesses complex fundamental mechanisms, and similar to other manufacturing processes, the product quality and performance are affected by several factors such as; raw material properties [108-110], equipment design [102, 111, 112] and process parameter [112-115].

Studies [95, 108] have shown that raw material properties such as, particle size and shape affect the ribbons porosity, post-milled granule particle size distribution, flowability and compaction properties of the tablets. However, the compaction properties of plastically materials (e.g.

microcrystalline cellulose) are more prone to change due to particle size compared to brittle materials (e.g. lactose) [109]. Also the morphological form affects the product quality. In a study by Bacher et al. [108] they manage to produce tablets with acceptable mechanical strengths by choosing the proper morphological forms [108, 109].

Previous studies [97, 102, 116] have shown that the critical process parameters (CPPs), roll pressure (RP) and roll speed (RS), have an important influence on the ribbon porosity and hence on the granule and tablet characteristics. RP controls the compaction pressure applied to the powder material; while the RS controls the dwell time of the powder under pressure in the compaction region and eventually the throughput of the RC. As an example higher RP results in ribbons with lower porosity and larger granules [117]. Larger granules have better flow properties. Nevertheless, larger granules prepared by roll compaction often results in tablets with unacceptable surfaces and inferior tensile strength compared to direct compression [95, 105, 118]. This phenomenon of inferior tablet tensile strength has been attributed to different effects. 1) The increased granule size reduces surface area for particle to particle bonding, during tableting; 2) Work-hardening of materials that leads to higher resistance towards further permanent plastic deformation [110, 118, 119]. Materials with plastic deformation properties such as microcrystalline cellulose (MCC) are more sensitive to this phenomenon [110] while brittle materials are not. Fines generated during RC, is undesirable as it often leads to material loss and reduced granule flow properties [109].

Additionally, the interaction between roll speed and feed screw speed (FSS) is also important and can influences ribbon quality (e.g. porosity). According to Hanpin Lim et al. [116] increased FSS will decrease ribbon porosity at higher RS whereas it slightly increase the ribbon porosity at lower RS. At slower FSS the feed delivers less powder into the compaction region which means there is a lower bulk density and higher porosity of the powder which enables more entrapped air to remain inside the powder in the compaction region. Therefore, faster RS, slower FSS gives the highest porosity. At higher FSS and high RS the porosity of the ribbons decreased due to less permeation of entrapped air as a consequence of the higher speed. At lower RS the FSS has minimal effect on ribbon porosity due to the longer dwell time [116].

On industrial scale, fines are often regranulated to improve the yield. However, a negative influence of recycling on API-conformity was reported [120]. The study by Jones et al. suggested that fines can either promote or inhibit the granule flow, since granule flow is dependent on the amount fines, size of fines and the characteristics of the bulk solid [121]. Therefore, a balance between the proportion of large and small sized granules in a granule population is needed to improve overall granules flowability. The maintenance of constant roll parameters throughout the entire roller

compaction process does not necessarily guarantee homogeneous quality of ribbons, for example, when powder feeding is inconsistent or when material properties have changed [98].

Therefore, a deeper understanding of the process is required in order to consistently produce and maintain the desired product quality. The roll compaction process is complex and sample sensitive. Although roll compaction has been the target for research in the last few decades, it is still not well understood primarily due to the diversity in the controlling factors and material properties. Insufficient process understanding hinders an optimal process design. The trial-and-error method is often applied in the pharmaceutical manufacturing when working with new formulations, because no complete scientific theory or universal model is suitable for all powders. The time and cost consumption in trial-and-error study for industrial application is a driving force to include QbD in order to understand the process and control the process to archive product with predefined qualities. Utilizing the PAT tools and suitable chemometric models it is possible to closely monitor the intermediate and final product quality during operation. Especially, NIRS and NIR-CI spectroscopy have gained the most interest due to their many advantages, such as fast measuring time in a nondestructive way [97, 104, 106, 122].

2.4 Tablet compression

Tablets are the most used solid dosage form since they are accepted and trusted by professionals and patients/consumers alike, they are easily administrated and simple to dose. The most used processing technologies to manufacture tablets are: direct compression and dry granulation or wet granulation followed by tablet compression [123].

Direct compression (DC) is a popular and simple process to manufacture tablets since it provides the fastest, most effective and least complex way to produce tablets. In DC the API and excipients are blended and compressed directly into tablets. The powder formulation has to possess certain properties such as good flowability and compressibility for successful operation. Therefore, the selections of excipients are very critical and important compared to granulation processes [123, 124]. A main challenge with respect to DC is when aiming for manufacturing of high or low dose tablet. Many APIs tend to have poor compressibility, which influences the quality of the tablets especially when high API content tablets have to be manufactured. Conversely, manufacturing of low API content tablets is also a challenge since it is difficult to accurately blend a small amount of API in a large amount of excipient to achieve the desired uniformity and homogeneity [125]. As an example segregation of the different components can occur during tableting. This will lead to problems with weight variation and content uniformity. The main factor causing segregation is due to particle size differences between the API and excipients. In most cases the particle size of the API is significantly

lower compared to the particle size of the excipients. Indeed, there is an increased possibility of segregation, where the smaller API particles 'slip through' the bigger particle sized excipients [124, 125]. If a powder formulation suffers from bad flowability, compressibility, segregation and dustability problems the manufacture may include a granulation step before tableting. The granulation process narrows the particle size distribution of a tablets powder formulation and reducing the segregations tendency. This reveals greater compressibility and permits to manufacture tablets with higher amount of API with a better uniformity. The granulation step may either be based on wet-granulation or dry granulation. However, dry granulation is a more flexible and cost-effective manufacturing process compared to wet-granulation [103, 125]. In order to define the quality of tablets several labour intensive tests (e.g. hardness, dissolution, disintegration ability, friability and uniformity), must be conducted and comply with certain requirements. Pharmaceutical industries invests considerable amounts of time and money in developing and verifying these tests to assure the final quality of the final tablet product. Using NIRS or NIR-CI some of the traditional tests may be replaced. As examples NIRS and NIR-CI based approaches have been developed in order to determine uniformity [126-128], hardness [42, 129] and dissolution [47, 130] of tablets.

3. AIMS OF THE STUDY

The overall aim of the present thesis was to develop and implement innovative analytical methods in QbD context for process monitoring and indeed enhance process understanding of solid dosage forms. The specific intense were as follows:

- To develop and implement an algorithm for blend end-point detection using Near-Infrared Spectroscopy.

- To investigate the influence of raw material quality and blend fill level on blend end-point based on Design of Experiments and material characterization.

- To investigate the influence of roll pressure and roll speed on ribbon, granule and tablet quality based on Design of Experiments.

- To develop and implement analytical methods based on Near-Infrared Chemical Imaging to monitor the critical quality attributes of ribbons, granules and tablets during processing.

- To create an overall understanding of the blending, roller compaction and tableting process prior continuous manufacturing.

4. MATERIALS AND METHODS

4.1.1 Raw materials, formulations and flowability

As model active pharmaceutical ingredient (API), acetylsalicylic acid (ASA), was used. The excipients used were microcrystalline cellulose (MCC) and two grades of calcium carbonates ($CaCO_3$) with different shapes, namely angular and equant, (Figure 7). Throughout this study the different types of $CaCO_3$ are noted as $CaCO_3$-A and $CaCO_3$-E, respectively.

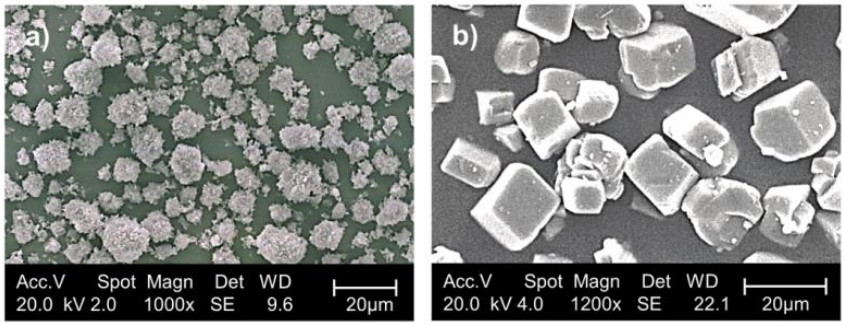

Figure 7. SEM images of (a) $CaCO_3$-A and (b) $CaCO_3$–E.

Two powder formulation batches, called formulation-I and formulation-II, were prepared and blended in triplicates using a Bohle Bin Blender mounted with a 10 L vessel. Formulation-I and formulation-II consisted of 5% (w/w) ASA, 35% (w/w) MCC and 60% (w/w) $CaCO_3$ (A or E). Blender fill level and number of revolutions were kept constant at respectively 50% and 120 for all blending runs. Flowability of the two pure $CaCO_3$ grades and the powder formulations were measured using a Schulze ring shear tester.

4.1.2 Algorithm for blending end-point detection

In order to visualize the blending profile and determine the blending end-point (homogeneity) an algorithm was developed. The algorithm is a simple and straightforward method, which use mean square successive difference test (MSSDT) applied to the obtained PCA scores.

4.1.3 Design of Experiments for blending study

The blending experiments based on formulation-I and formulation-II together with a two-factor two-level full factorial design were used to model the influences of the different $CaCO_3$ grades and the

process parameters blender fill level and number of revolutions on the blending time. $CaCO_3$ grade and fill level were chosen as experimental factors and blending time was chosen as the response for the DoE. The results were analysed with the DoE software, MODDE 10.1.

4.2.1 Materials and Roller Compaction settings

Roller compacted ribbons either pure or mixed ribbons were produced using an Alexanderwerk WP120 lab-scale roller compactor. Pure model roller compacted ribbons (PuR) were produced with microcrystalline cellulose (MCC), and mixed model roller compacted ribbons (MiXR) were produced with a powder formulation of 60% (w/w) MCC and 40% (w/w) acetylsalisylic acid (ASA), as the active pharmaceutical ingredient, API. In order to produce ribbons with porosity variation seven roll pressure (RP) conditions were analysed (2.5, 3.5, 4.5, 5.5, 6.5, 8.5, 10.5 MPa) PuRs and five RP conditions were analysed (2.5, 3.0, 4.0, 5.0, 6.0 MPa) for the MixRs.

4.2.2 Ribbon porosity measurements

The porosity, bulk density and true density of ribbon were determined using mercury intrusion porosimeter and the oil absorption method. Ribbons were weighed and subsequently placed in a petri dish containing liquid paraffin oil. The petri dish was transferred into a desiccator and the vacuum was applied. The vacuum was released and the samples were allowed to absorb oil into their internal pores. The excess of oil was removed by wiping the ribbons cautiously with a Kleenex paper. The oil saturated ribbons were weighed and the weight gain (final, volume of oil) of ribbons was used to estimate the pore volume using the oil density.

4.2.3 Ribbon porosity mapping based on NIR-CI and PCA

Two principal component analysis (PCA) models were developed for PuR and MixR, in order to gain an insight into the variation between each ribbon settings. Each score vector can be re-folded to a score surface image in order to illustrate the relative distribution map for each principal component (PC). By including the loading vectors and corresponding score surface image, it is possible to relate each PC with any variability source in the sample.

4.2.4 Ribbon porosity prediction based on NIR-CI and PLS-R

Two Partial Least Squares (PLS) regression models, based on NIR-CIs of respectively, PuR and MixR were developed to predict ribbon porosity using oil absorption method as reference method

4.3.1 Roller compaction and Design of Experiments

Experiments based on a two-factor two-level full factorial design, was used to probe the influences of two key roller compactor process parameters, roll pressure (RP) and roll speed (RS), on the properties of ribbons after roll compaction and granules after milling. The RP and RS were varied in range from 2.5 to 4.5 MPA and from 6 to 10 rpm, respectively. The critical quality attributes (CQAs) of the RC ribbons and granules were determined by six responses, termed as characteristics, including ribbon porosity, amount of fines (measured by sieve analysis and laser diffraction) and the 10%, 50% and 90% fractions of the granule size distribution. The results were analysed with the DoE software, MODDE 10.1.

4.3.2 Granule characterization

Amount of fines was measured via sieve analysis and laser diffraction. Fines were defined as granules with particles size ≤125μm and ≤138μm for sieve analysis and laser diffraction, respectively. Granule particle size was measured using laser diffraction.

4.3.3 Tablet compression

Granules from each experimental run were tableted at 358 ± 8.5 MPa using a rotary tablet press and 8 mm round flat-faced punch aiming for 320 mg tablets.

4.3.4 Tablet characterization

Tablet weight and tensile strength was measured automatized weight and tablet hardness tester.

4.3.5 Instrumentation and data acquisition

NIR spectra were recorded continuously during blending using a wireless NIRS device from NIR-Online. Spectra were recorded in diffuse reflectance mode over the wavelength range 1100-1700 nm with a resolution of 5 nm. Offline NIR-chemical images of samples were obtained with a spectrometer (Headwall Photonics model 1002A-00371,). This NIR chemical imaging camera is a prototype kindly provided by FOSS A/S. NIR-chemical images of samples were recorded in the wavelength range of 1100–1700 nm. The spectrometer was adapted to a line mapping configuration with a line of 320 pixels and pixel dimensions of 312x50 μm^2. Spectra were recorded in the diffuse reflectance mode.

4.3.6 Spectral data processing

All spectral data processing was performed by using MATLAB 7.1 software and in-house routines under the name of HYPER-Tools together with PLS Toolbox 6.5.

4.3.7 Chemometric models

A surrogate method based on NIR-and a Principal Component Analysis (PCA) model was developed to map the porosity distribution for each ribbon (section 4.2.3). NIR-CI and Partial Least Squares (PLS) regression model was developed to map and predict the pixel distribution and content of API in ribbons and tablets. A calibration-set consisting of seven homogenous powder mixtures of ASA and MCC (25, 30, 35, 40, 45, 50, 55 % w/w, of ASA) was used. In order to determine the pixel homogeneity of the distribution of a component in a sample, histograms and standard statistical values (mean, standard deviation, skewness and kurtosis) were used.

5. RESULTS AND DISCUSSION

In order to implement QbD and PAT for a pharmaceutical production line it is important to understand the process at each production stage within the production line. Using QbD and PAT approaches at each unit operation the CPPs which influence the CQAs of the material and their interaction can be understood. Monitoring and control methods can be developed and implemented to ensure constant product quality.

In this chapter the major finding of paper I-III are presented. The research presented in this thesis concerns the following unit operations; blending, roller compaction and tablet compression. For each unit operation QbD and PAT approaches have been implemented.

The first part of the results is focused on development of an algorithm based on mean square successive difference test (MSSDT) applied to NIRS and PCA scores to monitor and determine the blending profile and to statistically assess the end-point in the statistical stabile phase. A design of experiment was conducted to identify how the calcium carbonate grades and the fill level of the blender bin affect the blending end-point. For all blending experiments samples were withdrawn from each batch and investigated off-line by UV-VIS spectroscopy to determine the active pharmaceutical ingredient uniformity, thereby validating the ability of the algorithm to detect the blending end-point.

The second part of the results will deal with development of surrogate methods based on NIR-CI together with PCA and PLS-R to visualize the porosity distribution and estimate the mean porosity value of roller compacted ribbons. The model ribbons were prepared from either pure MCC or from a mixture of model API and MCC.

The last part of the results concern establishing a design space and understanding the impact of process parameters RP and RS on ribbon and granule properties through a full factorial Design of Experiments. This paper focuses also on the development and implementation of methods based on NIR-CI spectroscopy together with chemometric methods for process monitoring and control of intermediate and final product during roller compaction and tableting processes. Utilizing NIR-CI and chemometric models methods concerning, ribbon porosity, ribbon API content, relationship between ribbon NIR-CI porosity and granule size and tablet API content were developed. The final part of this chapter concerns the optimization of the optimal process setting based on tensile strength and tablet weight of the tablets produced from several batches.

5.1.1 Monitoring of blending process and detection of end-point for initial formulations using NIRS and blending algorithm

In order to access the ability of the algorithm to determine the correct blending end-point two powder formulations, compromised of different calcium carbonate grades, were investigated. Powder formulation-I and formulation-II were blended and monitored by NIRS in order to assess the ability of the algorithm in detecting the end-point (homogeneity). In all cases one PC was sufficient to explain more than 95% of the total variance. Judging from the results in Figure 8, it is clear to see that all replicates of formulation-I need ~1.5 min or ~30 revolutions to reach a steady state of the blending profile. After reaching the steady state the mean end-point for formulation-I was detected at 3.1±0.3 min where the extra time is explained by the algorithmic requirement to reach N=30 spectral recordings inside the stable zone of the profile. For comparison all replicates of formulation-II needs ~1 min or ~20 revolutions to reach steady state (Figure 9). The determined mean end-point for formulation-II is 2.0±0.0 min, which is significantly different (p = 0.02) from the mean end-point of formulation-I.

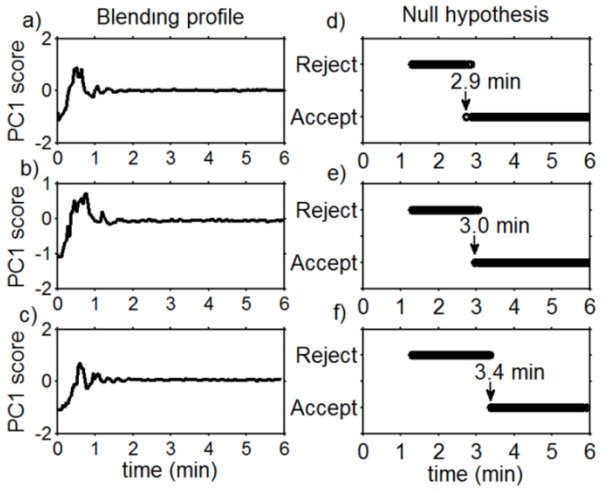

Figure 8. Blending profiles of formulation-I in triplicate. Left and right columns shows respectively, blend profile and blend uniformity end-point detection.

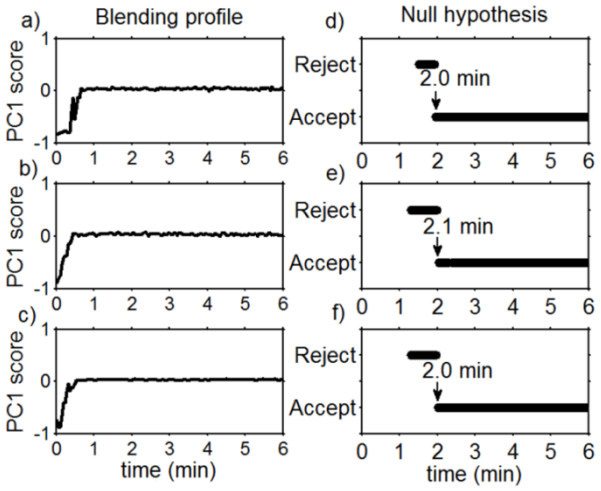

Figure 9. Blending profiles of formulation-II in triplicate. Left and right columns shows respectively, blend profile and blend uniformity end-point detection

The homogeneity of the final blends determined and quantified by UV-VIS spectroscopy. The mean API concentration for formulation-I and formulation-II were 97.5% and 98.1% with corresponding standard deviations of 2.1% and 2.3%, respectively. These results clearly demonstrate the accuracy of applying NIRS and the developed algorithm to determine the blend uniformity end-point.

A number of authors have proposed various methods based on PCA in order to monitor and estimate the blend homogeneity [81, 82, 85, 87, 88, 131]. However, none of these methods give reliable and clear end-point detection as they do not fully describing what the detection is based on. In this sense, Puchert et al. [66] proposed a new approach called ‘‘principal component score distance analysis’’ (PC-SDA). This method establishes a time window where spectral variability in the blend is lower than a preset threshold value and uses Hotelling’s T^2 statistics to monitor and report blend homogeneity. Nevertheless, Puchert et al. [66] did not only consider the process stability to detect the end-point but rather stability compared to a target spectrum. This hampers the method for real-time usage, because the method is strictly depending on knowing beforehand the spectral profile of the final blend. And this is not feasible in many occasions. The difference between already proposed methods and our method is that our algorithm considers the process stability to detect the blending end-point using mean square successive difference test (MSSDT) [132-135].

5.1.2 Flowability of pure $CaCO_3$ grades and powder formulations

To understand why different mean blending end-point are obtained between formulation-I and formulation-II the flow properties of the formulations and pure calcium carbonate grades were investigated by the ring shear tester. Figure 10 shows the flow function for pure $CaCO_3$-A, $CaCO_3$-E, formulation-I and formulation-II. The consolidation stress interval of interest in this study is between 500 to 1000 Pa, since this interval corresponds closest to the shear stress present in bin blenders of up to 20L. Using this narrowed interval, $CaCO_3$-A and $CaCO_3$-E are very cohesive and cohesive, respectively. The flowability for formulation-I and formulation-II varied, respectively, between 2.0±0.7 (very cohesive) to 2.1±0.1 (cohesive) and 3.3±0.1 (cohesive) to 4.1±0.2 (easy flowing). The main cause as to why we obtain different mean end-points for formulation-I and formulation-II may thus be due to the difference in flow properties of the $CaCO_3$ grades used. Difference in flow properties can be explained by the difference in morphology of the $CaCO_3$ particles. Equant shaped particles with a smooth surface (i.e. $CaCO_3$-E) will often have a lower frictional interaction and flow more easily compared to angular shaped particles with a rougher surface (i.e. $CaCO_3$-E), assuming all other features are identical. In addition, particles with rougher surface are more prone to morphological interaction during blending and hence prolonged the blending time compared to smooth particles [71, 75, 136].

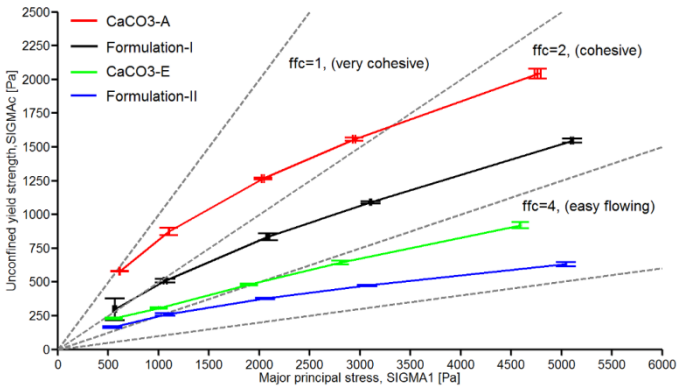

Figure 10. Flow functions of pure calcium carbonate grades and their formulations.

5.1.3 Design of Experiments for blending study

A design of experiment was conducted to identify how the calcium carbonate grades and the fill level of the blender bin, affect the blending end-point (Table 1). The blending end-point ranged for formulation-I and II from 2.64 min to 4.98 min and 1.72 to 2.69 min, respectively, as fill level increases.

Table 1. Experimental design (centre-point runs are in bold)

Run no.	$CaCO_3$	Fill level (%)	End-point (min)	ASA Concentration (%)
R1.1	A	35	2.40	98.9
R1.2	A	35	2.64	98.2
R2.1	E	35	2.02	96.7
R2.2	E	35	1.73	96.3
R3.1	A	65	4.98	96.2
R3.2	A	65	4.90	96.9
R4.1	E	65	2.10	95.3
R4.2	E	65	1.93	96.2
R5.1	**A**	**50**	**3.06**	**97.5**
R5.2	**A**	**50**	**2.95**	**97.3**

The coefficient plot (Figure 11) indicates that both $CaCO_3$-A and $CaCO_3$-E had a significant positive ($p = 0.001$) and significant negative ($p = 0.001$) effect on the blend uniformity end-point. Formulations compromised of $CaCO_3$-E reached the end-point faster compared to formulations compromised of $CaCO_3$-A, when similar process settings were used. As discussed earlier, these differences in end-point are likely due to difference in flow properties of the calcium carbonate grades. The process parameter fill level was significant positive ($p = 0.02$), indicating that fill level has an influence on the uniformity end-point. For both formulations types at highest fill level (65%) longer blending time was

needed to reach the blend uniformity end-point, respectively ~5 min for runs with $CaCO_3$-A and ~2 min for runs with $CaCO_3$-E.

A theoretical explanation as to why fill level has an influence on blend uniformity end-point may likely be found in the reduced void space in the powder bed at increased fill level. When the powder is loaded into the blender compression forces due to the weight create a static bed. During blending shear force becomes active in the blender, which dilates the material in the blender resulting in expansion of the powder bed. Bed expansion created void spaces which enhance the inter-particulate movement and promotes the blending process. Higher fill level will lead to a decreased void space in the bed and more shear force, e.g. due to longer blending time, is needed in order to archive uniformity [75]. The importance of fill level has previously been investigated e.g. by Llusa et al. [137] and Brone et al. [138]. These authors found that as the fill level in a bin blender increased, blending efficiency decreases, and additionally blending time was needed to obtain uniformity. The impact of fill level on blending efficiency was greater for shorter blending times. Brone et al [138] also reported that using blenders with baffles (as used in his study) increased the axial mixing rate and achieved homogeneity slightly faster. Both interaction-terms, $CaCO_3$-A*Fill and $CaCO_3$-E*Fill, had significant positive ($p = 0.04$) and significant negative ($p = 0.04$) effect on the blend uniformity end-point.

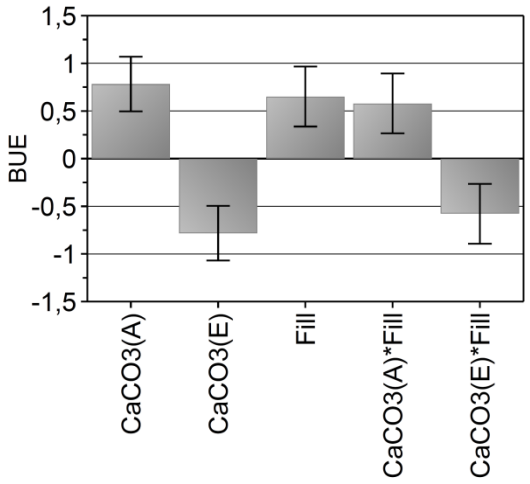

Figure 11. The Coefficient plot for the significant response (blend uniformity end-point) based on the full factorial design with $CaCO_3$ grades and blend fill level and their interactions as process variables.

For all blending experiments samples were withdrawn from each batch and investigated off-line by UV-VIS spectroscopy to determine the active pharmaceutical ingredient uniformity, thereby validating the ability of the algorithm to detect the blending end-point. The blend uniformity concentration of formulation-I and formulation-II runs ranged, respectively, from 96.6 to 98.5 % API and 95.8 to 96.5 % API. These results clearly demonstrate the potential of applying NIR and the developed algorithm to determine the blend uniformity end-point.

5.2.1 Ribbon porosity measurements

The average porosity of pure ribbons (PuRs) was determined by oil absorption methods (OAM) and mercury intrusion method (MIM). The average porosity of ribbons from different roller compaction settings ranged from 12.1 to 26.4, (%) porosity. A decrease in ribbon porosity was observed as the RP increases. In order to assess the accuracy of the OAM, the porosity results were correlated with the porosity results obtained by MIM by a simple linear regression model. The R-square (R^2=0.98) and the Root Mean Square Error (RMSE) values indicates a good correlation.

5.2.2 Ribbon porosity mapping based on NIR-CI and PCA

Figure 12a, represents the NIR spectra of pure ASA, MCC and a mixture of ASA:MCC (50:50). The NIR spectra are sensitive to porosity variation for both PuR and MiXR, respectively Figure 12b and Figure 12c. As compression force increases, ribbon gets denser and porosity decreases due to a decrease in the air–particle boundary surface and thereby diffuse scattering decreases and ultimately, less light will reach the detector [139]. Which results to an apparently higher absorbance, especially at longer wavelengths [128, 139]. These findings are consistent with the literature, where e.g. Kirsch and Drennen [140] observed upward baseline shifts when using single point NIRS as the tablet compaction pressure increased. This effect can be used to study the porosity phenomena in ribbons.

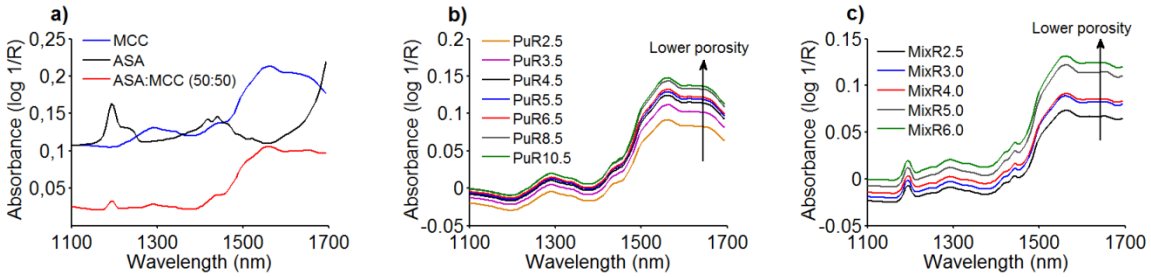

Figure 12. Pure NIR-spectrum of microcrystalline cellulose (MCC) and acetylsalicylic acid (ASA) powder, b) and c) Spectra of roller compacted ribbons of respectively pure and mixed ribbon. For both ribbon formulation an upward spectral shift is seen due to higher roll pressure

Two individual Principal Component Analysis (PCA) models were used for identifying the main variation within NIR-CIs of PuRs and MixRs in the spectral range from 1100-1700 nm. The PC1 for PCA-model-PuR explained 96.3%, of the variation. In order to explain the variation captured by the PCA model one should investigate the score surfaces image (Figure 13a) and corresponding loading (Figure 13b). For every pixel (spectra) a score value is obtained, which is the weight of its corresponding loading present in the pixel. The PC1 loading is highly correlated to the pure spectrum of MCC, shown in Figure 12a. An upward shift can be observed for the loading at longer wavelengths (1650-1700nm). The variation captured by the first principal component can be related to the physical variation (porosity variation), since there is no chemical variation in PuRs. This is evident from the score surface image, as depicted in Figure 13a, and less porous ribbons tend to have regions with higher score values, which relate to less porous regions.

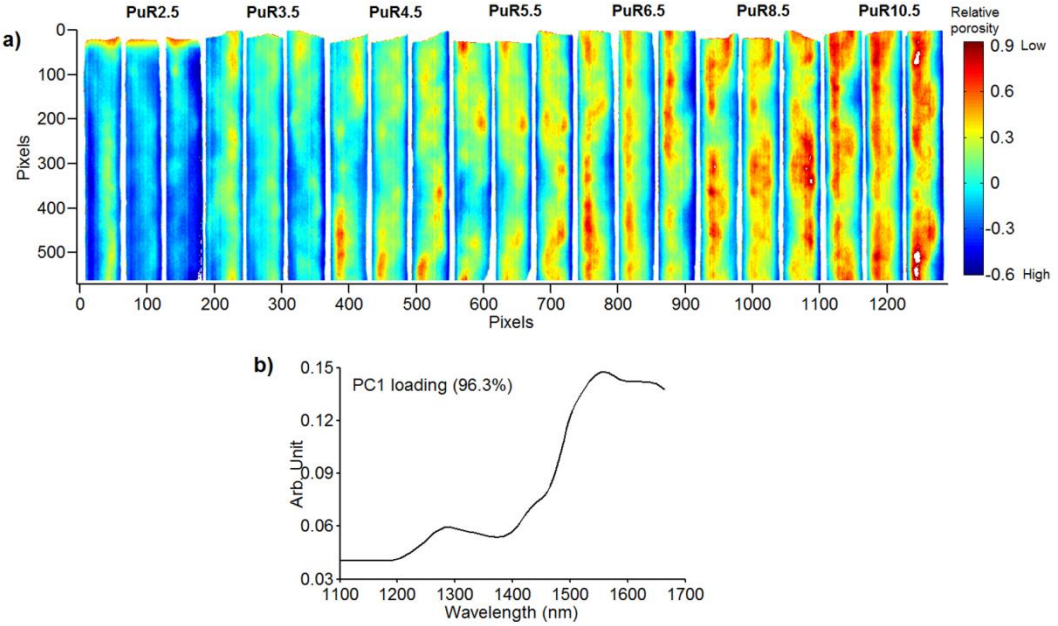

Figure 13. a) and b), represents, respectively, the score surface image and loading plot of the first principal component PC1 of pure MCC ribbons compacted at different pressures. Dark red colour indicates higher score values, were dark blue colour indicates low score values. Width and length of the ribbons approx. 35 and 140 mm, respectively.

The score surfaces image and loading of PC1 for PCA-model-MixR is depicted in Figure 14a, and Figure 14b, respectively. The PC1 explained 95.1%, of the variation and is highly correlated to the average spectrum of MCC and ASA. The variation obtained by the PC1 loading is mainly due to baseline shift caused by physical variation (porosity variation). By looking into the score surface image ribbons compacted at higher pressure tend to have narrow regions associated with higher score values, which can correspond to less porous regions. The score surface image and loading of PC2, depicted in Figure 14c and Figure 14d respectively. The PC2 loading explained 3.7%, of the variation and pattern of this loading is very similar to the pure ASA spectrum. It can be assumed that the score image in Figure 14c, provide the ASA distribution information. The score surfaces image and loading of PC3 is depicted in Figure 14e and Figure 14f, respectively. The features from 1200 to 1380nm in the PC3 loading could be related to the MCC content, since the pure MCC spectrum has similar absorption region. However, care should be taken since the explained variation is 1.1%.

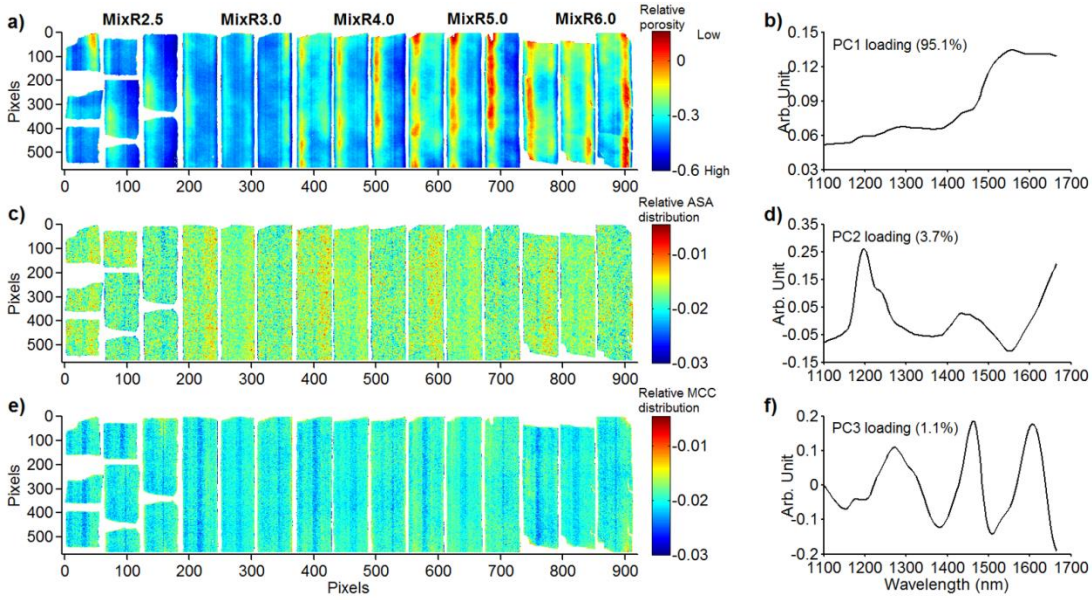

Figure 14. a,c,e) and b,d,f), represents, respectively, the score surface images and loading plots of the first, second and third principal components of the mixed ribbons compacted at different pressures. Dark red colour indicates higher score values, were dark blue colour indicates low score values. Width and length of the ribbons approx. 35 and 140 mm, respectively.

The score surface image demonstrated in Figure 13a and Figure 14a, shows heterogeneous porosity regions within each roller compacted ribbon. Roller compacted ribbons produced at higher compression pressure (less porosity) are associated with higher heterogeneity. Guigon *et al*. found that the feed screw results in heterogeneous porosity distribution along the roller-compacted ribbons caused by non-continuous densification feeding process. [102]. Based on our results, the non-continuous densification feeding process may be amplified at higher compaction pressures.

5.2.3 Ribbon porosity prediction based on NIR-CI and PLS-R

In order to evaluate the feasibility of the application of NIR-CI for the prediction of ribbon porosity for PuRs and MixRs, two PLS-models, respectively, PLS-model-PuR and PLS-model-MixR were developed and evaluated. NIR-CIs were used as the X-variables and single point porosity values (determined by the OAM), were used as the y variable. The correct number of latent variables (LVs) of the PLS models were assessed by The Root Mean Square Error of Calibration (RMSEC) and cross-validation (RMSECV), indicating the fit between NIR spectra and porosity values. Cross-validation was done by full cross-validation and the Root Mean Square Error of Cross Validation (RMSECV) was calculated.

The PLS-model-PuR resulted in two latent variables (Lvs), explaining 99.6% of the variation (Fig. 5a). The calibration and prediction error for this model are each small (R^2=0.98, RMSEC = 0.42%, RMSECV= 0.55%).

The PLS-model-MixR resulted in two sufficient LVs, explaining 99.8% of the variation. The calibration- and prediction error for this model are each small (R^2=0.98, RMSEC = 0.46%, RMSECV= 0.64%). In order to test the reliability of each PLS-model, two independent test sets of smaller ribbon sections (n=23) were used (one for each PLS-model). Each ribbon within the test-sets was measured by NIR-CI and the porosity result was predicted by the corresponding PLS-model, and plotted against the single point porosity measured by OAM via simple linear regression model.

Two prediction curves for respectively PuR and MixR, Figure 15 a and b, are obtained with strong correlation of R^2=0.96 for both curves. Therefore NIR-CI is able to characterize differences in porosity as a function of position on the ribbon and predict the porosity of the roller compacted ribbon.

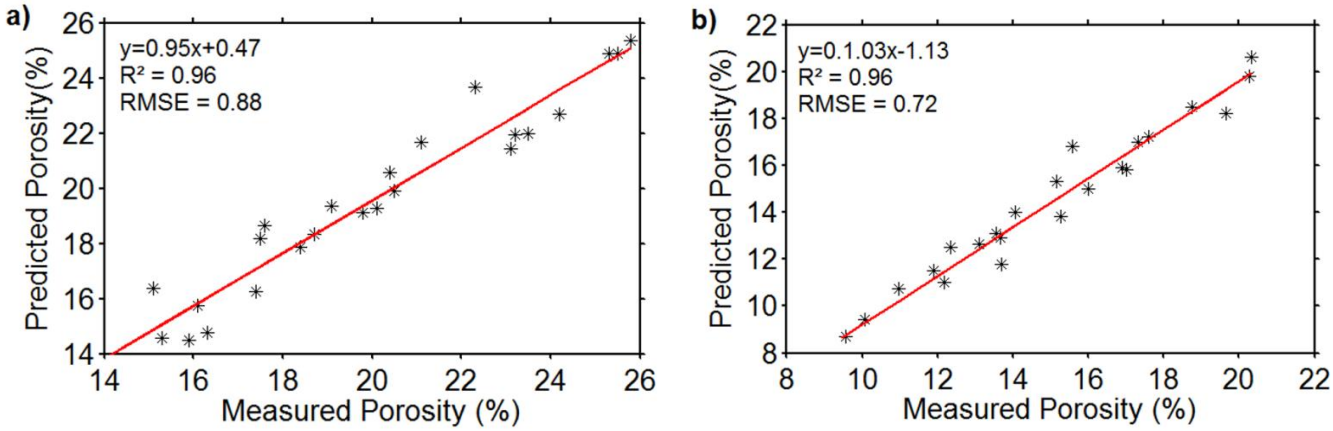

Figure 15. a) and b) Correlation of the predicted porosity and the lab measured porosity (oil absorption method) for respectively, pure ribbons and mixed ribbons.

In a previous study by Lim. et al. [116] the porosity of single component ribbons has been investigated using NIR-CI. They authors related the mean spectral absorbance at a single wavelength for different ribbons with their measured reference porosity values. Generally when working with NIR images, it is crucial to ensure that the measured signal is not influenced by other sources of variation. Hence, only the spectral information related to the component of interest should be correlated with the information from the component. If other sources of variation contribute to the signal, the results will be biased and it might be challenging to detect possible incorrect results. Also, when working with samples containing more than one ingredient, the NIR spectra are composed of broad and highly overlapped bands, which make it more difficult to find distinct and selective absorption bands for each ingredient

in the sample. These limitations are overcome by applying a multivariate data analysis approach (e.g. PCA), which is able to use the entire spectral profile to extract the useful information from the whole data set [62, 126, 141-144].

An alternative way of measuring ribbon porosity has recently been proposed by Souihi et al [145]. In their study, the authors used a roller compacter equipped with an instrumented roll technology allowing the measurement of normal stress (roll pressure) on ribbon using three sensors across the roll width. Normal Stress recorded from the middle sensor was used for data analysis and it was found to vary directly with roll pressure and inversely with the ratio of screw speed to roll speed. Ribbon porosity was found to mainly be a function of normal stress (or roll pressure) as a quadratic relationship between the normal stress and ribbon porosity. Using only the middle region of the ribbon to determine ribbon porosity may be biased as the feed screw often will result in heterogeneous porosity distribution along the roller-compacted ribbons due to non-continuous densification feeding process [102]. As demonstrated in our study and other studies the ribbon porosity is lower in the middle region compared to edges of the ribbon [98, 102, 116]. Therefore, measuring and using only the middle region to determine ribbon porosity will not provide the overall ribbon porosity as it does by e.g. using NIR-CI.

5.3.1 Roller compaction and Design of Experiments

The measured characteristics of the ribbons and milled granules from the full factorial design are presented in Table 2. The effects of each process variable, RS and RP, on each response (model) are shown in the coefficient plots in Figure 16. These will be discussed in turn in the following sections.

Table 2. Summary of the design experiments (means, ±SD, n=3).

Run ID	Porosity [%]	Fines $_{sieve}$ (≤125 µm) [%]	Fines $_{LD}$ (≤138 µm) [%]	$d_{0.1\ LD}$ [µm]	$d_{0.5\ LD}$ [µm]	$d_{0.9\ LD}$ [µm]
R1	25.9 ± 0.7	23.4 ± 0.5	63.5 ± 0.6	8.6 ± 0.3	96.5 ± 2.2	293.8 ± 20.2
R4	22.2 ± 0.9	20.8 ± 0.6	56.8 ± 0.6	8.1 ± 0.3	115.6 ± 1.8	518.5 ± 33.8
R2	18.9 ± 0.7	18.9 ± 1.0	54.1 ± 1.6	8.7 ± 0.3	125.6 ± 2.4	613.3 ± 32.1
R3	17.1 ± 1.1	17.3 ± 0.3	53.5 ± 0.5	8.5 ± 0.2	127.0 ± 1.2	706.8 ± 34.0
R5	14.1 ± 0.7	13.2 ± 0.7	42.8 ± 1.2	9.3 ± 0.5	177.1 ± 7.3	951.0 ± 14.5

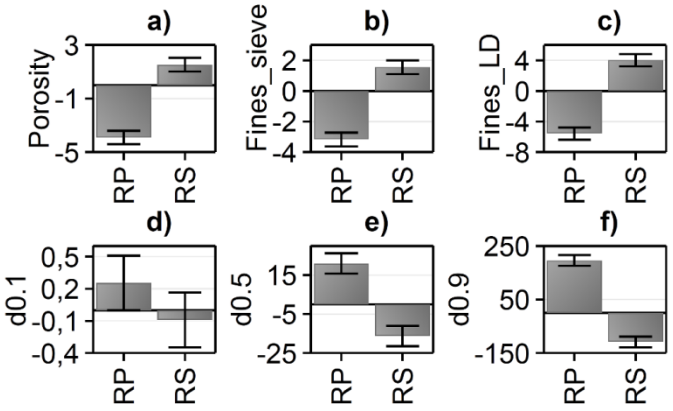

Figure 16. Coefficient plot for the significant responses based on the full factorial design with RP and RS as process variables.

5.3.2 Ribbon characteristic

Ribbon porosity ranged from 14.1 to 25.9 % for the five batches of ribbon (Table 2). The coefficient plot (Figure 16a) indicates that RP affects the ribbon porosity, where higher RP leads to lower porosity (p-value = $5x10^{-9}$), and higher RS leads to higher ribbon porosity with p-value = $5x10^{-5}$. The conditions for producing ribbons with lowest (14.1%) and highest (25.9%) mean porosity were RP/RS = 4.5 MPa/6 rpm and 2.5 MPa/10 rpm, respectively. The mean porosity decreases as the RP increases from 2.5 to 4.5 MPa and RS decreases from 10 to 6 rpm. Higher RP leads to more powder consolidation and thereby lower ribbons porosity. Under a constant powder feeding rate and roll gap, faster RS produces mechanically weaker ribbons with higher mean porosity. These findings are in accordance with the literature [95, 97, 104, 116].

5.3.3 Granule characteristics

The amounts of fines were determined based on results from sieve analysis and laser diffraction. The amount of fines ranged respectively from 13.2 to 23.4 % by weight and from 42.8 to 63.5 % by volume. The effect of RP on the amount of fines measured by sieve analysis is significantly negative while that of RS is positive (Figure 16b), with p-values $4x10^{-9}$ and $5x10^{-5}$, respectively. Similar effects were observed based on fines % measured by laser diffraction (Figure 16c). A high R^2 (0.96) was found between sieve analysis and laser diffraction results. The particle size diameters measured by laser diffraction ranged from 8.1 to 9.3 µm for $d_{0.1}$, 95.6 to 177.3 µm for $d_{0.5}$ and 293.8 to 951.0 µm for $d_{0.9}$. The coefficient plot (Figure 16d) indicates that RP had respectively significant positive (p = 0.009)

effect on $d_{0.1}$. Both RP and RS had a respectively significant positive ($p = 6x10^{-10}$, $4x10^{-10}$, $8x10^{-7}$) and significant negative ($p = 10x10^{-9}$, $2x10^{-7}$, 0.003) effect on respectively, $d_{0.5}$, and $d_{0.9}$ (Figure 16e-f). Based on the DoE it is clear that RP and RS had a huge influence on the ribbon and granule characteristics. The combination of higher RP and lower RS leads to stronger ribbons with lower porosity, larger granule size, less fines and broader granule size distribution. These findings are in accordance with the literature, [108, 113, 115, 146]. All models except $d_{0.1}$ could be considered as good models as they meet all acceptance criteria, (Table 3).

Table 3. Assessment of the responses (models) according to the acceptance criteria

Model	R^2 - Q^2 < [0.2 - 0.3]	Q^2 > 0.5	Model validity > 0.25	Reproducibility > 0.5	Description
Porosity	0.03	0.94	0.51	0.96	Accepted
Fines $_{sieve}$	0.02	0.95	0.93	0.96	Accepted
Fines $_{LD}$	0.02	0.96	0.98	0.98	Accepted
$d_{0.1\ LD}$	0.3	0.38	0.94	0.57	Rejected
$d_{0.5\ LD}$	0.02	0.96	0.64	0.98	Accepted
$d_{0.9\ LD}$	0.06	0.92	0.96	0.97	Accepted

5.3.4 Ribbon porosity map based on NIR-CI and PCA

PCA was used for identifying the main variation within NIR-CIs of the ribbons in the spectral range of 1100-1700 nm. The first PC loading explained 92.5% of the variation. The pattern of this loading plot was similar to the averaged spectra of the ASA:MCC (50:50) mixture (Figure 17a). This indicates that the main variation captured could be attributed to intensity (absorbance) of the spectra, which in turn affected by the porosity variation. The NIR spectra are sensitive to porosity variation, with lower porosity (higher density) ribbons having a higher apparent slope and more baseline shift [128, 140]. Therefore, the established PCA model can be used as surrogate method for estimation of surface porosity distribution**.** This was also demonstrated in previous section (5.2.2). From (Figure 17b) it is evident that ribbons with lower porosity (measured by oil method) have higher score values. Figure 17b also shows heterogeneous score value distribution (porosity distribution) within each roller compacted ribbon, an effect that is more pronounced for ribbons with lower porosity.

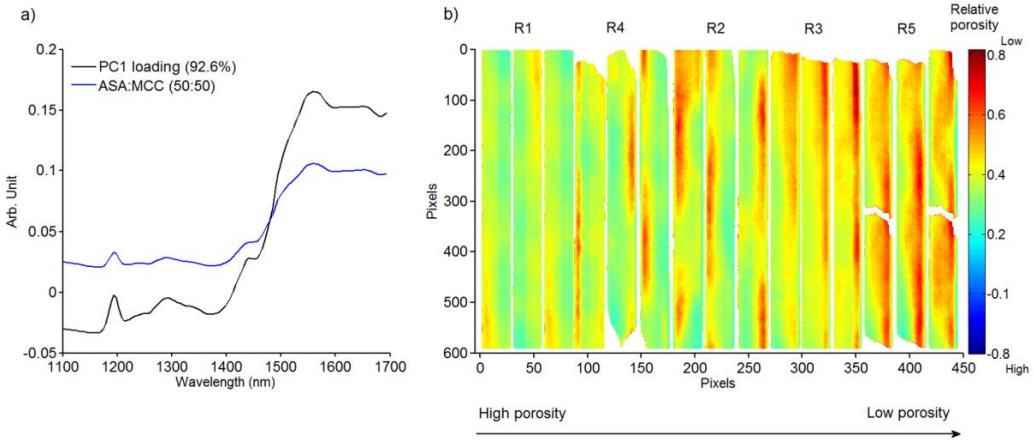

Figure 17. a) Loading plot of PC1 and the average NIR spectrum of 50:50 ASA:MCC powder mixture. b) The PC1 score surface image of roller compacted ribbons (n=3) with varying porosity. Replicated samples are placed side by side. Dark red colour indicates higher score values (lower relative prosotiy), were dark blue colour indicates low score values (higher relative porosity). Width and length of the ribbons approx. 35 and 140 mm, respectively.

5.3.5 Ribbon chemical map based on NIR-CI and PLS-R

Spectra extracted from NIR-CIs of ribbons were used as the X matrix and the nominal API concentration of the powder mixtures (calibration-set) were used as the y vector. The correct number of latent variables (LVs) of the PLS-R model was assessed by The Root Mean Square Error of Calibration (RMSEC) and cross-validation (RMSECV), indicating the fit between NIR spectra and API concentration values. Cross-validation was done by full cross-validation. The PLS-R model resulted in two latent variables (Lvs), explaining 98.3% of the variation. The calibration and cross-validation error for this model were relatively small (RMSEC = 1.1 %, RMSECV= 1.6%), (Figure 18).

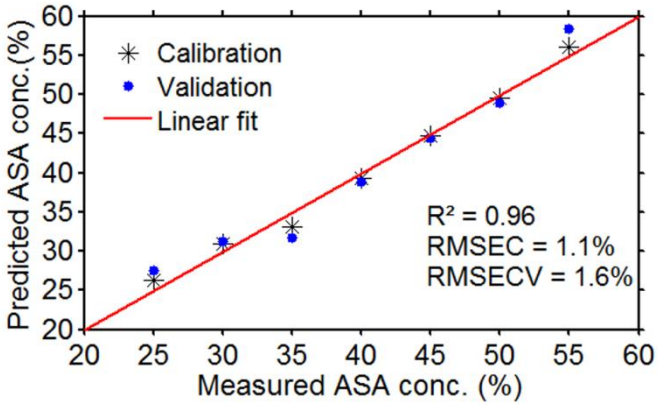

Figure 18. PLS-model for prediction of API content.

The API quantification was performed by applying the quantitative PLS-R model to the complete NIR-CI of the ribbons. The pixel distribution map (API distribution map) of all ribbons in the image are shown in (Figure 19). The concentration values for individual ribbon settings shown in (Figure 20) yielded mean API concentration ranging from 37.7 to 40.5 relative API (%) concentrations, which suggests the mean predicted API concentration values of the five ribbon settings are close to the nominal 40% (w/w) API concentration in the initial powder blend. However, the predicted API concentration is seen to decrease with decreasing mean ribbon porosity. The homogeneity of the distribution of API in the ribbons was assessed from the chemical images histogram. The histogram of all ribbon settings spans over a narrow range of API concentration values with relatively small standard variation values, ranging from 0.2 to 0.5, (Figure 20). The kurtosis and skewness values ranged 3.8 - 4.1 and -0.2 - 0.7, respectively. For ribbon setting R4, kurtosis and skewness values are very close to normal distribution. The small kurtosis and skewness value means that the API is homogenously distributed, at least at the ribbon surfaces. This is in contract to the relatively non-homogeneous density distribution in these ribbons.

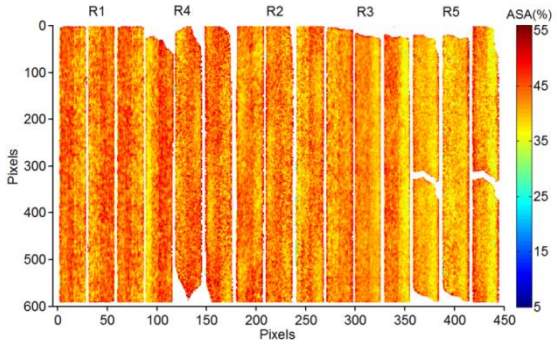

Figure 19. Predicted API concentration distribution map for ribbons (n=3) by the PLS-R model. Width and length of the ribbons approx. 35 and 140 mm, respectively

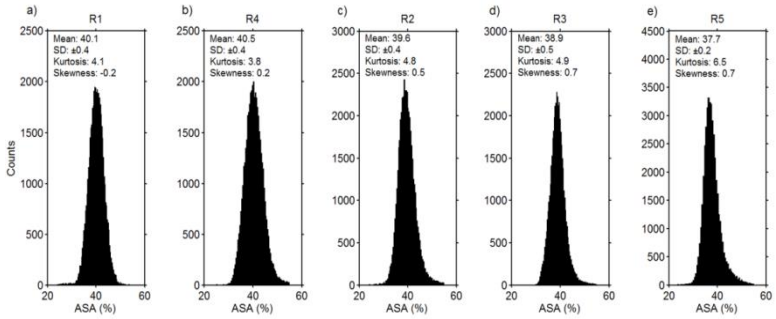

Figure 20. a-e) Mean API concentration histograms of the different ribbon settings (n=3).

5.3.6 Relationship between ribbon NIR-CI porosity distribution and granule size distribution

Each pixel in the score image contains a score value, which can be related to a porosity value per the PCA model. Again, histograms were used to study the NIR-CI score value distribution (porosity distribution), of each ribbon setting. Further, the 10%, 50% and 90% fractions (f0.1, f0.5, f0.9) PC1 score distribution was calculated for each distribution. The NIR-CI score value distribution (surrogate

estimation of porosity distribution) of each ribbon setting was compared to its corresponding average granule size distribution measured by laser diffraction (Figure 21). As the ribbon porosity decreases (score values increases) shown in Figure 21 a-e, all granule particle fractions; $d_{0.1}$ (8.3 to 9.3 µm), $d_{0.5}$ (95.6 to 177.3 µm) and $f_{0.9}$ (293.8 to 951.5 µm), shown in Figure 21 f-j. Linear correlations were established between porosity and granule size fractions. The correlation values (R^2) of the linear fitting are 0.02, 0.88 and 0.96 respectively for 10%, 50% and 90% fractions (Figure 22a-c). This trend is consistent with the observed relationship that lower ribbon porosity leads to larger granules in previous section. However, the trend with the $d_{0.1}$ fraction is not clear, which indicates a limitation of the NIR-CI prediction.

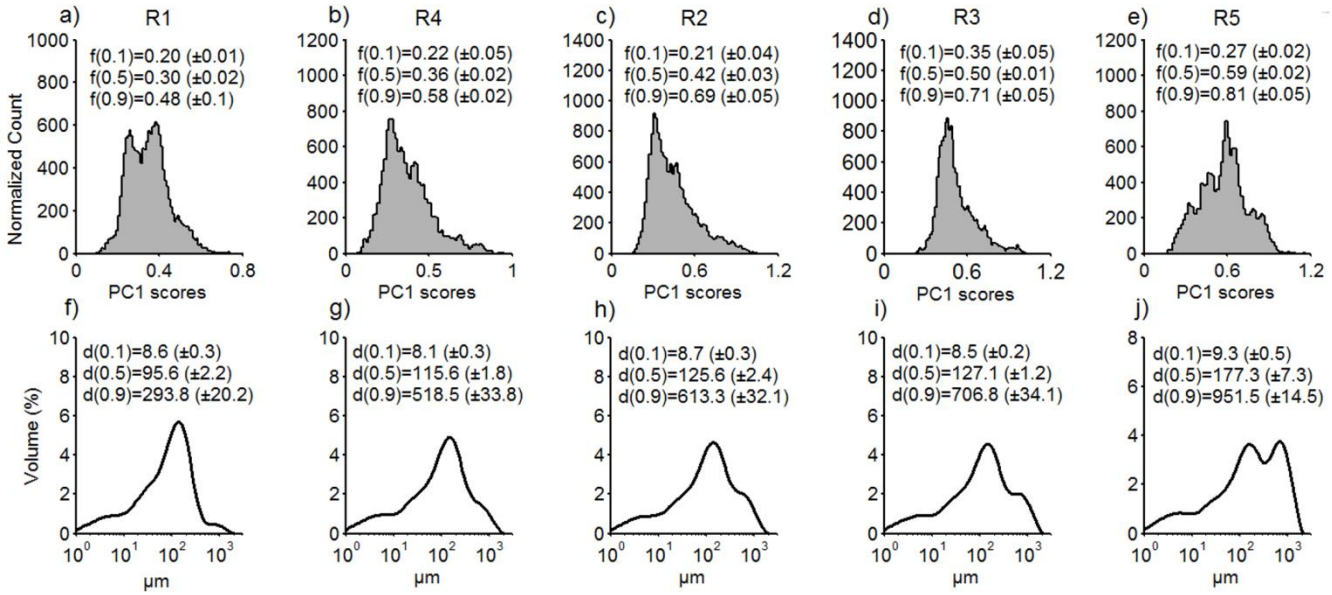

Figure 21. a-e) represents, respectively, PC1 score distribution of each ribbon setting and f-i), granule size distribution of corresponding ribbon settings.

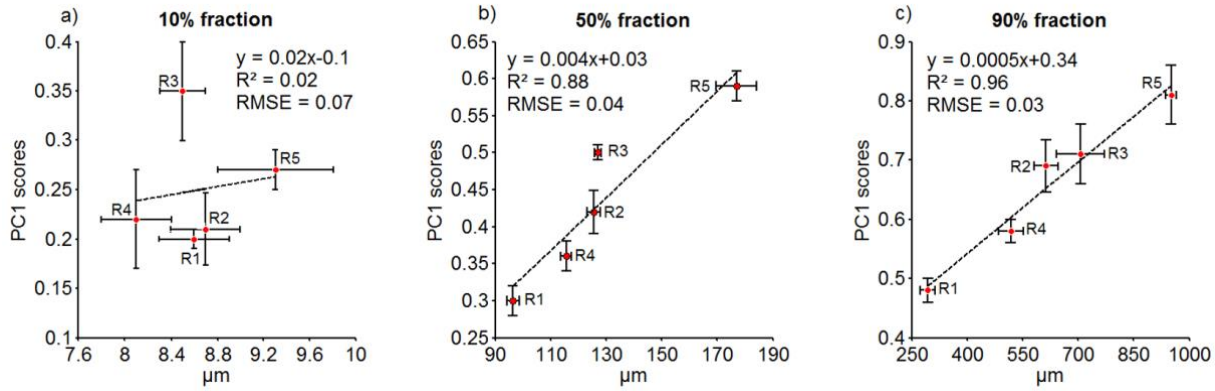

Figure 22. a-c), represents, respectively, the correlation between the 10, 50 and 90% fraction of the PC1 score values of ribbons with the corresponding granule size distribution.

5.3.7 Tablet characteristics

Tablets produced based on these different granule batches (R1 to R5) were named “tablet run” (TR) followed by the run setting number. The tablet tensile strength (TTS) for compacted tablets varied from 0.9 to 1.3 MPa, (Table 4). Figure 23a, shows a strong correlation R^2 = 0.97) between TSS and granule median size ($d_{0.5}$). Granules with larger median size revealed tablets with lower TTS, due to work-hardening and reduced surface area for bonding. These findings are in accordance with the literature [110, 118, 119]. Additionally, strong correlations $R^2_{\text{sieve analysis}}$ = 0.97 and $R^2_{\text{laser diffraction}}$ = 0.98 were also obtained between TTS and amount of fines measured by two different methods, shown in respectively Figure 23b and Figure 23c.

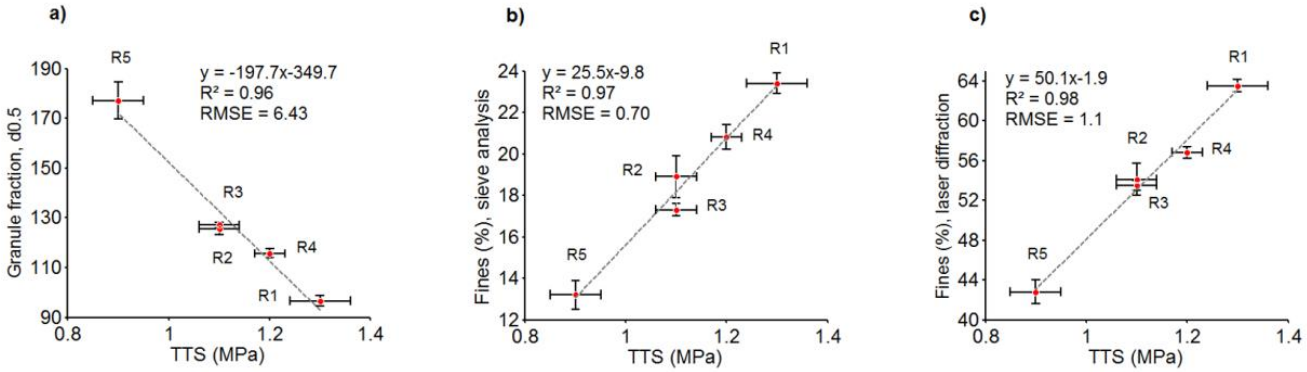

Figure 23. Linear correlation between tablet tensile strength and respectively median granule size, a), fines measured by sieve analysis, b) and fines measured by laser diffraction c) , (n=3).

The weight of tablets varied between 318.1 to 319.4 mg (Table 4) and all measured tablets complied with the mass uniformity requirement of single-dose preparation test from European Pharmacopoeia [147]. Previous studies have shown that tablet weight uniformity is mainly affected by several factors, such as tableting speed, tooling size, level of powder in the hopper (head pressure), particle size, density (porosity) and powder flow on the tablet press [148].

Table 4. Tablet tensile strength (TTS) and tablet weight (TW) made from granules (means, ± SD, n=20).

Run	TTS [MPa]	TW [mg]
TR1	1.3 ± 0.06	319.3 ± 2.9
TR4	1.2 ± 0.03	319.4 ± 1.2
TR2	1.1 ± 0.04	318.1 ± 1.9
TR3	1.1 ± 0.04	318.8 ± 2.1
TR5	0.9 ± 0.05	318.4 ± 2.2

5.3.8 Tablet chemical map based on NIR-CI and PLS-R

Using NIR-CI together with appropriate chemometric model is a fast and reliable approach to determine the surface chemical distribution [142, 143, 149]. The surface API content and distribution of tablet for each process setting was predicted using NIR-CI and the quantitative PLS-R model, described in previous section (3.3). The pixel distribution map (API distribution map) of all tablets in the image is shown in (Figure 24). The API content of these tablets varied between 39.2 to 39.6% (Figure 25), which is close to the nominal API content of 40%. Based on an analysis of variance (ANOVA) no significant ($p = 0.91$) differences were obtained between the different tablet batches.

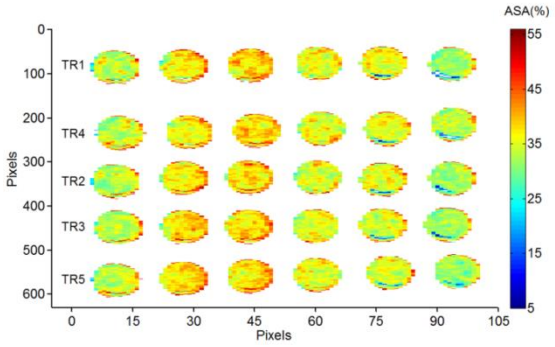

Figure 24. API distribution map of tablets (n=6) predicted by PLS-R model.

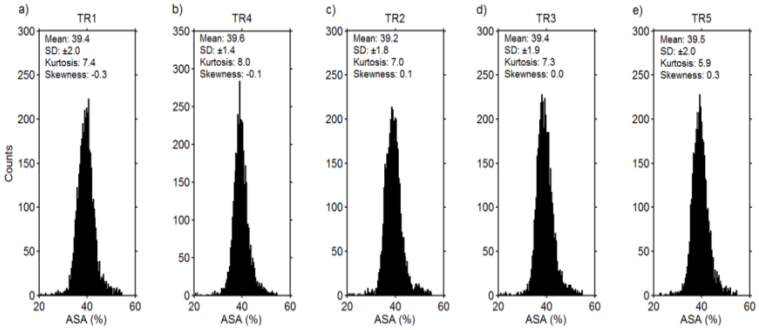

Figure 25. Mean API concentration histograms of the different tablets (n=6). For each histogram mean concentration, standard deviation, kurtosis and skewness are presented

However, the SD values among these tablets are significantly different, ranging from 1.4 to 2.0, (Figure 25). Higher SD values are an indication of less homogeneous API distribution. The kurtosis and skewness values ranged from 5.9 to 8.0 and -0.1 to 0.3, respectively. Higher kurtosis and skewness values, indicates, respectively, broadening of the peaks and tailing towards higher API concentration values. Since Run 4 with the process settings of RP (2.5 MPa) and RS (6 rpm) is the optimum because it results in tablets (TR4) with lowest SD for tensile strength and weight, this settings is chosen as the optimal process setting despite it yields the second highest amount of fines and second smallest granule.

6. CONCLUSIONS

Quality by Design approaches such as Risk assessment (RA), Design of Experiments (DoE) and Process analytical technology (PAT) tools were applied for a pharmaceutical production line consisting of blending, roller compaction and tableting. Using RA and DoE it was possible to identify the critical quality attributes and critical process parameters of each unit operation. Utilizing DoE it was possible to understand the influences of CPPs on CQAs and their interactions and indeed statistical predictive cause-effect relationships between CPPs and CQAs were developed. Developing and implementation analytical methods for each unit operation it was possible to monitor and asses the current CQAs. Analytical methods based on Near-Infrared Spectroscopy, Near-Infrared Chemical Imaging, mean squares successive difference test, Principal Component Analysis and Partial Least Squares regression was used. Applying abovementioned QbD approaches a more comprehensive process understanding was archived which will a huge advantage in order to shift from batch to continuous processing.

Initially, an algorithm based on mean squares successive difference test applied to Near-Infrared Spectroscopy data and Principal Component Analysis scores was developed to monitor and determine the blending profile and to statistically assess the end-point in the statistical stabile phase. Two powder formulation batches, formulation-I and formulation-II, with different grade of $CaCO_3$, were weighted and blended in a bin blender. Based on the ring shear test results, formulation-II had better flow properties compared to formulation-I, caused by a difference of the $CaCO_3$ shapes. In order to determine the blend uniformity end-point of the powder formulations, the developed algorithm was applied. Formulation-II with higher flowability reached blend uniformity end-point faster compared to formulation-I with lower flowability. Additionally, a design of experiment was conducted to identify how the calcium carbonate grades and fill level affect the blending end-point. The DoE revealed that calcium carbonate grades and the fill level have a significant influence on bend uniformity end-point. This study indicates that Near-Infrared spectroscopy together with the developed algorithm and ring shear are powerful tools to determine blend end-point and knowledge about the degree of powder flowability.

Next, the physical properties of roller compacted ribbons with varying porosity were visualized using near-infrared chemical imaging. Further, it was also demonstrated that the use of oil absorption method for measuring the ribbon porosity is a robust and safe alternative reference technique as compared to the mercury intrusion method. Finally, it was demonstrated that Near-Infrared Chemical

Imaging in combination with multivariate data analysis can be used as a non-destructive tool to visualize the porosity distribution and determine porosity values of pure and mixed ribbons.

Finally, the effects of roll pressure (RP) and roll speed (RS) on the ribbon porosity, granule properties, and tableting performance were investigated. A surrogate method based on Near-Infrared Chemical Imaging (NIR-CI) and Principal Component Analysis (PCA) was used to map the ribbon porosity distribution. The ribbon porosity distribution gained from the PCA based NIR-CI was used to develop quantitative/predictive models for granule size fractions. Partial least squares regression was used to visualize and predict the API distribution and content for both roller compacted ribbons and corresponding tablets. Higher RP and lower RS led to ribbons with lower porosity, larger granules with lower amount of fines, and tablets with lower tensile strengths. It was demonstrated that NIR-CI together with chemometric models can be utilized, as a non-destructive tool, to monitor roller compaction to deliver granules exhibiting robust tableting performance.

These analytical methods presented in the current work have the potential to be implemented as a quality control tools for the continuously operating manufacturing lines, involving blending, roller compaction and tableting.

7. PERSPECTIVES

At this stage of time, process analytical technology tools may be applied to single unit operations included in batch processing, where it is used for substituting part of the costly and labour intensive off-line laboratory testing of product quality. However, many pharmaceutical industries are moving slowly towards more use of spectroscopic Process analytical technology (PAT) tools for raw material and process control, as well as designing with quality in mind. Implementation of Quality by Design (QbD) and PAT will continue to improve the way risk is approached and it will increase the understanding and control of the manufacturing processes. It will increase product quality and help the pharmaceutical industry to reduce development and manufacturing cycle times and costs in the process. QbD & PAT may, possibly in combination with other tools, e.g. Lean and Six Sigma, be the prospective leading tool for developing, manufacturing and controlling the pharmaceutical products. Successful adaption will be to the benefits of us all.

There is also an increased trend of shifting from batch to continuous or, at least semi-continuous processing. Continuous manufacturing (CM) is defines as a process without interruption over a sustained period of time. As an example, GSK has demonstrated significant reduction in scale-up time and cost during development by switching from batch to continuous granulation [38]. Another example is the collaboration between a university and a pharmaceutical industry where they managed to establish an end-to-end continuous manufacturing line consisting of the primary and secondary manufacturing steps in order to produce solid dosage forms [150].

Therefore, there is an increased need for real-time process monitoring and control, to ensure acceptable product quality. Indeed, PAT and QbD will be appropriate and necessary tools to achieve this. Figure 26 demonstrates a continuous manufacturing line for the secondary manufacturing part where QbD and PAT are applied. Using risk management and Design of Experiments it is possible to establish design space for each unit operation or the overall process. Once the design space is established and the statistical predictive cause-effect models between critical process parameters (CPPs) and critical quality attributes (CQAs) are obtained PAT analyzers can be implemented. Utilizing the state-of-art PAT analyzers for in-line process monitoring and using the statistical predictive cause-effect relationship models developed from the DoE, it is possible to implement control and feed-back-loops in order to achieve an automatized process.

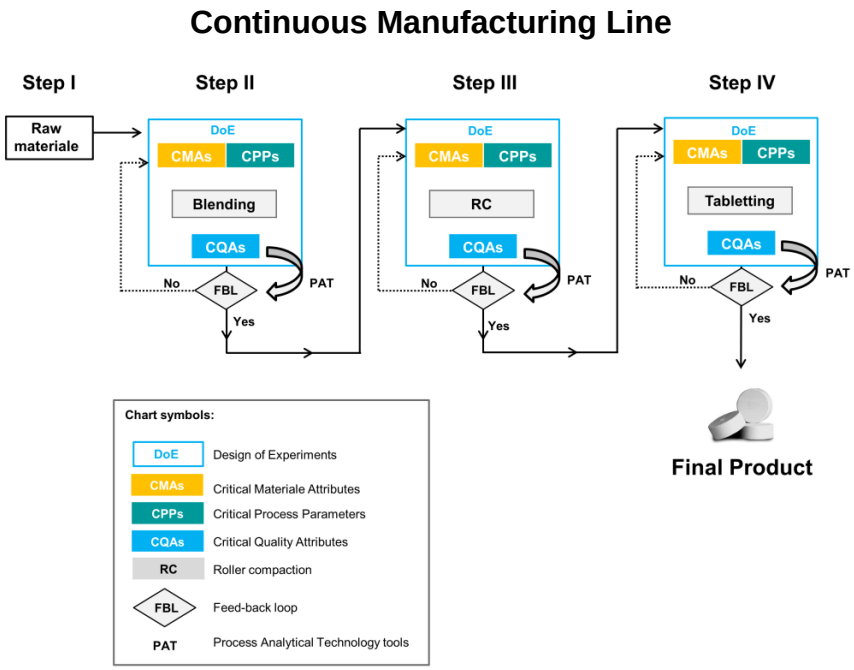

Figure 26. Schematic overview of a continuous manufacturing line

The most applied PAT tools are NIRS and NIR-CI. Nevertheless, NIRS is a single point spectroscopic technique and e.g. patterns of homogeneity are not usually reflected in such measurements, because a bulk NIR spectrum represents an average composition of the measured sample. Therefore, the most advantageous tool to implement will be the NIR-CI. Future improvements in precision and speed in NIR-CI are likely to arise with increased computer processing speeds, improved cameras, faster hardware, more accurate and efficient algorithms. Further applications could be merging with other PAT tool e.g. Terahertz or Raman spectroscopy. In order to reduce data load and increase processing speed in chemical imaging innovative spectrometer have to be designed and developed. An exciting technique, known as Integrated Chemical Imaging is able to reduce the data load and increase processing speed by enabling the sensing detector to do some of the data analysis [151].

Adoption of CM in QbD context in the pharmaceutical industry requires interdisciplinary expertise and cross-functional collaboration in areas such as upper management, regulatory, supply-chain, drug formulation, analytical chemistry, chemometrics, process engineering, process automation and manufacturing. In addition more collaboration between academia/universities, pharmaceutical

industries and regulatory bodies should be established in order to overcome barriers the pharmaceutical industry and regulatory will face when CM is implemented.

8. REFECENCES

[1] A. Mullard 2015. 2014 FDA drug approvals. Nat Rev Drug Discov 14:77-81.

[2] Pwc 2012. From vision to decision Pharma 2020.
http://www.pwc.com/pharma2020. Acessed on March 2015.

[3] J. A. DiMasi, H. G. Grabowski 2007. The cost of biopharmaceutical R&D: is biotech different?
MDE Manage Decis Econ 28:469-479.

[4] D. W. Light, R. Warburton 2011. Demythologizing the high costs of pharmaceutical research. BioSocieties 6:34-50.

[5] M. Herper 2012. The Truly Staggering Cost of Inventing New Drugs. Forbes.
http://www.forbes.com/forbes/2012/0312/strategies-pharmaceuticals-lilly-stagger-cost-inventing-new-drugs.html. Acessed on March 2015.

[6] R. Mullin 2011. Paying Attention to Manufacturing. Chem Eng News 89:18-22.

[7] B. Wang, J.J. Gagne, N.K. Choudhry 2012. The epidemiology of drug recalls in the United States. Arch Intern Med 172:1110-1111.

[8] L. Taylor 2011. India plans to price-control 60% of pharma market. PharmaTimes.
http://www.pharmatimes.com/Article/11-11-01/India_plans_to_price-control_60_of_pharma_market.aspx. Acessed on March 2015.

[9] Turkey issues new unilateral Health Application Announcement 2011. PharmaLetter.
http://www.thepharmaletter.com/article/turkey-issues-new-unilateral-health-application-announcement. Acessed on March 2015

[10] P. Suresh, P.K. Basu 2008. Improving Pharmaceutical Product Development and Manufacturing: Impact on Cost of Drug Development and Cost of Goods Sold of Pharmaceuticals. J Pharm Innov 3:175-187.

[11] J.D. Rockoff 2015. Drug Making Breaks Away From Its Old Ways. 'Continuoius-Manufacturing' Process Can Improve Quality Control, Speed output. The Wall Street Journal. http://www.wsj.com/article_email/drug-making-breaks-away-from-its-old-ways-1423444049-lMyQjAxMTI1NjE1MjYxNDIxWj. Acessed on Februrary 2015.

[12] J.S. Srai, C. Badman, M. Krumme, M. Futran, C. Johnston 2015. Future supply chains enabled by continuous processing-opportunities and challenges. May 20-21, 2014 continuous manufacturing symposium. J Pharm Sci 3:840-849.

[13] B.R. Conway 2008. Solid dosage form. In: S.C. Gad, editor. Pharmaceutical manufacturing handbook: Production and Processes, 1st ed., New Jersy: John Wiley & Sons Ltd. p 235-260.

[14] P. McKenzie, S. Kiang, J. Tom, A.E. Rubin, M. Futran 2006. Can pharmaceutical process development become high tech? AIChE J 52:3990-3994.

[15] EMA 2012. Guidline on Real Time Release Testing.
http://www.ema.europa.eu/docs/en_GB/document_library/Scientific_guideline/2012/04/WC500125401.pdf. Acessed on Janurary 2015.

[16] US FDA 2004. Pharmaceutical cGMPs for the 21at Century: A Risk-Based Approach.
http://www.fda.gov/Drugs/DevelopmentApprovalProcess/Manufacturing/QuestionsandAnswersonCurrentGoodManufacturingPracticescGMPforDrugs/ucm137175.htm. Acessed on Janurary 2015.

[17] US FDA 2004. PAT – A Framework for Innovative Pharmaceutical Manufacturing and Quality Assurance.
http://www.fda.gov/downloads/Drugs/Guidances/ucm070305.pdf. Acessed on Janurary 2015.

[18] US FDA 2011. Process Validation: General Principles and Practices. http://www.fda.gov/downloads/Drugs/Guidances/UCM070336.pdf. Acessed on Janurary 2015.
[19] ICH 2009. Q8(R2) Pharmaceutical Development. http://www.fda.gov/downloads/Drugs/Guidances/ucm073507.pdf. Accessed on February 2015.
[20] ICH 2005. Q9 Quality Risk Management. http://www.ich.org/fileadmin/Public_Web_Site/ICH_Products/Guidelines/Quality/Q9/Step4/Q9_Guideline.pdf Accessed on February 2015.
[21] ICH 2008. Q10 Pharmaceutical Quality system. http://www.fda.gov/downloads/Drugs/Guidances/ucm073517.pdf. Accessed on February 2015.
[22] ICH 2012. Q11 Development and Manufacture of Drug Substances. http://www.fda.gov/downloads/Drugs/Guidances/UCM261078.pdf. Accessed on February 2015.
[23] IBM Business Conculting Services 2005, The metamorphosis of manufacturing - from art to science. http://www-935.ibm.com/services/us/imc/pdf/ge510-4034-metamorphosis-of-manufacturing.pdf. Acessed on Janurary 2015.
[24] N. Shah 2004. Pharmaceutical supply chains: key issues and strategies for optimization. Comput Chem Eng 28:929-941.
[25] K. Plumb 2005. Continuous Processing in the Pharmaceutical Industry. Chem Eng Res Des 83:730-738
[26] B. Aksu, T. De Beer, S. Folestad, J. Ketolainen, H. Linden, J.A. Lopes, M. de Matas, W. Oostra, J. Rantanen, M. Weimer 2012. Strategic funding priorities in the pharmaceutical sciences allied to Quality by Design (QbD) and Process Analytical Technology (PAT). Eur J Pharm Sci 47:402-405.
[27] A. Rogers, A. Hashemi, M. Ierapetritou 2013. Modeling of Particulate Processes for the Continuous Manufacture of Solid-Based Pharmaceutical Dosage Forms. Process 1: 67-127
[28] S.D. Schaber, D.I. Gerogiorgis, R. Ramachandran, J.M.B. Evans, P.I. Barton, B.L. Trout 2011. Economic Analysis of Integrated Continuous and Batch Pharmaceutical Manufacturing: A Case Study. Ind Eng Chem Res 50:10083-10092.
[29] L.X. Yu 2008. Pharmaceutical quality by design: product and process development, understanding and control. Pharm Res 25:781-791
[30] K. Nepveux, J.P. Sherlock, M. Futran M. Thien, M. Krumme 2015. How development and manufacturing will need to be structured-heads of development/manufacturing. May 20-21, 2014 continuous manufacturing symposium. J Pharm Sci 104:850-864.
[31] S. Byrn, M. Futran, H. Thomas, E. Jayjock, N. Maron, R.F. Meyer, A.S. Myerson, M. Thien, B.L. Trout 2015. Achieving continuous manufacturing for final dosage formation: challenges and how to meet them. May 20-21, 2014 continuous manufacturing symposium. J Pharm Sci 3:792:802.
[32] I. R. Baxendale, R. D. Braatz, B. K. Hodnett, K. F. Jensen, M. D. Johnson, P. Sharratt, J. P. Sherlock, A. J.Florence 2015. Achieving continuous manufacturing: technologies and approaches for synthesis, workup, and isolation of drug substance. May 20-21, 2014 continuous manufacturing symposium. J Pharm Sci 3:781-791.
[33] C. Badman, B. L. Trout 2015. Achieving continuous manufacturing. May 20-21, 2014 continuous manufacturing symposium. J Pharm Sci 3:779:780.
[34] A.S. Myerson, M. Krumme, M. Nasr, H. Thomas, R.D. Braatz 2015. Control systems engineering in continuous pharmaceutical manufacturing. J Pharm Sci 104:832-839. [35] T.D. Page, H. Fillipi, G. Guidat, R. Patnaik, S. Poechlauer, P. Shering, P. Guinn, M. McDonnell, P. Johnston, C., Journal of pharmaceutical sciences, 104 (2015) 821-831.
[36] G. Allison, Y. T. Cain, C. Cooney, T. Garcia, T. Bizjak, H. Gooen, J. Oyvind, K. Nirdosh, K. Bekki, K. Evdokia, M. Dora, M. Rapti, M. Elaine, F. Montgomery, M. Nasr, W. Randolph, J. L. Robert, D. Rudd, D. Zezza 2015. Regulatory and Quality

Considerations for Continuous Manufacturing. May 20-21, 2014 Continuous Manufacturing Symposium. J Pharm Sci 3:803:812.

[37] K. B. Konstantinov, C. L. Cooney 2015. White paper on continuous bioprocessing. May 20-21, 2014 continuous manufacturing symposium. J Pharm Sci 3:812:820.

[38] J. Robertson 2013. Implementation of small scale continuous granulation in the pharmaceutical industry. 6th International Conference on Granulation, Sheffield, UK.

[39] R.P. Cogdill, J.K. Drennen 2008. Risk-based Quality by Design (QbD): A Taguchi Perspective on the Assessment of Product Quality, and the Quantitative Linkage of Drug Product Parameters and Clinical Performance. J Pharm Innov 3:23-29.

[40] B. S. Riley, X. Li 2011. Quality by design and process analytical technology for sterile products--where are we now?. AAPS PharmSciTech 12:114-118.

[41] A.L. Pomerantsev, O.Y. Rodionova 2012. Process analytical technology: a critical view of the chemometricians. J Chemometrics 26:299-310.

[42] Y. Roggo, P. Chalus, L. Maurer, C. Lema-Martinez, A. Edmond, N. Jent 2007. A review of near infrared spectroscopy and chemometrics in pharmaceutical technologies. J Pharm Biomed Anal 44:683-700.

[43] M. Blanco, J. Coello, H. Iturriaga, S. Maspoch, C. de la Pezuela C 1998. Near-infrared in the pharmaceutical industry. Analyst 123:135-150.

[44] R.C. Lyon, E.H. Jefferson, C.D. Ellison, L.F. Buhse, J.A. Spencer, M.M. Nasr, A.S. Hussain 2003. Exploring pharmaceutical applications of near-infrared technology. Amer Pharma Rev 6:62-70.

[45] G. Reich 2005. Near-infrared spectroscopy and imaging: basic principles and pharmaceutical applications. Adv Drug Deliv Rev 57:1109-1143.

[46] E.W. Ciurczak, 2001. Principles of near-infrared spectroscopy. In: D.A. Burns, E.W. Ciurczak, editor. Handbook of NearInfrared Analysis, 2nd ed., New York/Basel: Marcel Dekker Inc. p 7-18.

[47] E. Rasanen, N. Sandler 2007. Near infrared spectroscopy in the development of solid dosage forms. J Pharm Pharmacol 59:147-159.

[48] J. Luypaert, D.L. Massart, Y. Vander Heyden 2007. Near-infrared spectroscopy applications in pharmaceutical analysis. Talanta 72: 865-883.

[49] K.H. Norris 1996. History of Near Infrared Spectroscopy. J Infrared Spectrosc 4:31-37.

[50] L. Bokobza 2002. Origin of near-infrared absorption bands. In: H.W. Siesler, Y. Ozaki, S. Kawata, H.M. Heise, editor. Infrared Spectroscopy: Principles, Instruments, Applications 1st ed., Weinheim, Wiley-VCH Verlag GmbH. p 11-41.

[51] Y. Roggo, L. Duponchel, J.-P. Huvenne 2004. Quality Evaluation of Sugar Beet (Beta vulgaris) by Near-Infrared Spectroscopy. J Agric Food Chem 52:1055-1061.

[52] M.S. Larrechi, M.P. Callao 2003. Strategy for introducing NIR spectroscopy and multivariate calibration techniques in industry. Trends Anal Chem 22:634-640.

[53] B.V. Alander J. A., Martinkauppi B., Saranwong S., Mantere T 2013. A Review of Optical Nondestructive Visual and Near-Infrared Methods for Food Quality and Safety. Int J Spec 2013:1-36.

[54] F.C. Clarke, S.V. Hammond, R.D. Jee, A.C. Moffat 2002. Determination of the Information Depth and Sample Size for the Analysis of Pharmaceutical Materials Using Reflectance Near-Infrared Microscopy. Appl Spectrosc 56:1475-1483.

[55] T. De Beer, A. Burggraeve, M. Fonteyne, L. Saerens, J. Remon, C. Vervaet 2011. Near infrared and Raman spectroscopy for the in-process monitoring of pharmaceutical production processes. Int JPharm 417: 32-47.

[56] J.M. Amigo 2010. Practical issues of hyperspectral imaging analysis of solid dosage forms. Anal Bioanal Chem 398:93-109.
[57] M. Zeaiter, J.M. Rogger, V. Bellon-Maurel 2005. Robustness of models developed by multivariate calibration. Part II: The influence of pre-processing methods. TrAC 24:437-445.
[58] O. Rodionova, A. Pomerantsev 2010. NIR-based approach to counterfeit-drug detection. TrAC 29:795-803.
[59] R. J. Barnes, M. S. Dhanoa, S. J. Lister 1989. Standard normal variate transformation and de-trending of near-infrared diffuse reflectance spectra. Appl Spectrosc 43:772-777.
[60] T. Næs, T. Isaksson, T. Fearn, T. Davies 2003. A user-friendly guide to multivariate calibration and classification. J. Chemometrics 17:571-572.
[61] K.H. Esbensen, D. Guyot, F. Westad, L.P. Houmøller 2002. Multivariate data analysis – in practice. K.H. Esbensen, editor. An introduction to multivariate data analysis and experimental design, 5th ed., Esbjerg/Oslo: Aarlborg University/Camo. p 19-97.
[62] P. Geladi, H. Isakson, L. Lindquist, S. Wold, K. Esbensen 1989. Principal component analysis of multivariate images. Chemom. Intell. Lab. Syst 5:209-220.
[63] S. World, M. Sjöström ,Eriksson L 2001. PLS-regression a basic tool of chemometrics. Chemom Intell Lab Syst 58:109-130.
[64] K. Varmuza, P. Filzmoser 2009. Calibration. In: K. Varmuza, P. Filzmoser editor. Introduction to Multivariate Statistical Analysis in Chemometrics 1st ed., New York: CRC Press Inc. p. 103-194.
[65] L. Nørgaard, R. Bro, S.B. Engelsen 2009. Krydsvalidering. Dansk Kemi 90:28-29.
[66] T. Puchert, C.V. Holzhauer, J.C. Menezes, D. Lochmann, G. Reich 2011. A new PAT/QbD approach for the determination of blend homogeneity: combination of on-line NIRS analysis with PC Scores Distance Analysis (PC-SDA). Eur J Pharm Biomed 78:173-182.
[67] L.T. Fan, S.J. Chen, C.A. Watson 1970. Solid mixing. Ind. Eng. Chem 62:53-69.
[68] T.P. Garcia, S.J. Wilkinson, J.F. Scott 2001. The development of a blend-sampling technique to assess the uniformity of a powder mixture. Drug Dev Ind Pharm 27:297-307.
[69] F.J. Muzzio, P. Ribinson, C. Wightman, D. Brone 1997. Sampling practices in powder blending. Int J Pharm 155:153-178.
[70] M.C.R. Johnson 1975. The effect of particle size upon mixture homogeneity. Pharm. Acra Helv 50:60-63.
[71] M. Poux, P. Fayolle, J. Bertrand, D. Bridoux, J. Bousquet 1991. Powder mixing: some practical rules applied to agitated systems. Powder Technol, 68:213-234.
[72] T.R. Speiser, R. Tawashi 1962. The mixing action of pharmaceutically used powder mixers. Pharm. Acra Helv 37:529-543.
[73] R.D. Maesschalck, F.C. Sanchez, D.L. Massart, P. Doherty, P. Hailey 1998. On-Line Monitoring of Powder Blending with Near-Infrared Spectroscopy. Appl Spectrosc 52:725-731.
[74] U. Sindel, A Schweiger, I. Zimmermann 1998. Determination of the optimum mixing time for a mixture of lactose and colloidal silicon dioxide. J Pharm Sci 87:524-526.
[75] T.P.Garcia., J.K.Prescoot 2008. Blending and Blend uniformity. L. L. Augsburger, S. W. Hoag, editor. Pharmaceutical Dosage Forms: Tablets 3rd ed., New York: Informa Healthcare. p 111-174.
[76] O. Scheibelhofer, N. Balak, P.R. Wahl, D.M. Koller, B.J. Glasser, J.G. Khinast 2013. Monitoring blending of pharmaceutical powders with multipoint NIR spectroscopy. AAPS PharmSciTech 14:234-244.

[77] A.S. El-Hagrasy, F. D'Amico, J.K. Drennen 2005. A Process Analytical Technology approach to near-infrared process control of pharmaceutical powder blending. Part I: D-optimal design for characterization of powder mixing and preliminary spectral data evaluation. J Pharm Sci 95:392-406.
[78] L.J. Bellamy, A. Nordon, D. Littlejohn 2008. Real-time monitoring of powder mixing in a convective blender using non-invasive reflectance NIR spectrometry. Analyst, 133:58-64.
[79] A.S. El-Hagrasy, M. Delgardo-Lopez, J.K. Drennen 2005. A Process Analytical Technology approach to near-infrared process control of pharmaceutical powder blending: Part II: Qualitative near-infrared models for prediction of blend homogeneity. J Pharm Sci 95:407-421.
[80] S.S. Sekulic, H.W. Ward, D.R. Brannegan, E.D. Stanley, C.L. Evans, S.T. Sciavolino, P.A. Hailey, P.K. Aldridge 1996. On-line monitoring of powder blend homogeneity by near-infrared spectroscopy. Anal Chem 68:509-513.
[81] S.S. Sekulic, J. Wakeman, P. Doherty, P.A. Hailey 1998. Automated system for the on-line monitoring of powder blending processes using near-infrared spectroscopy. Part II. Qualitative approaches to blend evaluation. J Pharm Biomed Anal 17:1285-1309.
[82] A.S. El-Hagrasy, H.R. Morris, F. D'Amico, R.A. Lodder, J.K. Drennen 2001. Near-infrared spectroscopy and imaging for the monitoring of powder blend homogeneity. J Pharm Sci 90:1298-1307.
[83] H. Zhang, Z. Jiang, J.Y. Pi, H.K. Xu, R. Du 2009. On-line monitoring of pharmaceutical production processes using Hidden Markov Model. J Pharm Sci 98:1487-1498.
[84] H. Wu, M. Tawakkul, M. White, M.A. Khan 2009. Quality-by-Design (QbD): An integrated multivariate approach for the component quantification in powder blends. Int J Pharm 372: 39-48.
[85] D.J. Wargo, J.K. Drennen 1996. Near-infrared spectroscopic characterization of pharmaceutical powder blends. J Pharm Biomed Anal 14:1415-1423.
[86] J.J. Moes, M.M. Ruijken, E. Gout, H.W. Frijlink, M.I. Ugwoke 2008. Application of process analytical technology in tablet process development using NIR spectroscopy: blend uniformity, content uniformity and coating thickness measurements. Int J Pharm 357:108-118.
[87] F.C. Sánchez, J. Toft, B. Bogaert, D.L. Massart, S.S. Dive, P. Hailey 1995. Monitoring powder blending by NIR spectroscopy. Anal Chem 352:771-778.
[88] D. Ely, S. Charmarthy, M. T. Carvajal 2006. An investigation into low dose blend uniformity and segregation determination using NIR spectroscopy. Colloids Surf 288:71-76.
[89] J. Rantanen, H. Wikström, R. Turner, S.L. Taylor 2005. Use of In Line Near Infrared Spectroscopy in Combination with Chemometrics for Improved Understanding of Pharmaceutical Processes . Anal Chem 77:556-563.
[90] E.T. Skibsted, H.F. Boelens, J.A. Westerhuis, D.T. Witte, A.K. Smilde 2006. Simple assessment of homogeneity in pharmaceutical mixing processes using a near-infrared reflectance probe and control charts. J Pharm Biomed Anal 41:26-35.
[91] A.S. El-Hagrasy, F. D'Amico, J.K. Drennen 2005. A Process Analytical Technology approach to near-infrared process control of pharmaceutical powder blending. Part III: Quantitative near-infrared calibration for prediction of blend homogeneity and characterization of powder mixing kinetics. J Pharm Sci 95:422-434.
[92] Z. Shi, R.P. Cogdill, S.M. Short, C.A. Anderson 2008. Process characterization of powder blending by near-infrared spectroscopy: blend end-points and beyond. J Pharm Biomed Anal 47:738-745.
[93] Y. Sulub, M. Konigsberger, J. Cheney 2011. Blend uniformity end-point determination using near-infrared spectroscopy and multivariate calibration. J Pharm Biomed Anal 55:429-434.

[94] I. Storme-Paris, I. Clarot, S. Esposito, J.C. Chaumeil, A. Nicolas, F. Brion, A. Rieutord, P. Chaminade 2009. Near InfraRed Spectroscopy homogeneity evaluation of complex powder blends in a small-scale pharmaceutical preformulation process, a real-life application. Eur J Pharm Biopharm 72:189-198.
[95] P. Kleinebudde 2004. Roll compaction/dry granulation: pharmaceutical applications. Eur J Pharm Biopharm 58:317-326.
[96] J.R. Johanson 1965. A rolling theory for granular solids. J Appl Mech 32:842-848.
[97] A.K. Samanta, A.D. Karande, K.Y. Ng, P.W. Heng 2013. Application of near-infrared spectroscopy in real-time monitoring of product attributes of ribbed roller compacted flakes. AAPS PharmSciTech 14:86-100.
[98] O. Simon, P. Guigon 2003. Correlation between powder-packing properties and roll press compact heterogeneity. Powder Technol 130:257-264.
[99] Y. Funakoshi, T. Asogawa, E. Satake 1977. The use of a Novel Roller Compactor with a Concavo-Convex Roller pair to Obtain Uniform Compacting Pressure. Drug Dev Ind Pharm 3:555-573.
[100] R.W. Miller 1994. Advances in Pharmaceutical Roller Compactor Feed System Designs. Pharm Technol 18:154-162.
[101] G. Shlieout, R.F Lammens, P. Kleinebudde 2000. Dry granulation with a roller compactor. Part I: The functional units and operation modes. Pharma Technol 12:24-35.
[102] P. Guigon, O. Simon 2003. Roll press design—influence of force feed systems on compaction. Powder Technol 130:41-48.
[103] R.W. Miller, 2010. Roller Compaction. In: D.M. Parikh, editor. Handbook of Pharmaceutical Granulation Technology, 3rd ed., New York: Informa Healthcare. p. 163-180.
[104] D. Acevedo, A. Muliadi, A. Giridhar, J.D. Litster, R.J. Romanach 2012. Evaluation of three approaches for real-time monitoring of roller compaction with near-infrared spectroscopy. AAPS PharmSciTech 13:1005-1012.
[105] A.M. Falzone, G.E. Peck, G.P. Mccabe 1992. Effects of changes in roller compactor parameters on granulations produced by compaction. Drug Dev Ind Pharm 18:469-489.
[106] A. Gupta, G.E. Peck, R.W. Miller, K.R. Morris 2005. Real-time near-infrared monitoring of content uniformity, moisture content, compact density, tensile strength, and Young's modulus of roller compacted powder blends. J Pharm Sci 94:1589-1597.
[107] P.J. Sheskey, R.W. Miller 2006. Roller Compaction Technology for the Pharmaceutical Industry. In: J. Swarbrick, editor. Encyclopedia of Pharmaceutical Technology, 3rd ed., Informa Healthcare. p 3159-3176.
[108] C. Bacher, P.M. Olsen, P. Bertelsen, J. Kristensen, J.M. Sonnergaard 2007. Improving the compaction properties of roller compacted calcium carbonate. Int J Pharm 342:115-123.
[109] S.J. Wu, C. Sun 2007. Insensitivity of compaction properties of brittle granules to size enlargement by roller compaction. J Pharm Sci 96:1445-1450.
[110] C.C. Sun, M.W. Himmelspach 2006. Reduced tabletability of roller compacted granules as a result of granule size enlargement. J Pharm Sci 95:200-206.
[111] P.D. Daugherity, J.H. Chu 2007. Investigation of serrated roll surface differences on ribbon thickness during roller compaction. Parm Dev Technol 12:603-608.
[112] P.J. Sheskey, J. Hendren 1999. The effects of roll compaction equipment variables, granulation technique, and HPMC polymer level on a controlled-release matrix model drug formulation. Pharm Technol 23:90-106.
[113] F. Freitag, P. Kleinebudde 2003. How do roll compaction/dry granulation affect the tableting behaviour of inorganic materials? Comparison of four magnesium carbonates. Eur J Pharm Sci, 19:281-289.

[114] F. Freitag, K. Reincke, J. Runge, W. Grellmann, P. Kleinebudde 2004. How do roll compaction/dry granulation affect the tableting behaviour of inorganic materials? Microhardness of ribbons and mercury porosimetry measurements of tablets. Eur J Pharm Sci 22:325-333.
[115] S. Inghelbrecht, J.P. Remon 1998. Roller compaction and tableting of microcrystalline cellulose/drug mixtures. Int J Pharm 161:215-224.
[116] H. Lim, V.S. Dave, L. Kidder, E. Neil Lewis, R. Fahmy, S.W. Hoag 2011. Assessment of the critical factors affecting the porosity of roller compacted ribbons and the feasibility of using NIR chemical imaging to evaluate the porosity distribution. Int J Pharm 410:1-8.
[117] J.F. Gamble, M. Tobyn, A.B. Dennis, T. Shah 2010. Roller compaction: application of an in-gap ribbon porosity calculation for the optimization of downstream granule flow and compactability characteristics. Pharm Dev Technol 15:223-229.
[118] S. Malkowska, K.A. Khan 1983. Effect of recompression on the properties of tablets prepared by dry granulation. Drug Dev Ind Pharm 9:331-347.
[119] M.G. Herting, P. Kleinebudde 2008. Studies on the reduction of tensile strength of tablets after roll compaction/dry granulation. Eur J Pharm Biopharm 70:372-379.
[120] P.J. Sheskey, T.D Cabelka, R.T. Robb, B.M. Boyce 1994. Use of Roller Compaction in the Preparation of Controlled-Release Hydrophilic Matrix Tablets Containing Methylcellulose and Hydroxypropyl Methylcellulose Polymers. Pharm Technol 18:132-150.
[121] T.M. Jones, N. Pilpel 1966. The flow of granular magnesia. J Pharm Pharmac 18: 429-442.
[122] A.A. Gowen, C.P. O'Donnell, P.J. Cullen, S.E. Bell 2008. Recent applications of Chemical Imaging to pharmaceutical process monitoring and quality control. Eur J Pharm BioPharm 69:10-22.
[123] G. Kumar, D. C. Pallavi 2013. Direct Compression - An Overview. Int J Res Pharm Biomed Sci 4:155-158.
[124] M.C. Gohel 2004. A review of co-processed directly compressible excipients. J Pharm Pharmaceut Sci 8:76-93.
[125] B.C. Hancock, S. Garcia-Munoz 2013. How do formulation and process parameters impact blend and unit dose uniformity? Further analysis of the product quality research institute blend uniformity working group industry survey. J Pharm Sci 102:982-986.
[126] S. Sasic 2007. An in-depth analysis of Raman and near-infrared chemical images of common pharmaceutical tablets. Appl Spectrosc 61:239-250.
[127] C. Ravn, E. Skibsted, R. Bro 2008. Near-infrared chemical imaging (NIR-CI) on pharmaceutical solid dosage forms-comparing common calibration approaches. J Parm Biomed Anal 48:554-561.
[128] M. Donoso, D.O. Kildsig, E.S. Ghaly 2003. Prediction of tablet hardness and porosity using near-infrared diffuse reflectance spectroscopy as a nondestructive method. Pharm Dev Technol 8:357-366.
[129] R.K. May, K. Su, L. Han, S. Zhong, J.A. Elliott, L.F. Gladden, M. Evans, Y. Shen, J.A. Zeitler 2013. Hardness and density distributions of pharmaceutical tablets measured by terahertz pulsed imaging. J Pharm Sci 102:2179-2186.
[130] Y. Hattori, M. Otsuka 2011. NIR spectroscopic study of the dissolution process in pharmaceutical tablets. Vibrat Spec 57:275-281.
[131] S. Virtanen, O. Antikainen, J. Yliruusi 2007. Uniformity of poorly miscible powders determined by near infrared spectroscopy. Int J Pharm 345:108-115.
[132] P.G. Moore 1955. The Properties of the Mean Square Successive Difference in Samples From Various Populations. J Amer Statist Assoc 50:434-456.

[133] J. Keen, D.J. Page 1953. Estimating Variability from the Differences Between Successive Readings. J ROY STAT SOC C-APP 2:13-23.
[134] R.S. Bingham 1968. Approximations for Mean Square Successive Difference Critical Values. Technometrics 10:397-400.
[135] H. J. Zar 2010. Serial Randomness Measurements: Parametric Testing, in: Biostatistical Analysis, Fifth Edition, (2010), pp. 599-602.
[136] E.G. Rippie, M. D. Feiman, M. K. Pramoda 1967. Segregation kinetics of particulate solids systems IV. Effect of particle shape on energy requirements. J Pharm Sci 56:1523-1525.
[137] M. Llusa, F.J. Muzzio 2005. The Effect of Shear Mixing on the Blending of Cohesive Lubricants and Drugs. Pharm Tech 12:36-45.
[138] D. Brone, A. Alexander, F.J. Muzzio 1998. Quantitative characterization of mixing of dry powders in V-blenders. AIChE J 44:271-278.
[139] S.M. Short, R.P. Cogdill, P.L. Wildfong, J.K. Drennen, C.A. Anderson 2009. A near-infrared spectroscopic investigation of relative density and crushing strength in four-component compacts. J Pharm Sci 98:1095-1109.
[140] J.D. Kirsch, J.K. Drennen 1995. Near-Infrared Spectroscopy: Applications in the Analysis of Tablets and Solid Pharmaceutical Dosage Forms. Appl Spectrosc Rev 30:139-174.
[141] J. Cruz, M. Blanco 2011. Content uniformity studies in tablets by NIR-CI. J Pharm Biomed Anal 56:408-412.
[142] J.M. Amigo, J. Cruz, M. Bautista, S. Maspoch, J. Coello, M. Blanco 2008. Study of pharmaceutical samples by NIR chemical-image and multivariate analysis. TrAC 27:696-713.
[143] J.M. Amigo, C. Ravn 2009. Direct quantification and distribution assessment of major and minor components in pharmaceutical tablets by NIR-chemical imaging. Eur J Pharm Sci 37:76-82.
[144] R. Bro 2003. Multivariate calibration. Anal Chim Acta 500:185-194.
[145] N. Souihi, G. Reynolds, P. Tajarobi, H. Wikstrom, G. Haeffler, M. Josefson, J. Trygg 2015. Roll compaction process modeling: Transfer between equipment and impact of process parameters. Int J Pharm 484:192-206.
[146] M. Allesø, A. S. Torstenson, M. Bryder, P. Holm 2013. Presenting a rational approach to QbD-based pharmaceutical development: A roller compaction case study. Eur Pharm Rev 18:3-10.
[147] European Pharmacopoeia 2014. Uniformity of Mass of single-dose preparations Units. p. 297-298.
[148] N. Souihi, M. Josefson, P. Tajarobi, B. Gururajan, J. Trygg 2013. Design Space Estimation of the Roller Compaction Process. Ind Eng Chem Res 52:12408-12419.
[149] A. Palou, J. Cruz, M. Blanco, J. Tomàs, J. de los Ríos, M. Alcalà 2012. Determination of drug, excipients and coating distribution in pharmaceutical tablets using NIR-CI., J Pharml Anal 2:90-97.
[150] S. Mascia, P.L. Heider, H. Zhang, R. Lakerveld, B. Benyahia, P.I. Barton, R.D. Braatz, C.L. Cooney, J.M. Evans, T.F. Jamison, K.F. Jensen, A.S. Myerson, B.L. Trout 2013. End-to-end continuous manufacturing of pharmaceuticals: integrated synthesis, purification, and final dosage formation. Angew Chem Int Ed Engl 52:12359-12363.
[151] L. A. Cassis, A. Urbas, R. A. Lodder 2005. Hyperspectral integrated computational imaging. Anal Bioanal Chem 382: 868-872.

9. LIST OF APPENDICES

I. **M. Khorasani**, J.M. Amigo, P. Bertelsen, F. van den Berg, J. Rantanen. Detecting blending end-point using mean squares successive difference test and near-infrared spectroscopy. Journal of Pharmaceutical Sciences, **(2015).**

II. **M. Khorasani**, J.M. Amigo, J. Sonnergaard, P. Olsen, P. Bertelsen, J. Rantanen. Visualization and prediction of porosity in roller compacted ribbons with near-infrared chemical imaging (NIR-CI). Journal of Pharmaceutical and Biomedical analysis, 109 (**2015**) 11-17.

III. **M. Khorasani**, J.M. Amigo, Changquan Calvin Sun, P. Bertelsen, F. van den Berg, J. Rantanen. Near-infrared chemical imaging (NIR-CI) as a process monitoring solution for a production line of roll compaction and tableting. European Journal of Pharmaceutics and Biopharmaceutics, 93 (**2015**) 293-302.

I

Detecting Blending End-Point Using Mean Squares Successive Difference Test and Near-Infrared Spectroscopy

MILAD KHORASANI,[1] JOSÉ M. AMIGO,[2] POUL BERTELSEN,[3] FRANS VAN DEN BERG,[2] JUKKA RANTANEN[1]

[1]Faculty of Health and Medical Sciences, Department of Pharmacy, University of Copenhagen, Copenhagen, Denmark
[2]Faculty of Science, Department of Food Science, University of Copenhagen, Copenhagen, Denmark
[3]Takeda Pharma A/S, Roskilde, Denmark

Received 22 February 2015; revised 30 April 2015; accepted 6 May 2015

Published online in Wiley Online Library (wileyonlinelibrary.com). DOI 10.1002/jps.24533

ABSTRACT: An algorithm based on mean squares successive difference test applied to near-infrared and principal component analysis scores was developed to monitor and determine the blending profile and to assess the end-point in the statistical stabile phase. Model formulations consisting of an active compound (acetylsalicylic acid), together with microcrystalline cellulose and two grades of calcium carbonate with dramatically different particle shapes, were prepared. The formulation comprising angular-shaped calcium carbonate reached blending end-point slower when compared with the formulation comprising equant-shaped calcium carbonate. Utilizing the ring shear test, this distinction in end-point could be related to the difference in flowability of the formulations. On the basis of the two model formulations, a design of experiments was conducted to characterize the blending process by studying the effect of $CaCO_3$ grades and fill level of the bin on blending end-point. Calcium carbonate grades, fill level, and their interaction were shown to have a significant impact on the blending process.

Keywords: process analytical technology (PAT); near-infrared spectroscopy; blending; mean squares successive difference test; multivariate analysis; principal component analysis; ring shear testing; design of experiments; blend uniformity analysis; UV–Vis spectroscopy; mixing

INTRODUCTION

One of the most critical unit operations during manufacturing of solid dosage forms is the blending operation. Achieving a uniform mixture of the active pharmaceutical ingredient (API) and the needed excipients is particularly important. Problems incurred during blending can lead to inadequate final product quality, such as content uniformity, disintegration time, and/or dissolution behavior. All these performance parameters can directly impact the final dosage form efficacy, *in vivo* performance, and ultimately patient safety. For this reason, homogeneity of powder blends and unit dosage forms is especially importance.[1]

A blend, in the classical pharmaceutical sense, is considered to be homogeneous when the API content of the blend samples is within specification, while assuming that all excipients are also evenly distributed.[2] Blending is a reshuffling process involving the random movement of individual groups of particles. Competing process with the powder blending process are segregation and/or demixing.[3,4] Three main mechanisms are responsible for blending, namely, diffusion, convention, and shear. The degrees to which these mechanisms influence a blending process depend on the flow properties of the powders being blended, the specific equipment selected, and the process parameters/settings.[3,5] Several factors such as particle size, shape, density, electrostatic charge, and surface moisture content have a considerable impact on the flow properties of powders.[6,7] As an example, spherical- and cubic-shaped particles often exhibit good flow properties and therefore promote blending. But at the same time, well-flowing material can also be more prone to demixing/segregation. Plate- and needle-shaped particles, for example, have poor flow properties and are more likely to agglomerate, making it more difficult to achieve a uniform blend. However, an advantage of blending these plate and needle-shaped particles is that once they are well blended, they are more likely to stay as uniform blend.[3,4,8]

In industrial practice, the homogeneity of a powder blend is determined by invasive thief sampling followed by a time-consuming off-line chemical analysis of the sampled material.[5] An alternative method to determine the homogeneity is by using near-infrared spectroscopy (NIRS) that is a powerful non-invasive analytical technique and is sensitive to both chemical and physical properties in the measured sample. In addition, NIRS is a fast and easy method to interface with the process for real-time monitoring.[2] Several researchers have used NIRS and different classical statistic, univariate and multivariate approaches, to develop qualitative[2,9–19] and quantitative[13,20–24] methods for studying the blend homogeneity. The qualitative methods are typically simple to use, whereas the quantitative methods are more complex but provide information about the mixture composition. The interested reader is referred to reviews by De Beer et al.,[25] Reich,[26] Roggo et al.,[27] and a book chapter in Drennen and Ciurczak.[28]

One of the most prominent qualitative methods providing reliable results is the use of the multivariate data analysis method, principal component analysis (PCA).[29] A number of authors have used PCA[11,12,15,17,18,30] in order to monitor and estimate the blend homogeneity. One approach is plotting the score values of the first principal component (PC1) against process time and assuming blend homogeneity to be reached when the score level stabilizes around one (arbitrary) point as a function of time.[11,31] Another approach is plotting the first two PCs for replicate target blends (blends that are assumed to be

Correspondence to: Jukka Rantanen (Telephone: +45-35336585; Fax: +45-35306030; E-mail: jukka.rantanen@sund.ku.dk)

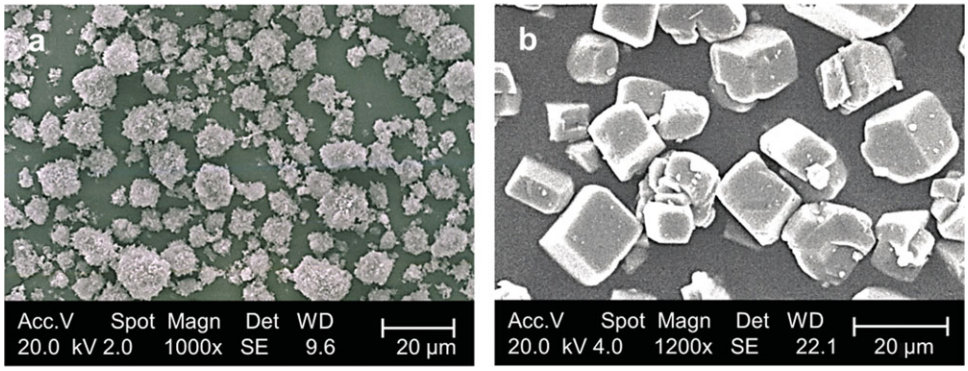

Figure 1. Scanning electron microscope images of (a) $CaCO_3$-A and (b) $CaCO_3$-E.

homogeneous) and test blends in a two-dimensional score plot. If the target blends cluster together in this score plot, then test blends that have reached homogeneity should be close to or overlapping with the target blends cluster.[11,12] However, the establishment of a reliable and coherent end-point detection method with a solid statistical rationale is the keystone where many of the already proposed methods fail, as they do not fully describe what the detection is based on.

In this sense, Puchert et al.[2] proposed a new approach called "principal component score distance analysis." This method establishes a time window where spectral variability in the blend is lower than a preset threshold value and uses Hotelling's T^2 statistics to monitor and report blend homogeneity. However, Puchert et al.[2] did not only consider the process stability to detect the end-point but rather stability compared with a target spectrum. This hampers the method for real-time usage, because the method is strictly depending on knowing beforehand the spectral profile of the final blend. And this is not feasible in many occasions.

In order to have a stable process when working with real-time series data points, it is important to have an understanding of the types of expected variation in the data. Two important classes of variation are the following ones: (1) controlled variation, which is characterized by a stable and constant pattern of (hopefully minor) variation over time. This type of variation comes in a random order and depicts a uniform fluctuation about a constant level; the process is said to be in a state of statistical control. (2) Uncontrolled variation, which is characterized by a pattern of variation that changes over time. This type of variation indicates that the process is not yet in a state of statistical control and further processing (i.e., blending) is required. A process is considered stable if the average process value is constant and the variation is random.[32,33] One approach to evaluate process stability in serial-related data points is the application of the mean square successive difference test (MSSDT) for serial randomness.[34–37]

Using this knowledge, our main aim was, therefore, to develop an algorithm based on MSSDT applied to near-infrared (NIR) and PCA scores to monitor and determine the blending profile and to statistically assess the end-point in the statistical stabile phase. In order to access the ability of the algorithm to determine the correct blending end-point, two powder formulations, composed of different calcium carbonate grades, were investigated. The flow properties of the pure calcium carbonate grades and their powder formulations were determined by a ring shear tester. A design of experiment was conducted to identify how the calcium carbonate grades and fill level of the blender bin affect the blending end-point. For all blending, experiments samples were randomly withdrawn from the surface of each batch in order prevent local segregation because of the thief sampling process. Subsequently, samples were investigated off-line by UV–Vis spectroscopy to determine the API uniformity, thereby validating the ability of the algorithm to detect the blending end-point.

EXPERIMENTAL

Materials and Instrumental Setup for Online NIRS

As a model API, acetylsalicylic acid (ASA) USP grade (Rhodine® 3080; Rhodia, Saint-Fons, France) was used. The excipients used were microcrystalline cellulose (MCC), Comprecel® PH 101 USP grade (MINGTAY Chemical, Taoyan city, Taiwan), and two grades of calcium carbonates ($CaCO_3$) with different shapes, namely, angular $CaCO_3$ Sturcal L® (Specialty Minerals, Lifford, Great Britian) and equant $CaCO_3$ Scoralite D® (Scora S.A., Caffiers, France).

Figure 1 shows scanning electron microscope images of the two $CaCO_3$ grades. Angular-shaped particles are sharp-edged, polyhedral-shaped particles with a rougher (i.e., bumpy, uneven) surface. Equant-shaped particles are cubic or spherical-shaped particles with similar width, length, and thickness and smoother surface.[38] Throughout this study, $CaCO_3$ Sturcal L® and $CaCO_3$ Scoralite D® are noted as $CaCO_3$-A and $CaCO_3$-E, respectively.

After accurate weighing, the ingredients of each formulation batch were transferred to a 10-L bin-blender with baffles (LM 40; L.B.Bohle Maschinen & Verfahren GmbH, Ennigerloh Haan, Germany). A Prozess Analysator spectrometer controlled with the SX-center software (NIR-Online GmbH, Walldorf, Germany) was used for spectral acquisition in diffuse reflectance mode over the wavelength range 1100–1700 nm with a resolution of 5 nm for sample measurements. This enabled acquisition of six scans (integration time: 30 µs) that were averaged into one spectrum for each blender revolution. A schematic drawing of the instrumental setup is shown in Figure 2. The spectrometer was mounted directly onto the Bohle bin blender via a custom-build lid from Bohle. The spectrometer has a built in sensor to determine the orientation and whenever the instrument was located at the bottom position during a bin rotation a triggering device signalled the start of a new spectral recording; a trigger angle of −45° to 45° was

 DOI 10.1002/jps.24533

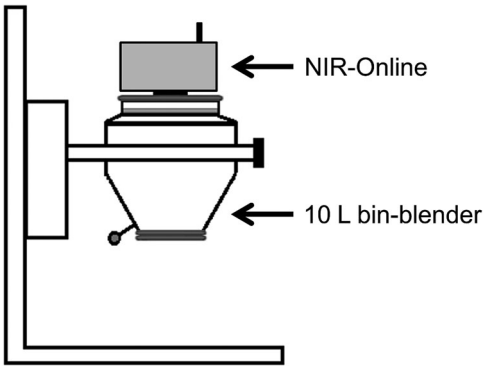

Figure 2. Instrumental setup for online NIRS blending monitoring.

used in the current study. Recorded spectra were transferred via the built-in wireless network from the spectrometer to the computer. White and dark reference measurements were obtained prior to all experimental runs. Acquisition settings were similar to those used in sample measurements. The blender was programmed to run in one direction during the course of blending.

Initial Blending Experiments

In order to study the feasibility of the developed blending end-point detection algorithm, two powder formulation batches, called formulation-I and formulation-II, were prepared and blended in triplicates. Formulation-I and formulation-II consisted of 5% (w/w) ASA, 35% (w/w) MCC, and 60% (w/w) $CaCO_3$ (A or E). Blender fill level and number of revolutions were kept constant at 50% and 120 for all blending runs. Number of revolution is calculated as blending time multiplied by the rotation speed, 6 min and 20 rpm, respectively. A Student's *t*-test was performed to determine whether the differences in estimated end-point were significant between the powder formulation batches. The level of significance used was: $\alpha = 0.05$ with $n = 3$.

Flowability

Sample Division and Preparation

After each blending run, a large composite sample of 600 mL was withdrawn based on six randomly chosen locations inside the powder bed. Subsequently, the withdrawn sample was split into 8 × 75 mL measurements units using an automated sample divider with eight divisions (PT100; Retsch, Haan, Germany). For the ring shear testing, 3 × 75 mL randomly selected units were used and the remaining 5 × 75 mL samples were discarded. The same procedure was conducted for the pure powder of $CaCO_3$ grades. In order to archive homogenous moisture content, the measurement samples were conditioned at 25°C and 43 ± 5% RH for 5 days as studies have shown that flow properties are dependent on the powders' moisture content.[39,40]

Ring Shear Testing

Flowability of the two pure $CaCO_3$ grades and the powder formulations were measured using a Schulze ring shear tester (RST-XS.s; Dr. Ing. Dietmar Schulze Schüttgutmesstechnik, Wolfenbüttel, Germany). A bulk sample of 70 mL was prepared in a XS-Lr0 shear cell. The sample was then evaluated using a customized shear program including testing at $\sigma_{pre} = 250$, 500, 1000, 1500, and 2500 Pa with three σ_{sh} points being measured. These points were selected so that the normal stress at shear to failure (σ_{sh}) were 20%, 50%, and 80% of the σ_{pre}. A flow property from shear testing that is often used in comparative studies is ff_c. It expresses the flowability of a powder and is defined as the relationship of the consolidation stress (σ_1) to the unconfined yield strength (σ_c). Generally, the greater the value, the better flowing the powder is. However, it should be noted that the powder flowability is also influenced by several other factors, such as the nature of the blending container. All samples were measured three times and the mean value of ff_c was calculated according to Eq. (1), and plotted as function of σ_1, yielding a flow function curve.

$$ff_c = \sigma_1/\sigma_c \quad (1)$$

A higher value of ff_c is an indication of better (more desirable) flow properties for the current system.[41] Table 1 shows the relationship of ff_c values with flow properties.[39]

Table 1. Correlation of ff_c Values with Flow Properties[39]

$ff_c < 1$	Nonflowing
$1 < ff_c < 2$	Very cohesive
$2 < ff_c < 4$	Cohesive
$4 < ff_c < 10$	Easy flowing
$10 < ff_c$	Free flowing

Design of Experiments

The blending experiments based on formulation-I and formulation-II together with a two-factor two-level full factorial design were used to model the influences of the different $CaCO_3$ grades and the process parameter blender fill level on the blending time (end-point). $CaCO_3$ grade and fill level were chosen as experimental factors and blending time (end-point) was chosen as the response for the design of experiment. The fill level of the blender covered a range from 35% (v/v) to 65% (v/v) of the 10-L bin. The rotational speed of the blender was set at 20 rpm and the total blending time was set to 5 min. Five runs in duplicate were carried, including two center-points (Table 2). The results were analyzed with the

Table 2. Experimental Design

Run Number	$CaCO_3$	Fill Level (%)	End-Point (min)	ASA Concentration (%)
R1.1	A	35	2.40	98.9
R1.2	A	35	2.64	98.2
R2.1	E	35	2.02	96.7
R2.2	E	35	1.73	96.3
R3.1	A	65	4.98	96.2
R3.2	A	65	4.90	96.9
R4.1	E	65	2.10	95.3
R4.2	E	65	1.93	96.2
R5.1	**A**	**50**	**3.06**	**97.5**
R5.2	**A**	**50**	**2.95**	**97.3**

Centre-point runs are in bold.

Design of Experiment software, MODDE 10.1 (Umetrics AB, Umeå, Sweden) using multilinear models.

Spectral Preprocessing

Near-infrared spectra were recorded continuously during blending. In order to reduce the multiplicative interferences of scatter and physical characteristics of the powder, the raw spectra were preprocessed by standard normal variate (SNV). Afterwards, mean-centering (mncn) of the data matrix was applied for subsequent PCA model. No wavelength truncation was performed prior to the spectral preprocessing and the spectral decomposition.

Algorithm for Blending End-Point Detection

The approach presented in this study is a simple and straightforward method, which uses MSSDT applied to the obtained PCA scores to visualize the blending profile and determine the blending end-point (homogeneity). PCA is a multivariate statistical technique commonly used for variable reduction of data sets (e.g., NIR spectra collected over time). PCA captures the main variation in the spectra with a few PCs. Each spectrum is plotted as a single point in the multidimensional space, resulting in a cluster of single-point spectra in n-dimensional space. The first PC captures the major source of variation within the spectral data, the second PC captures the second greatest source, and so forth, until all relevant sources of variation have been explained.[42,43]

The MSSDT can be used as a tool to determine stability in terms of randomness in a sequence (N) of successive numbers or data points, and hence to determine blend uniformity end-point using the scores for the obtained PCs.[34–37] Stability can be determined by the fluctuations based on the sequence of data points being random or nonrandom distributed. If the sequence of data points shows a random order, the process has reached a stabile statistical phase (is in statistical control), whereas if the numbers indicate a nonrandom order, the blending process has not yet reached a stabile statistical phase. Establishing a null and alternative hypothesis—H_0, data sequence has random variability and H_1 data sequence has nonrandom variability—by employing the MSSDT, it is possible to evaluate whether the sequences of data points are random.

Initially, the estimated population variance of the sequence of data points is calculated by Eq. (2).

$$s^2 = \frac{\Sigma_{i=1}^{N}(X_i - \bar{X})^2}{N-1} \tag{2}$$

where s^2 is the estimated variance of the population, N is the number of data points, X_i the ith element from the population (a PCA score value in this case), and $\bar{X}$ is the population mean.

Next, the MSSDT is employed to evaluate whether the sequence of data points is random. The MSSDT is conceptualized as an alternative unbiased measure of variance that is compared with the estimated population variance, Eq. (3).

$$s_*^2 = \frac{\Sigma_{i=1}^{N-1}(X_{i+1} - X_i)^2}{2(N-1)} \tag{3}$$

Finally, Eq. (4) is employed in order to calculate the test statistic, which is designated as C.[37]

$$C = 1 - \frac{s_*^2}{s^2} \tag{4}$$

In order to accept the null hypothesis (H_0) and conclude that the sequence of data points is random, the absolute value of C must be equal to or lower than the tabled critical value of the C statistic at a defined level of significance. The level of significance used in this study was: $\alpha = 0.05$, and $n = 30$, yielding the critical $C_{0.05,30} = 0.291$.[37] The sufficient number of successive data points (n) was determined by preliminary blending studies (data not shown). If the sequence of data points obeys randomness, the process is finished and the last data point within the current sequence of numbers is an estimate of the time where the process is identified as stable, the blending end-point.

The strategy for determining the end-point of blending is divided in the following steps:

I. During blending, NIR spectra are recorded, preprocessed by SNV and collected into a data matrix that is growing as function of blending time.
II. When blending time in minutes is greater than a preset threshold (0.5 min) and the number of collected spectrum is greater than the preset moving window ($n = 30$), mncn and PCA is applied to the data matrix.
III. The score values of the first PC1 are plotted against process time to visualize the blending profile.
IV. The blending profile is fitted with a first-degree polynomial function with a moving window of $n = 30$ data points.
V. The residuals (sequence of data points) between the first-degree polynomial function and score values (blending profile) are calculated for the moving window.
VI. Null and alternative hypothesis are established, estimated population variance is calculated, and MSSDT is implemented.
VII. If the null hypothesis (H_0) is rejected, blending and NIR-spectral recording continued until the process reaches a predefined maximum time ($K = 20$ min).
VIII. Blend uniformity can be determined when the null hypothesis (H_0) is accepted within the predefined stop time, at which point the blending process is stopped.

A control flow sheet over the described steps for the blend end-point algorithmics is shown in Figure 3.

The obtained blending profiles can be divided into three phases: blending, steady state, and demixing. In the first phase (Fig. 4), there are large, nonrandom fluctuations in the score values. As the blend becomes more homogeneous over time, the fluctuations in the score values decrease. In the second phase (Fig. 4), the blend profile has reached a steady state, where there is equilibrium between blending and demixing rates, which results in the desired homogeneity of the blend. The third phase is dominated by demixing where the blend becomes less homogeneous and the fluctuations (oscillations) in the score values starts to increase again. However, demixing may not occur for all type of formulations (not observed for the profile in Fig. 4). Additionally, no demixing phenomena were observed in any of the blending profiles used in this study,

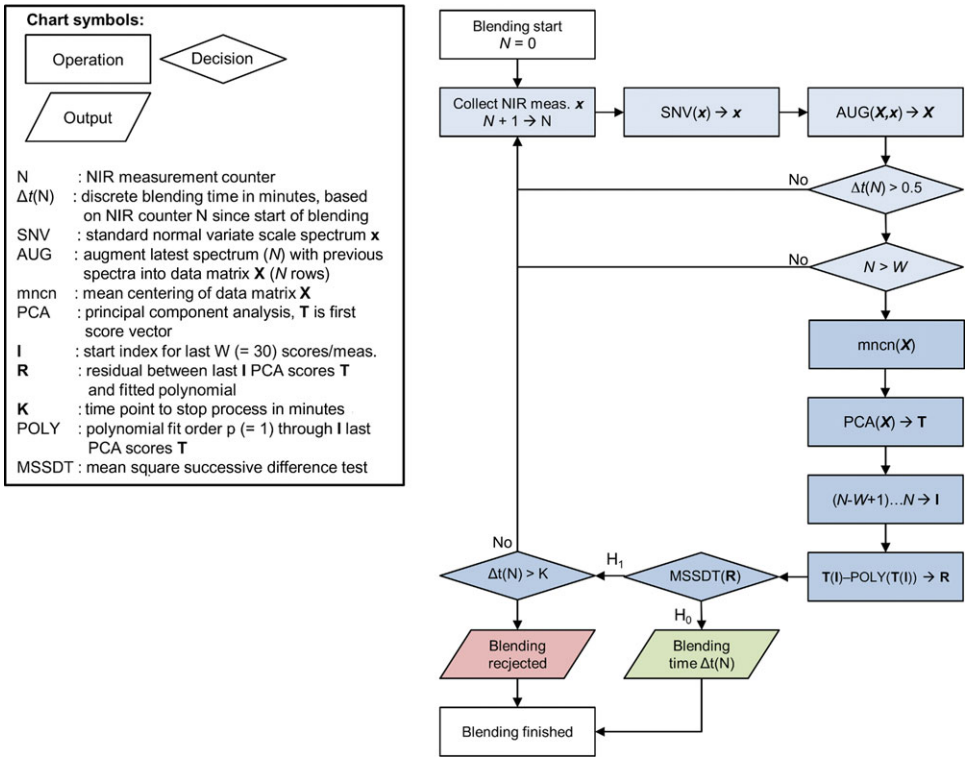

Figure 3. Flow-sheet over developed blend end-point algorithm.

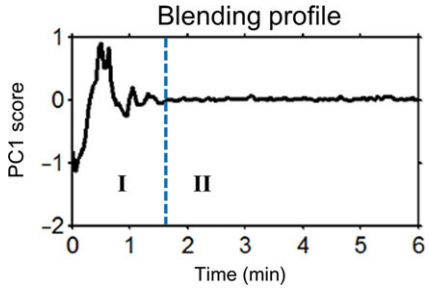

Figure 4. Blending profile (formulation-I) with (a) blending and (b) steady-state phases.

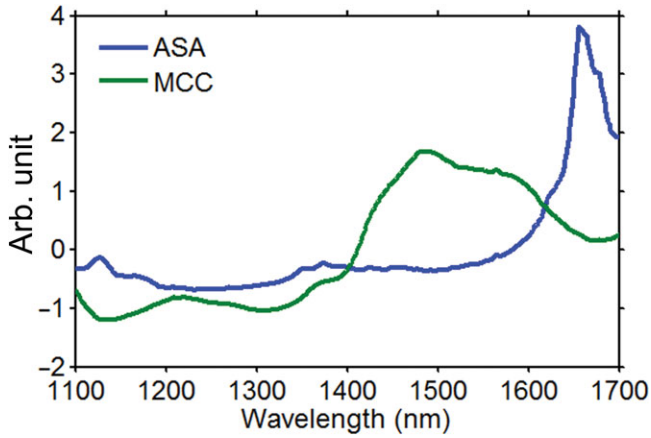

Figure 5. Near-infrared spectra of pure acetylsalicylic acid (ASA) and microcrystalline cellulose (MCC).

as can be appraised by the representative examples shown in Figures 7 and 8.

Reference Analysis of Powder Homogeneity

A standard assay method for ASA was used, albeit with slight modifications.[44] Using a sample thief powder samples (~5 g) were withdrawn at six randomly selected locations within the bin after each blending process has reached estimated blending uniformity end-point. Samples were only withdrawn from the powder surface in order to eliminate segregation. To dissolve the weighed powder samples, 0.1 N NaOH was chosen as solvent. All used chemical and solvent were of analytical grade. ASA concentrations were measured using a spectrometer (Lambda 850; PerkinElmer Company, Waltham, Massachusetts) at 297 nm. A calibration curve for ASA was created and found to be linear over the range 0.01–0.05 mg/mL ($R^2 = 0.99$). In order to evaluate the methods' precision, the calibration was prepared on three different days (RSD < 2.8%).

RESULTS AND DISCUSSION

Monitoring of Blending Process and Detection of End-Point for Initial Formulations

The pure raw spectra of ASA and MCC are depicted in Figure 5. ASA has characteristic bands at 1140 and 1660 nm, where MCC has characteristic bands at 1218 nm and a broad band ranging from 1400 to 1600 nm. The contribution of calcium carbonate in NIR spectra is very small because of the chemical structure of

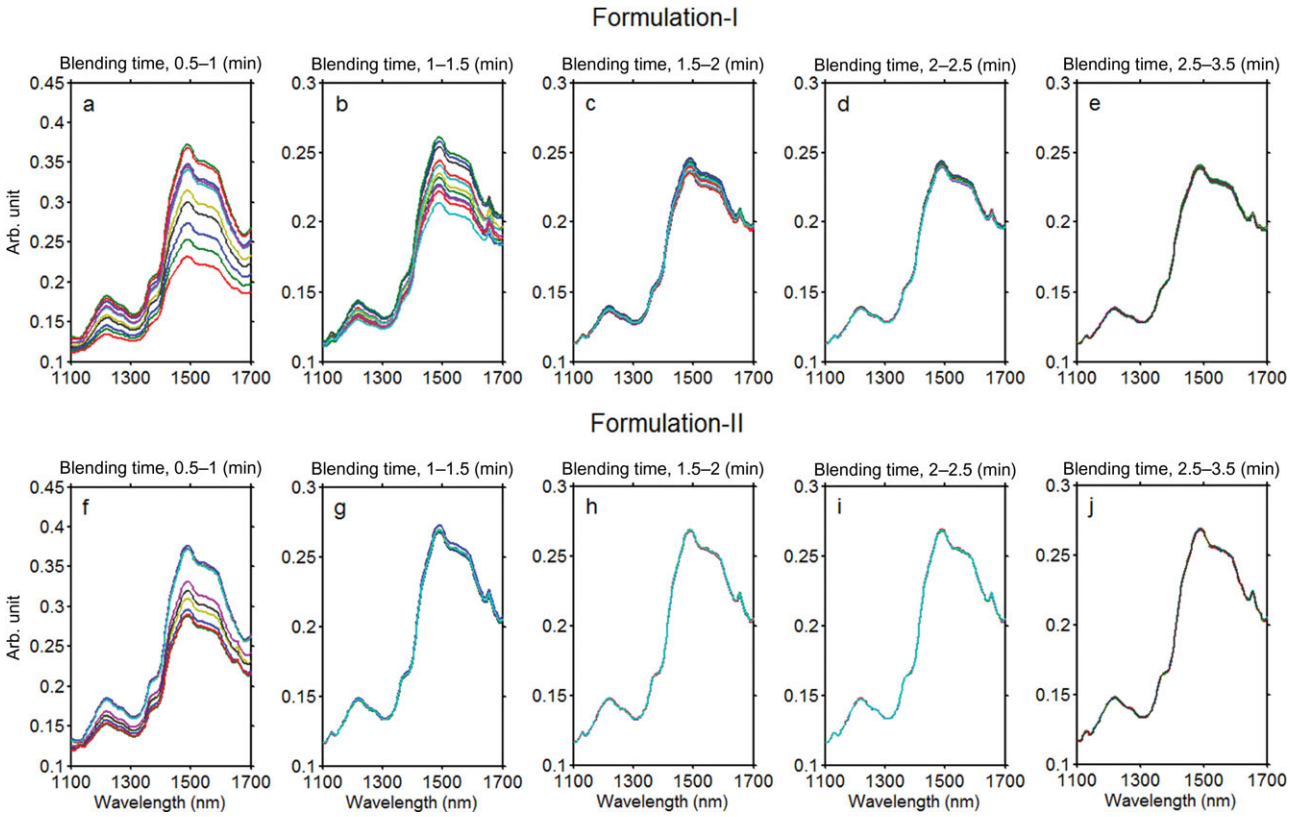

Figure 6. Near-infrared spectral evolution during blending of formulation-I (a–e) and formulation-II (f–j).

calcium carbonate. However, it has a band at 1410 nm related to surface moisture content (data not shown).

Initially, powder formulation-I and formulation-II were blended and monitored by NIRS. The raw spectral evolutions during blending at different blending time intervals (ranging from 0.5 to 3.5 min) are represented in Figures 6a–6e for formulation-I and in Figures 6f–6j for formulation-II, respectively, with a blender fill level of 50%. It is clear to see that the spectral variation decreases faster for formulation-II as compared with formulation-I. The spectral variation of formulation-I becomes stabile after 3.5 min of blending and characteristics band for ASA and MCC are clearly represented (Fig. 6e). In contrast, the spectral variation of formulation-II is already stable after 2 min of blending, where characteristic bands for ASA and MCC are expressed (Fig. 6h). This may indicate that formulation-II reach blending end-point faster compared with formulation-I.

In order to assess the ability of the algorithm in detecting the end-point (homogeneity), PCA was applied. In all cases, one PC was sufficient to explain more than 95% of the total variance (data not shown). Judging from the results in Figure 7, it is clear to see that all replicates of formulation-I need approximately 1.5 min or approximately 30 revolutions to reach a steady state of the blending profile. After reaching the steady state, the mean end-point for formulation-I was detected at 3.1 ± 0.3 min where the extra time is explained by the algorithmic requirement to reach $n = 30$ spectral recordings inside the stable zone of the profile. For comparison, all replicates of formulation-II needs approximately 1 min or approximately 20 revolutions to reach steady state (Fig. 8). The determined mean end-point for formulation-II is 2.0 ± 0.0 min, which is significantly different ($p = 0.02$) from the mean end-point of formulation-I.

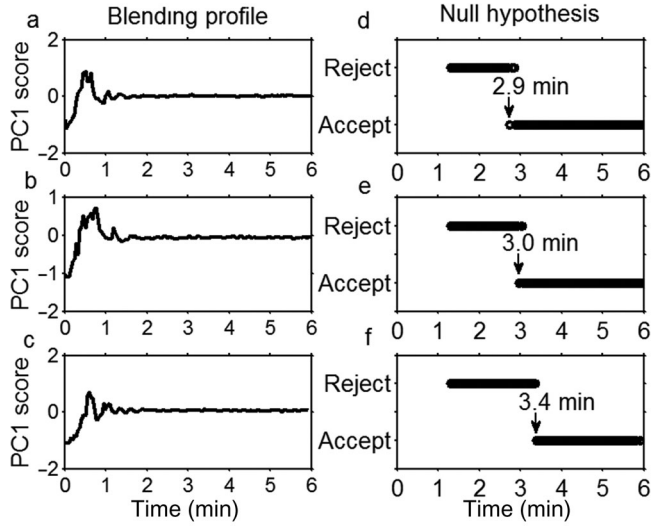

Figure 7. Blending profiles of formulation-I in triplicate. Left and right columns shows blend profile based on the first principal component (PC) and blend uniformity end-point detection.

To confirm the homogeneity of the final blends after reaching their estimated end-point, six powder samples were withdrawn using a thief probe and quantified by UV–Vis spectroscopy. The mean API concentration for formulation-I and formulation-II were 97.5% and 98.1% with corresponding

 DOI 10.1002/jps.24533

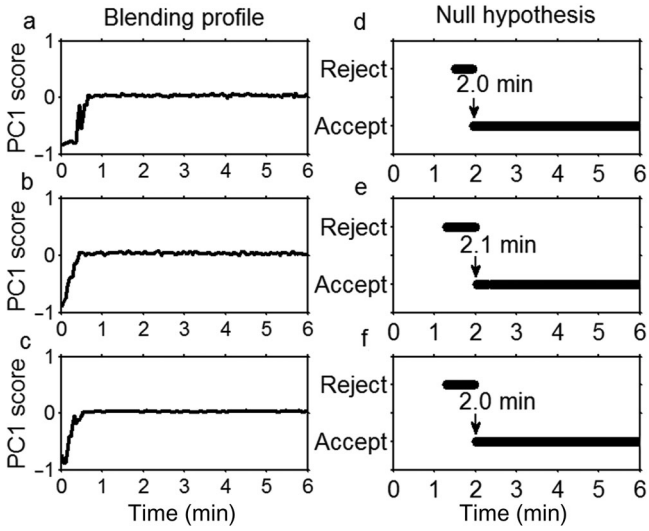

Figure 8. Blending profiles of formulation-II in triplicate. Left and right columns shows blend profile based on the first principal component (PC) and blend uniformity end-point detection.

standard deviations of 2.1% and 2.3%, respectively. These results clearly demonstrate the accuracy of applying NIR and the developed algorithm to determine the blend uniformity end-point.

Flowability of Pure $CaCO_3$ Grades and Powder Formulations

Figure 9 shows the flow function for pure $CaCO_3$-A, $CaCO_3$-E, formulation-I, and formulation-II. As can be seen, the flowability of pure $CaCO_3$-A and $CaCO_3$-E varied between 1.1 ± 0.0 (very cohesive) and 2.3 ± 0.0 (cohesive) and 2.4 ± 0.1 (cohesive) and 5.0 ± 0.1 (easy flowing). However, the consolidation stress interval of interest in this study is between 500 and 1000 Pa, as this interval corresponds closest to the shear stress present in bin blenders of up to 20 L. Using this narrowed interval, $CaCO_3$-A and $CaCO_3$-E are very cohesive and cohesive, respectively. The flowability for formulation-I and formulation-II varied, respectively, between 2.0 0.7 (very cohesive) and 2.1 ± 0.1 (cohesive) and 3.3 ± 0.1 (cohesive) and 4.1 ± 0.2 (easy flowing), in the 500–1000-Pa interval. The main cause as to why we obtain different mean end-points for formulation-I and formulation-II may thus be because of the difference in flow properties of the $CaCO_3$ grades used. Difference in flow properties can be explained by the difference in morphology of the $CaCO_3$ particles. Equant-shaped particles with a smooth surface (i.e., $CaCO_3$-E) will often have a lower frictional interaction and flow more easily compared with angular-shaped particles with a rougher surface (i.e., $CaCO_3$-A), assuming all other features are identical. In addition, particles with rougher surface are more prone to morphological interaction during blending and hence prolonged the blending time compared with smooth particles.

Additional information related to the flow properties of formulation-I and formulation-II can also be obtained from the flow function curve (Fig. 9). As an example, at shear stresses above 1000 Pa, which can be found in a bin blender larger than 20 L, formulation-I changes its flow properties from very cohesive to cohesive and formulation-II moves closer to the free flowing region. This preliminary information may be useful before upscaling, as flow properties have an important impact on the blending process and hence the blend uniformity end-point. However, this is not further investigated in the present study.

Design of Experiments Investigation of $CaCO_3$ Grades and Fillin Level on Blend End-Point

A full factorial experimental design (Table 2) was conducted to investigate how the $CaCO_3$ grades and blending process parameters affect the blend uniformity end-point. Table 2 shows the experimental design and the detected blend uniformity end-point for each run. The statistical significant model terms for the response blend uniformity end-point of the design of experiment are shown in the coefficient plot in Figure 10.

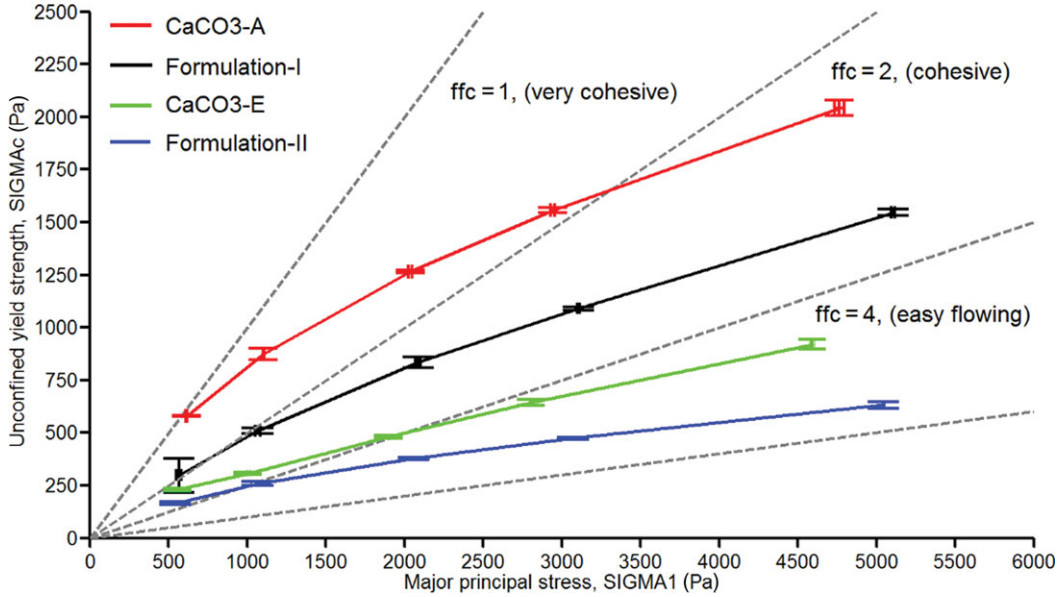

Figure 9. Flow functions of pure calcium carbonate grades and related formulations.

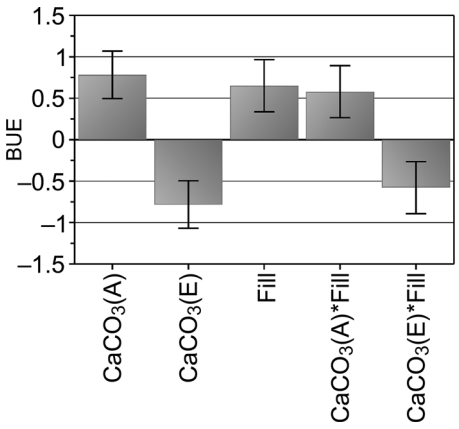

Figure 10. Coefficient plot, where *y*-axis is the response; blend uniformity end-point (BUE) and *x*-axis are the factors and intermediates.

The blending end-point ranged for formulation-I and II from 2.64 to 4.98 min and 1.72 to 2.69 min, respectively, as fill level increases. The coefficient plot (Fig. 10) indicates that $CaCO_3$-A and $CaCO_3$-E had, respectively, a significant positive ($p < 0.001$) and significant negative ($p < 0.001$) effect on the blend uniformity end-point. Formulations composed of $CaCO_3$-E reached the end-point faster as compared with formulations composed of $CaCO_3$-A, when similar process settings were used. As discussed earlier, these differences in end-point are likely because of difference in flow properties of the calcium carbonate grades. The process parameter fill level was significantly positive ($p = 0.02$; Fig. 10), indicating that fill level has an influence on the uniformity end-point. Longer blending times were required to reach the blend uniformity end-point for both formulations runs at the higher filling level (65%); approximately 5 and 2 min were required for runs with CaCO3-A and CaCO3-E, respectively. A theoretical explanation as to why fill level has an influence on blend uniformity end-point may likely be found in the reduced void space in the powder bed at increased fill level. When the powder is loaded into the blender, compression forces because of the weight create a static bed. During blending, shear force becomes active in the blender, which dilates the material in the blender resulting in the expansion of the powder bed. Bed expansion created void spaces that enhance the interparticulate movement and promotes the blending process. A higher fill level will lead to a decreased void space in the bed and more shear force. Consequently, a longer blend time is needed to achieve uniformity.[3] The importance of fill level has previously been investigated, for example, by Muzzio and Llusa[45] and Brone et al.[46] These authors found that as the fill level in a bin blender increased, blending efficiency decreased, and extra blending time was needed to obtain uniformity. The impact of fill level on blending efficiency was greater for shorter blending times. Brone et al.[46] also reported that using blenders with baffles (as used in this study) increased the axial mixing rate and achieved homogeneity slightly faster. Interaction terms, $CaCO_3$-A*Fill and $CaCO_3$-E*Fill, had significant positive ($p = 0.04$) and significant negative ($p = 0.04$) effect on the blend uniformity end-point.

To confirm the homogeneity of the final blends, six powder samples were withdrawn using a thief probe and analyzed by UV–Vis spectroscopy. The blend uniformity concentration results for all formulations in the experimental design are listed in Table 2. The blend uniformity concentration of formulation-I and formulation-II runs ranged, respectively, from 95.3% to 98.9% API and 96.2% to 96.7% API. These results clearly demonstrate the potential of applying NIR and the developed algorithm to determine the blend uniformity end-point.

CONCLUSIONS

In this study, an algorithm based on MSSDT applied to NIR and PCA scores was developed to monitor and determine the blending profile and to statistically assess the end-point in the statistical stabile phase. Two powder formulation batches, formulation-I and formulation-II, with different grade of $CaCO_3$, were weighted and blended in a bin blender. On the basis of the ring shear test results, formulation-II had better flow properties compared with formulation-I, caused by a difference of the $CaCO_3$ morphology. In order to determine the blend uniformity end-point of the powder formulations, the developed algorithm was applied. Formulation-II with higher flowability reached blend uniformity end-point faster compared with formulation-I with lower flowability. Additionally, a design of experiment was conducted to identify how the calcium carbonate grades and fill level affect the blending end-point. The design of experiment revealed that calcium carbonate grades and the fill level have a significant influence on bend uniformity end-point. This study indicates that NIRS together with the developed algorithm and ring shear are powerful tools to determine blend end-point and gain knowledge about the degree of powder flowability.

ACKNOWLEDGMENTS

Milad Khorasani acknowledges the Drug Research Academy (University of Copenhagen) and Takeda Pharma A/S for financial support. The authors also acknowledge funding from The Danish Council for Independent Research (DFF), Technology and Production Sciences (FTP), project 12-126515/0602-02670B. The authors gratefully acknowledge Søren Vinter Søgaard for his help with ring shear measurements.

REFERENCES

1. Maesschalck RD, Sanchez FC, Massart DL, Doherty P, Hailey P. 1998. On line monitoring of powder blending with near-infrared spectroscopy. Appl Spectrosc 52:725–731.

2. Puchert T, Holzhauer CV, Menezes JC, Lochmann D, Reich G. 2011. A new PAT/QbD approach for the determination of blend homogeneity: Combination of on-line NIRS analysis with PC scores distance analysis (PC-SDA). Eur J Pharm Biopharm 78:173–182.

3. Prescott JK, Garcia TP. 2008. Blending and blend uniformity. In Pharmaceutical dosage forms: Tablets; Augsburger LL, Hoag SW, Eds. 3rd ed. New York: Informa Healthcare, pp 111–174.

4. Poux FP, Bertrand M, Bridoux J, Bousquet D. 1991. Powder mixing: Some practical rules applied to agitated systems. Powder Technol 68:213–234.

5. Scheibelhofer O, Balak N, Wahl PR, Koller DM, Glasser BJ, Khinast JG. 2013. Monitoring blending of pharmaceutical powders with multipoint NIR spectroscopy. AAPS PharmSciTech 14:234–244.

6. Fu X, Huck D, Makein L, Armstrong B, Willen U, Freeman T. 2012. Effect of particle shape and size on flow properties of lactose powders. Particuology 10:203–208.

7. Soppela I, Airaksinen S, Murtomaa M, Tenho M, Hatara J, Räikkönen H, Yliruusi J, Sandler N. 2010. Investigation of the powder flow behaviour of binary mixtures of microcrystalline celluloses and paracetamol. J Excip Food Chem 1:55–67.
8. Rippie EG, Faiman MD, Pramoda MK. 1967. Segregation kinetics of particulate solids systems IV. Effect of particle shape on energy requirements. J Pharm Sci 56:1523–1525.
9. Bellamy LJ, Nordon A, Littlejohn D. 2008. Real-time monitoring of powder mixing in a convective blender using non-invasive reflectance NIR spectrometry. Analyst 133:58–64.
10. Sekulic SS, Ward HW, Brannegan DR, Stanley ED, Evans CL, Sciavolino ST, Hailey PA, Aldridge PK. 1996. On-line monitoring of powder blend homogeneity by near-infrared spectroscopy. Anal Chem 68:509–513.
11. Sekulic SS, Wakeman J, Doherty P, Hailey PA. 1998. Automated system for the on-line monitoring of powder blending processes using near-infrared spectroscopy. Part II. Qualitative approaches to blend evaluation. J Pharm Biomed Anal 17:1285–1309.
12. El-Hagrasy AS, Morris HR, D'Amico F, Lodder RA, Drennen JK. 2001. Near-infrared spectroscopy and imaging for the monitoring of powder blend homogeneity. J Pharm Sci 90:1298–1307.
13. Zhang H, Jiang Z, Pi PY, Xu HK, Du R. 2009. On-line monitoring of pharmaceutical production processes using hidden Markov model. J Pharm Sci 98:1487–1498.
14. Wu H, Tawakkul M, White M, Khan MA. 2009. Quality-by-Design (QbD): An integrated multivariate approach for the component quantification in powder blend. Int J Pharm 372:39–48.
15. Wargo DJ, Drennen JK. 1996. Near-infrared spectroscopic characterization of pharmaceutical powder blends. J Pharm Biomed Anal 14:1415–1423.
16. Moes JJ, Ruijken MM, Gout E, Frijlink HW, Ugwoke MI. 2008. Application of process analytical technology in tablet process development using NIR spectroscopy: Blend uniformity, content uniformity and coating thickness measurements. Int J Pharm 357:108–118.
17. Sánchez FC, Toft J, van den Bogaert B, Massart DI, Dive SS, Hailey P. 1995. Monitoring powder blending by NIR spectroscopy. Anal Chem 352:771–778.
18. Igne B, de Juan A, Jaumot J, Lallemand J, Preys S, Drennen JK, Anderson CA. 2014. Monitoring powder blending by NIR spectroscopy. Int J Pharm 473:219–231.
19. Rantanen J, Wikström H, Turner R, Taylor LS. 2005. Use of in line near infrared spectroscopy in combination with chemometrics for improved understanding of pharmaceutical processes. Anal Chem 77:556–563.
20. Skibsted ET, Boelens HF, Westerhuis JA, Witte DT, Smilde AK. 2006. Simple assessment of homogeneity in pharmaceutical mixing processes using a near-infrared reflectance probe and control charts. J Pharm Biomed Anal 41:26–35.
21. El-Hagrasy AS, Drennen JK. 2006. A process analytical technology approach to near-infrared process control of pharmaceutical powder blending. Part III: Quantitative near-infrared calibration for prediction of blend homogeneity and characterization of powder mixing kinetics. J Pharm Sci 95:422–434.
22. Shi Z, Cogdill RP, Short SM, Anderson CA. 2008. Process characterization of powder blending by near-infrared spectroscopy: Blend end-points and beyond. J Pharm Biomed Anal 47:738–745.
23. Sulub Y, Konigsberger M, Cheney J. 2011. Blend uniformity endpoint determination using near-infrared spectroscopy and multivariate calibration. J Pharm Biomed Anal 55:429–434.
24. Storme-Paris I, Clarot I, Esposito S, Chaumeil JC, Nicolas A, Brion F, Rieutord A, Chaminade P. 2009. Near infrared spectroscopy homogeneity evaluation of complex powder blends in a small-scale pharmaceutical preformulation process, a real-life application. Eur J Pharm Biopharm 72:189–198.
25. De Beer T, Burggraeve A, Fonteyne M, Saerens L, Remon JP, Vervaet C. 2011. Near infrared and Raman spectroscopy for the in-process monitoring of pharmaceutical production processes. Int J Pharm 417:32–47.
26. Reich G. 2005. Near-infrared spectroscopy and imaging: Basic principles and pharmaceutical applications. Adv Drug Deliv Rev 57:1109–1143.
27. Roggo Y, Chalus P, Maurer L, Lema-Martinez C, Edmond A, Jent N. 2007. A review of near infrared spectroscopy and chemometrics in pharmaceutical technologies. J Pharm Biomed Anal 44:683–700.
28. Drennen JK, Ciurczak EW. 2014. Blend uniformity analysis. In Pharmaceutical and medical applications of nearinfrared spectroscopy; Ciurczak EW, Igne B, Eds. 2nd ed. London, UK: CRC Press, pp 33–54.
29. Blanco M, Cueva-Mestanza R, Cruz J. 2012. Critical evaluation of methods for end-point determination in pharmaceutical blending processes. Anal Meth 4:2694.
30. Virtanen S, Antikainen O, Yliruusi J. 2007. Uniformity of poorly miscible powders determined by near infrared spectroscopy. Int J Pharm 345:108–115.
31. Huang J, Kaul G, Cai C, Chatlapalli R, Hernandez-Abad P, Ghosh K, Nagi A. 2009. Quality by design case study: An integrated multivariate approach to drug product and process development. Int J Pharm 382:23–32.
32. Hembree B. Assessing process stability. In NIST/SEMATECH e-handbook of statistical methods. Accessed February 21, 2014, at: http://www.itl.nist.gov/div898/handbook/ppc/section4/ppc45.htm.
33. FDA. 2006. ICH harmonised tripartite guideline: Quality risk management Q9. Accessed February 12, 2015, at: http://www.fda.gov/downloads/Drugs/GuidanceComplianceRegulatory Information/Guidances/ucm073511.pdf.
34. Moore PG. 1955. The properties of the mean square successive difference in samples from various populations. J Am Stat Assoc 50:434–456.
35. Keen J, Page DJ. 1953. Estimating variability from the differences between successive readings. J Roy Stat Soc C-App 2:13–23.
36. Bingham RS. 1968. Approximations for mean square successive difference critical values. Technometrics, Taylor & Francis, 4 Park Square, Milton Park, Abingdon, Oxfordshire, England 10:397–400.
37. Zar HJ. 2010. Serial randomness measurements: Parametric testing. In Biostatistical analysis. 5th ed. Northern Illinois University, New Jersey, US. pp 599–602.
38. United State Pharmacopoeia. 2012. Physical tests, optical microscopy, USP37, N32S2.pp 389–391.
39. Schultze D. 2008. Powders and bulk solids: Behavior, characterization, storage and flow. 1st ed. Berlin, Germany: Springer.
40. Teunou E, Fitzpatric. 1999. Effect of relative humidity and temperature on food powder flowability. J Food Eng 42:109–116.
41. Jenike AW. 1964. Storage and flow of solids. 1st ed. Utah: University of Utah, Salt Lake City, US.
42. Joanna LS, Gilmore IS. 2009. Principal component analysis. In Surface analysis—The principal techniques; Vickerman JC, Gilmore IS, Eds. 2nd ed. pp 571–579.
43. Brereton RG. 2002. Principal component analysis. In Chemometrics: Data analysis for laboratorty and chemcial plant; Brereton RG Ed. 1st ed. New York: Wiley, pp 190–200.
44. Bharate SS, Kolhe SR, Bharate SB. 2011. Development of validated spectrophotometric method for simultaneous estimation of acetylsalicylic acid and caffeine in pure and tablet dosage form. J Adv Sci Res 2:34–41.
45. Muzzio F, Llusa M. 2005. The effect of shear mixing on the blending of cohesive lubricants and drugs. Pharm Tech 12:36–45.
46. Brone D, Alexander A, Muzzio F. 1998. Quantitative characterization of mixing of dry powders in V-blenders. AIChE J 44:271–278.

II

Journal of Pharmaceutical and Biomedical Analysis 109 (2015) 11–17

Contents lists available at ScienceDirect

Journal of Pharmaceutical and Biomedical Analysis

journal homepage: www.elsevier.com/locate/jpba

Visualization and prediction of porosity in roller compacted ribbons with near-infrared chemical imaging (NIR-CI)

M. Khorasani [a], J.M. Amigo [b], J. Sonnergaard [a], P. Olsen [c], P. Bertelsen [c], J. Rantanen [a,*]

[a] Department of Pharmacy, Faculty of Health and Medical Sciences, University of Copenhagen, Denmark
[b] Department of Food Science, Faculty of Science, University of Copenhagen, Denmark
[c] Takeda Pharma A/S, Roskilde, Denmark

ARTICLE INFO

Article history:
Received 13 October 2014
Received in revised form 4 February 2015
Accepted 5 February 2015
Available online 14 February 2015

Keywords:
Roller compaction
NIR chemical imaging spectroscopy
Porosity
Principal component analysis
Partial least square

ABSTRACT

The porosity of roller compacted ribbon is recognized as an important critical quality attribute which has a huge impact on the final product quality. The purpose of this study was to investigate the use of near-infrared chemical imaging (NIR-CI) for porosity estimation of ribbons produced at different roll pressures. Two off-line methods were utilized as reference methods. The relatively fast method (oil absorption) was comparable with the more time-consuming mercury intrusion method (R^2 = 0.98). Therefore, the oil method was selected as the reference off line method. It was confirmed by both reference methods that ribbons compressed at a higher pressure resulted in a lower mean porosity. Using NIR-CI in combination with multivariate data analysis it was possible to visualize and predict the porosity distribution of the ribbons. This approach is considered important for process monitoring and control of continuously operating roller compaction line.

1. Introduction

Roller compaction is a widely applied dry granulation method used within pharmaceutical industry due to cost-effectiveness and the ability to produce free flowing agglomerates without using any solvents or heat. During roller compaction, starting material with small particle size is compressed between two counter rotating rollers into a dense ribbon. Subsequently ribbons are milled through screens to achieve a desired granule size distribution. One of the main advantages of roller compaction is the possibility for continuous manufacturing and thereby achieving faster throughput time and lower operational and maintenance costs [1,2].

The most important physical parameter as critical quality attribute (CQA) for roller compacted ribbons is the porosity (i.e., relative density or solid fraction) [3]. It has been demonstrated that ribbons with various porosities can influence subsequent process units (e.g. granulation and tableting). Ribbons with a higher porosity lead to granules with reduced flowability and hence, tablets with reduced tablet quality [4]. The most prominent critical process parameter (CPP) influencing the ribbon porosity is, roll pressure. Ribbons compacted at higher pressure were found to have a lower mean porosity and higher strength, due to densification and bonding between particles [3,5]. Another CPP, which has shown to influence the ribbon porosity is the screw feed rate. It has been shown that at constant feed screw speed, the last flight of the spiral feed screw creates fluctuations in the powder flow during feeding to the rolls, causing heterogynous porosity (relative density) distribution through the ribbon width and length [5]. This phenomenon is common for roller compactors with horizontal-feeding systems, were higher feed screw speed leads to higher ribbon porosity [2,6–8].

Traditional analytical methods for porosity measurements, such as mercury intrusion porosimetry and gas pycnometry are destructive and time consuming methods which cannot provide any information regarding the spatial distribution of porosity. Therefore, it is crucial to develop new methods for ensuring the desired product quality by monitoring the CQAs during the process. By using process analytical technology (PAT) tools such as near infrared spectroscopy (NIRS) or near infrared chemical imaging (NIR-CI) in combination with multivariate data analysis, one can obtain real-time process information that can be used to implement improved control strategies and better process understanding of the manufacturing process. Previous studies have demonstrated the feasibility of NIRS and NIR-CI as tools for real-time monitoring of several CQAs, e.g. content uniformity, water content and relative density from varying dosage forms [9–12]. Nevertheless,

* Corresponding author at: Department of Pharmacy, Faculty of Health and Medical Sciences, University of Copenhagen, Universitetsparken 2, 2100 Copenhagen, Denmark. Tel.: +45 35336585.
E-mail address: jukka.rantanen@sund.ku.dk (J. Rantanen).

http://dx.doi.org/10.1016/j.jpba.2015.02.008
0731-7085/

NIRS is a single point spectroscopic technique and e.g. patterns of homogeneity are not usually reflected in such measurements, because a bulk NIR spectrum represents an average composition of the measured sample. Other imaging techniques such as, Terahertz Pulsed Imaging has also been used for measuring the tablet hardness and density distribution [13]. However, NIR-CI is a faster method and has a higher spatial resolution compared to Terahertz Pulsed Imaging [14].

Previous studies have demonstrated the feasibility of NIRS and NIR-CI as tools for real-time monitoring of several CQAs, e.g. content uniformity, water content and relative density from varying dosage forms [9–12,15]. Previously, Lim et al. [8] has used NIR-CI to study the porosity distribution of single ingredient, roller compacted ribbons. They related the mean spectral absorbance at a single wavelength for different ribbons with their measured reference porosity values.

Generally when analysing NIR images, it is crucial to ensure that the measured signal is not influenced by other sources of variation. Hence, only the spectral information related to the analyte of interest should be correlated with the information from the analyte. If other sources of variation contribute to the signal, the results will be biased and it might be challenging to detect possible incorrect results. Also, when working with samples containing more than one ingredient, the NIR spectra are composed of broad and highly overlapped bands, which make it more difficult to find distinct and selective absorption bands for each ingredient in the sample. These limitations are overcome by applying a multivariate data analysis approach, which is able to use the entire spectral profile to extract the useful information from the whole data cube [16–21].

The aim of this study is to investigate the viability of NIR-CI for porosity estimation of ribbons produced using roller compaction. Two off-line methods were looked upon as reference. The relatively fast method (oil absorption) was comparable with the more time-consuming mercury intrusion method ($R^2 = 0.98$). It was confirmed by both reference methods that ribbons compressed at a higher pressure resulted in a lower mean porosity. For the NIR-CI the oil absorption method was selected as reference method, since this method is fast, low cost and non-toxic, compared with mercury intrusion method.

Finally, a surrogate method based on NIR-CI and multivariate data analysis (principal component analysis (PCA) and partial least squares (PLS) regression) was investigated to visualize the porosity distribution and estimate the mean porosity value of roller compacted ribbons. The model ribbons were prepared from either pure microcrystalline cellulose (MCC) or from a mixture of model active pharmaceutical ingredient (API) and microcrystalline cellulose.

2. Experimental

2.1. Materials

The pure model roller compacted ribbons were produced with microcrystalline cellulose (MCC), Comprecel® PH 101 USP grade (MINGTAY Chemical, Taoyan city, Taiwan) and mixed model roller compacted ribbons were produced with a powder formulation of 60% (w/w) MCC and 40% (w/w) acetylsalicylic acid (ASA) USP grade, (Rhodine 3080, Rhodia, Saint-Fons, France) as the active pharmaceutical ingredient, API. All weighed components, were blended for 3.5 min at 23 rpm in a Bohle bin blender (Bohle LM 40, Bohle Machinen & Verfahren GmbH, Haan, Germany).

2.2. Roller compaction

Roller compacted ribbons were prepared using a lab-scale roller compactor (Alexanderwerk® WP120 Pharma, Alexanderwerk GmbH, Remscheid, Germany) mounted with two counter rotating smooth surface rolls of 12 cm diameter and 4 cm wide and a single horizontal feed screw. For the experiments, the roll gap and roll speed were kept constant, respectively 2.5 cm and 6 rpm. The roller compactor was set at the automatic mode, whereas the speed of the feed screw was automatically adjusted through a control circuit to keep the gap constant. In order to produce ribbons with porosity variation seven roll pressure (RP) conditions were analyzed (2.5, 3.5, 4.5, 5.5, 6.5, 8.5, 10.5 MPa) for the pure ribbons (PuRs) and five RP conditions were analyzed (2.5, 3.0, 4.0, 5.0, 6.0 MPa) for the mixed ribbons (MixRs). Ribbons were collected after the roller compacter had reached a steady state (2–3 min). For PuR and MixR, respectively six and three ribbon samples of each ribbon settings were collected for porosity and NIR-CI measurements. Prior to investigations the ribbons were stored for at 25 °C and 45% relative humidity (RH).

2.3. Porosity measurements

2.3.1. Mercury intrusion method

The porosity, bulk density and true density of ribbon were determined using mercury intrusion porosimeter (AutoPore® IV 9510, Micromeritics Instruments Inc., Norcross, GA, USA). The mercury intrusion method was applied as a reference method. Three ribbon samples where each having width and length of, respectively of ~4 and ~14 cm, was collected for each experimental setting. In order to fill the sample chamber each ribbon was cut into smaller sections and weighted. A 3 cc penetrometer was used as sample chamber. The sample chamber contain ribbon were subjected to a pressure cycle starting at approximately 3.4×10^{-3} MPa, increasing to 413.7 MPa in predefined steps to give pore size/pore volume information.

2.3.2. Oil absorption method

Mercury intrusion is relatively slow and difficult technique to be applied as a routine reference technique. For that reason, faster and less toxic method would be needed. In the oil absorption method, three ribbon samples with a width and length of, respectively of ~4 and ~14 cm, were collected for each experimental setting. Ribbons were weighed and subsequently placed in a petri dish containing liquid paraffin oil (Ph. Eur. grade; Sigma–Aldrich, St. Louis, MO, USA). The petri dish was transferred into a desiccator and the vacuum was applied for 15 min. The vacuum was released and the samples were allowed to absorb oil into their internal pores for 30 min. The excess of oil was removed by wiping the ribbons cautiously with a Kleenex paper. The oil saturated ribbons were weighed and the weight gain (finally, volume of oil) of ribbons was used to estimate the pore volume using the oil density. Optimal experimental time conditions and selection of oil were determined based on a design of experiment study (data not shown). The ribbon porosity for the oil absorption method is calculated by Eq. (1)

$$P_{\text{Oil absorption}}\% = \frac{V_{\text{oil}}}{V_{\text{oil}} + V_{\text{ribbon}}} \times 100 \quad (1)$$

where $P_{\text{Oil absorption}}\%$ is the ribbon porosity measured by oil absorption method, V_{oil}, is the volume of oil absorbed and V_{ribbon}, is the volume of the ribbon and is calculated by dividing the weight of the unsaturated ribbon by the true density measured by gas pycnometer.

2.4. Instrumentation and data acquisition

Offline NIR-chemical images of roller compacted ribbons were obtained with a spectrometer (Headwall Photonics model 1002A-00371). This NIR chemical imaging camera is a prototype kindly provided by FOSS (FOSS A/S, Hilleroed, Denmark). NIR-chemical

images of roller compacted ribbons were recorded in the wavelength range of 1100–1700 nm. The spectrometer was adapted to a line mapping configuration with a line of 320 pixels and pixel dimensions of 312 μm × 50 μm. Spectra were recorded in the diffuse reflectance mode. Spectra were recorded in the diffuse reflectance mode.

2.4.1. Spectral correction

NIR-CI image data processing was performed by using MATLAB 7.1 (The Math-Works, Natick, MA, USA) software and in-house routines under the name of HYPER-Tools (freely available on demand) together with PLS Toolbox (Eigenvector Research Inc., Wenatchee, WA, USA). Since NIR-CI measurement is combined with information from both the sample and the instrument, background correction for the instrument information is necessary. The high reflectance standard Spectralon TM (Labsphere Inc., North Sutton, NH, USA) was used as background reference. Areas containing non-sample information were eliminated by masking. Savitzky–Golay smoothing with window size of 13 and polynomial order of 2 together with mean-centering was applied as pre-processing methods.

2.4.2. Unfold 3D hyperspectral data cube

NIR chemical image is a three-dimensional (3D) hyperspectral data cube. For the structure of D (*XxYxλ*), the *X* and *Y* axes represent spatial (pixel) information and the λ axis corresponds to the wavelength. Prior data processing it is necessary to unfold the 3D hyperspectral data cube to two-dimensional (2D) data matrix in which each row is a spectrum (sample) related to one of the pixels, D (*XYxλ*). The 2D data matrix is pre-processed by mean centring and refolded to the 3D hyperspectral cube after data analysis, where the chemical image can be obtained. Once all 3D hyperspectral cubes of ribbons are processed an overall chemical image can be created by adding individual images together.

2.4.3. Data analysis

Two principal component analysis (PCA) models were developed for PuR and MixR, in order to gain an insight into the variation between each ribbon settings. Each score vector can be re-folded to a score surface image in order to illustrate the relative distribution map for each principal component (PC). By including the loading vectors and corresponding score surface image, it is possible to relate each PC with any variability source in the sample [16,22]. Afterward, two partial least squares (PLS) regression models, based on respectively, PuR and MixR were developed to predict ribbon porosity using oil absorption method as reference method. PCA-models and PLS-models were developed using MATLAB 7.1 (The Math-Works, Natick, MA, USA) software and the toolbox HYPER-Tools.

3. Results and discussion

3.1. Porosity measurements

The average porosity of pure ribbons (PuRs) was determined by oil absorption methods (OAM) and mercury intrusion method (MIM) (Table 1). The average porosity of ribbons from different roller compaction settings ranged from 12.1 to 26.4, (%) porosity. Roller compacted ribbons compacted at a higher roll pressure lead to the formation of stronger ribbons with lower porosity. Similar findings have been reported earlier [2,6,23].

In order to assess the accuracy of the OAM, the porosity results were correlated with the porosity results obtained by MIM by a simple linear regression model, depicted in Fig. 1. The *R*-square (R^2 = 0.98) value indicates a good correlation.

Table 1
Summary of mean porosity values (in terms of percentage) for pure microcrystalline cellulose ribbons, (standard deviation between brackets).

Batch ID#	Roll pressure (MPa)	Oil absorption method (SD, *n* = 3)	Mercury intrusion method (SD, *n* = 3)
PuR2.5	2.5	25.6 (±0.5)	26.4 (±0.5)
PuR3.5	3.5	21.8 (±0.8)	22.1 (±0.5)
PuR4.5	4.5	20.2 (±0.6)	19.2 (±0.3)
PuR5.5	5.5	18.4 (±0.8)	18.8 (±0.3)
PuR6.5	6.5	17.7 (±0.7)	16.5 (±0.3)
PuR8.5	8.5	16.6 (±0.7)	14.1 (±0.2)
PuR10.5	10.5	15.5 (±0.4)	12.1 (±0.4)

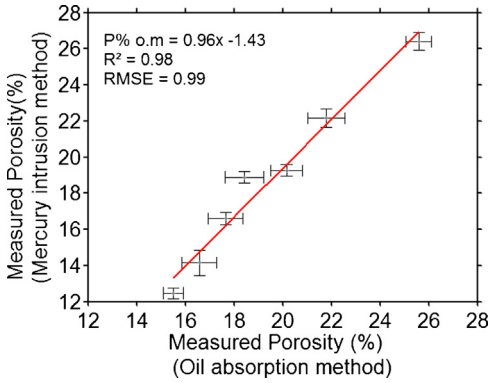

Fig. 1. Oil absorption method and Mercury intrusion.

The OAM results may be affected by several factors influencing the obtained porosity results. These factors include possible incomplete saturation of oil, dissolving of ribbon in the oil and inefficient removal of oil from the ribbon surface prior weighing. However the influences of the aforementioned factors are considered small in this study. The OAM is a low-cost and non-toxic alternative method for porosity measurement. It is also simple and fast to implement and feasible for routine measurements. In order to save time and reduce the porosity measurement expenses the OAM will be considered as the main porosity technique through this study. The average porosity and percent relative standard deviation of mixed ribbons (MixR) were determined by OAM shown in Table 2. The average porosity of ribbons from different roller compaction settings ranged from 10.7 to 17.8, (%) porosity.

Roller compacted ribbons compacted at a higher roll pressure lead to the formation of ribbons with lower porosity.

3.2. Near chemical imaging and principal component analysis

Near infrared reflectance spectroscopy is known to contain information related to both chemical and physical properties of the roller compacted ribbons. In this study the physical variability is the most interesting. In Fig. 2a, the NIR spectra of pure MCC and ASA are presented, and Fig. 2b and c presents the average NIR spectra of each ribbon settings, both pure ribbons (PuRs) and mixed ribbons (MixRs). The NIR spectra are sensitive to compaction pressure

Table 2
Summary of mean porosity values (in terms of percentage) for mixed ribbons (standard deviation between brackets).

Batch ID#	Roll pressure (MPa)	Oil absorption method (SD, *n* = 3)
MixR2.5	2.5	17.8 (±0.7)
MixR3.0	3.0	16.7 (±0.4)
MixR4.0	4.0	14.3 (±0.7)
MixR5.0	5.0	12.3 (±0.2)
MixR6.0	6.0	10.7 (±0.3)

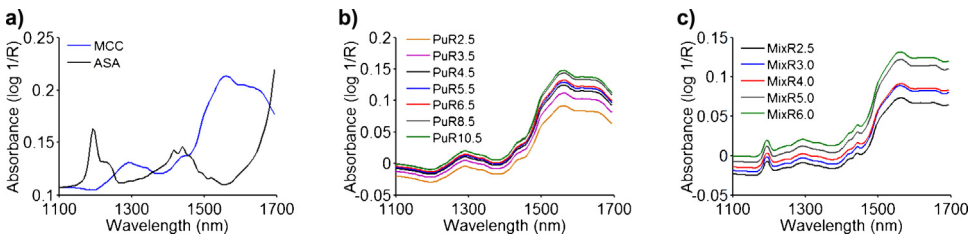

Fig. 2. (a) Pure NIR-spectrum of microcrystalline cellulose (MCC) and acetylsalicylic acid (ASA) powder. (b) and (c) Spectra of roller compacted ribbons of respectively pure and mixed ribbon. For both ribbon formulation an upward spectral shift is seen due to higher roll pressure.

and higher compaction pressure leads to increase in the apparent slope and a baseline shift. As compression force increases, ribbon gets denser and porosity decreases due to a decrease in the air-particle boundary surface and thereby diffuse scattering decreases and ultimately, less light will reach the detector [24].

Which results to an apparently higher absorbance, especially at longer wavelengths [24,25]. These findings are consistent with the literature, where e.g. Kirsch and Drennen [26] observed upward baseline shifts when using single point NIRS as the tablet compaction pressure increased. This effect can be used to study the porosity phenomena in ribbons.

Two individual principal component analysis (PCA) models were used for identifying the main variation within NIR-CIs of PuRs and MixRs in the spectral range from 1100 to 1700 nm. The PC1 for PCA-model-PuR explained 96.3%, of the variation. In order to explain the variation captured by the PCA model one should investigate the score surfaces image (Fig. 3a) and corresponding loading (Fig. 3b). For every pixel (spectra) a score value is obtained, which is the weight of its corresponding loading present in the pixel. The PC1 loading is highly correlated to the pure spectrum of MCC, shown in Fig. 2a). The loading plot shows positive features at 1290 and 1562 and a shoulder at 1442 nm which are respectively corresponding to the NIR bands of pure MCC and water in MCC [27]. An upward shift can be observed for the loading at longer wavelengths (1650–1700 nm).

The variation captured by the first principal component can be related to the physical variation (porosity variation), since there is no chemical variation in PuRs. This is evident from the score surface image, as depicted in Fig. 3a, and less porous ribbons tend to have regions with higher score values, which are related to less porous regions. High score values are represented by the dark red colour and low score values by the dark blue colour. The PC2 and PC3 loadings explained respectively 3.1% and 0.6% (data not shown) of the variation; however, these PCs did not include any additional information.

The score surfaces image and loading of PC1 for PCA-model-MixR is depicted in Fig. 4a and b, respectively. The PC1 explained 95.1%, of the variation and is highly correlated to the average spectrum of MCC and ASA. The features at 1190 nm and a shoulder at 1417 nm are corresponding to the bands of the pure ASA, Fig. 2a. The peak at 1290 nm is related to the bands of pure MCC, Fig. 2a. Overlapping peaks between ASA and MCC are observed at 1442 nm and from 1562 to 1700 nm. The variation obtained by the PC1 loading is mainly due to baseline shift caused by physical variation (porosity variation). By looking into the score surface image in Fig. 4a, ribbons compacted at higher pressure tend to have narrow regions associated with higher score values, which can correspond to less porous regions. The score surface image and loading of PC2, depicted in Fig. 4c and d, respectively. The PC2 loading explained 3.7%, of the variation and pattern of this loading is very similar to the pure ASA spectrum. It can be assumed that the score image in Fig. 4c, provide the ASA distribution information. The score surfaces image and loading of PC3 is depicted in Fig. 4e and f, respectively. The features from 1200 to 1380 nm in the PC3 loading could be related to the MCC content, since the pure MCC spectrum has similar absorption region. However, care should be taken since the explained variation

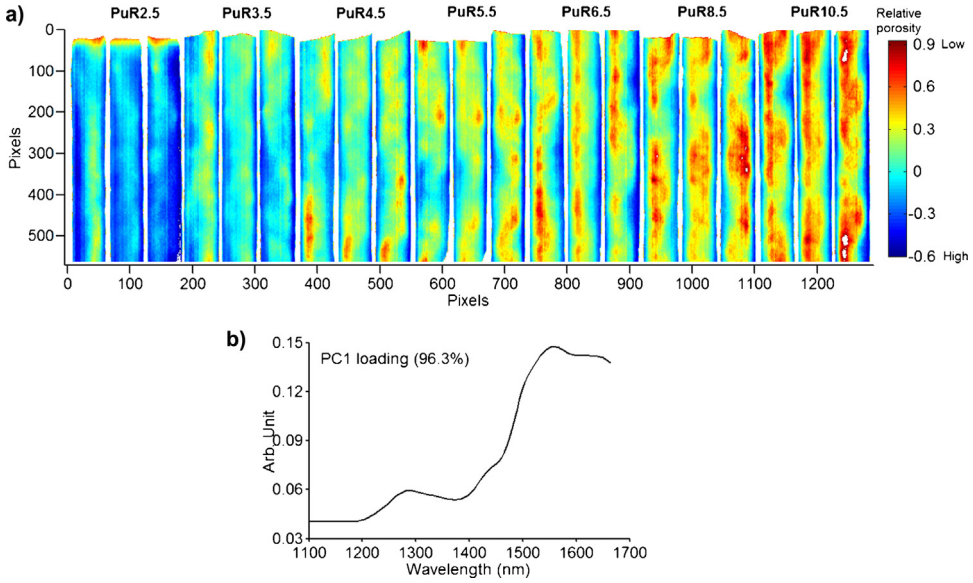

Fig. 3. (a) and (b), represents, respectively, the score surface image and loading plot of the first principal component PC1 of pure MCC ribbons compacted at different pressures. Dark red colour indicates higher score values, were dark blue colour indicates low score values. Width and length of the ribbons approx. 35 and 140 mm, respectively. (For interpretation of the references to colour in this figure legend, the reader is referred to the web version of this article.)

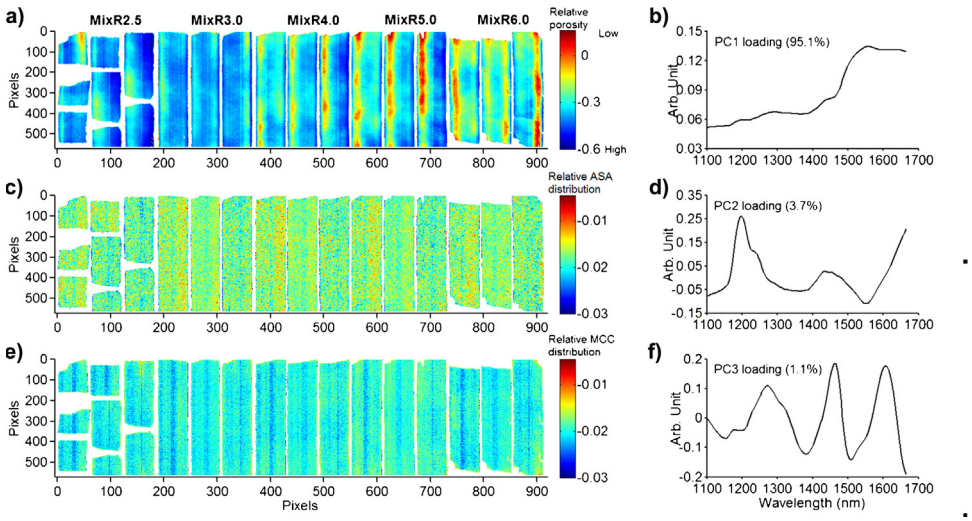

Fig. 4. (a, c, e) and (b, d, f), represents, respectively, the score surface images and loading plots of the first, second and third principal components of the mixed ribbons compacted at different pressures. Dark red colour indicates higher score values, were dark blue colour indicates low score values. Width and length of the ribbons approx. 35 and 140 mm, respectively. (For interpretation of the references to colour in this figure legend, the reader is referred to the web version of this article.)

is 1.1%. Based on Fig. 4c and d, it can be verified that the variation seen in Fig. 4a is not a consequence of de-mixing but porosity variation.

The score surface image demonstrated in Figs. 3a and 4a, shows heterogeneous porosity regions within each roller compacted ribbon. Roller compacted ribbons produced at higher compression pressure (less porosity) are associated with higher heterogeneity.

Guigon and Simon found that the feed screw results in heterogeneous porosity distribution along the roller-compacted ribbons caused by non-continuous densification feeding process [5]. Based on our results, the non-continuous densification feeding process may be amplified at higher compaction pressures.

3.3. Partial least squares modelling

In order to evaluate the feasibility of the application of NIR-CI for the prediction of ribbon porosity for PuRs and MixRs, two PLS-models, respectively, PLS-model-PuR and PLS-model-MixR were developed and evaluated. NIR-CIs were used as the *X* variables and single point porosity values (determined by the OAM), were used as the *y* variable. The correct number of latent variables (LVs) of the PLS models were assessed by The Root Mean Square Error of Calibration (RMSEC) and Cross-Validation (RMSECV), indicating the fit between NIR spectra and porosity values. Cross-validation was done by full cross-validation and the Root Mean Square Error of Cross Validation (RMSECV) was calculated. The PLS-model-PuR

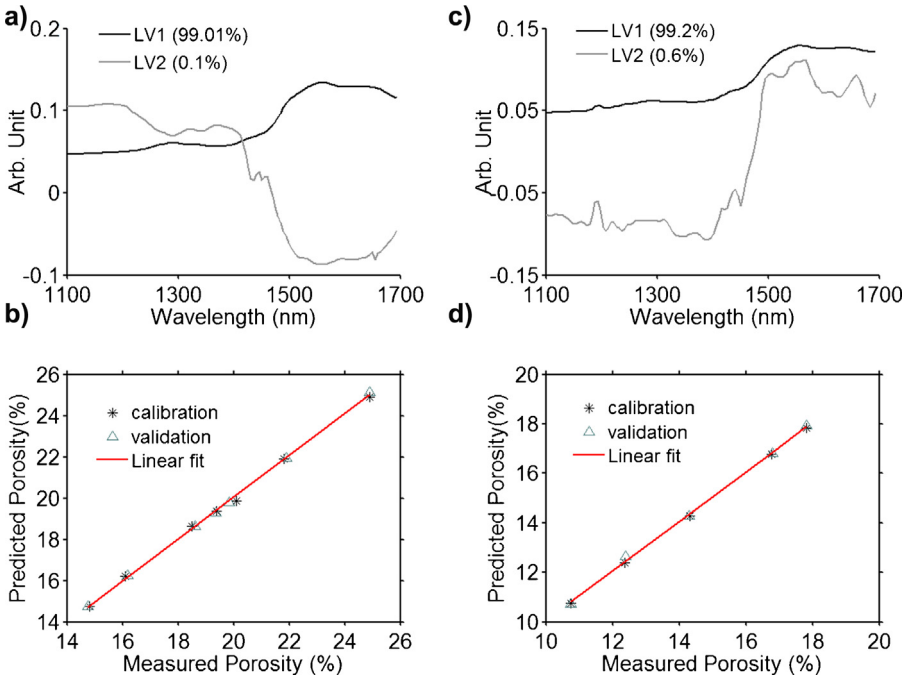

Fig. 5. (a) and (b), represents, respectively, the latent variable plot and the PLS regression of the pure MCC ribbons compacted at different pressures. Where (c) and (d) represents, respectively, the latent variable plot and the PLS regression of the mixed ribbons compacted at different pressures.

Table 3
Overview of the calibration results obtained for the PLS-models.

PLS-model	R^2 cal.	Number of latent variables	Explained variation	RMSEC	RMSECV
PuR	0.98	2	99.6%	0.42%	0.55%
MixR	0.98	2	99.8%	0.46%	0.64%

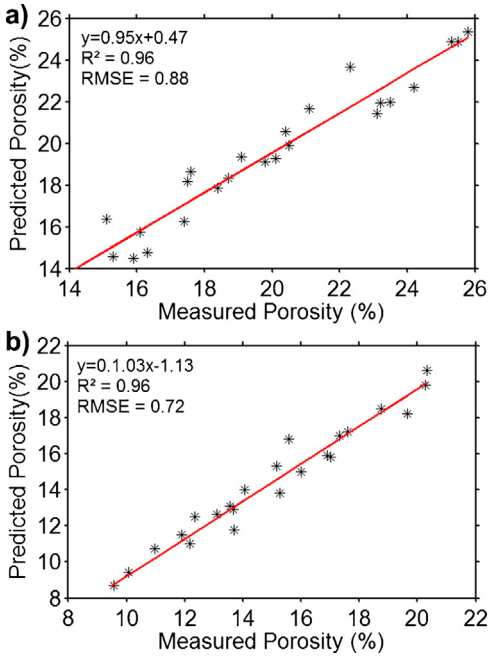

Fig. 6. (a) and (b) Correlation of the predicted porosity and the lab measured porosity (oil absorption method) for respectively, pure ribbons and mixed ribbons.

resulted in two latent variables (Lvs), explaining 99.6% of the variation (Fig. 5a). The calibration- and prediction error for this model are each small (R^2 = 0.98, RMSEC = 0.42%, RMSECV = 0.55%), shown in Table 3 and Fig. 5b.

The PLS-model-MixR resulted in two sufficient LVs, explaining 99.8% of the variation (Fig. 5c). The calibration- and prediction error for this model are each small (R^2 = 0.98, RMSEC = 0.46%, RMSECV = 0.64%), shown in Table 3 and Fig. 5d. In order to test the reliability of each PLS-model, two independent test sets of smaller ribbon sections (n = 23) were used (one for each PLS-model). Each ribbon within the test-sets was measured by NIR-CI and the porosity result was predicted by the corresponding PLS-model, and plotted against the single point porosity measured by OAM via simple linear regression model. Two prediction curves for respectively PuR and MixR, Figs. 6a and 6b, are obtained with strong correlation of R^2 = 0.96 for both curves. Therefore NIR-CI is able to characterize differences in porosity as a function of position on the ribbon and predict the porosity of the roller compacted ribbon.

4. Conclusions

In this study, the physical properties of ribbons with varying porosity were visualized using NIR chemical imaging. Further, it was also demonstrated that the use of oil absorption method for measuring the ribbon porosity is a robust and safe alternative reference technique as compared to the mercury intrusion method. Finally, it was demonstrated that NIR-CI in combination with multivariate data analysis can be used as a non-destructive tool to visualize the porosity distribution and determine porosity values of pure and mixed ribbons. This has potentially a large impact on quality control of continuously operating manufacturing lines, such as roller compaction process.

Acknowledgements

Milad Khorasani is acknowledging the Drug Research Academy (University of Copenhagen) and Takeda Pharma A/S for financing of the Ph.D. studies. Authors also acknowledge the funding from The Danish Council for Independent Research (DFF), Technology and Production Sciences (FTP), project 12-126515/0602-02670B. Dr. Mikko Juuti (VTT Technical Research Centre of Finland) is acknowledged for scientific discussions.

References

[1] P.J. Sheskey, R.W. Miller, Roller compaction technology for the pharmaceutical industry, in: Encyclopedia of Pharmaceutical Technology, 3rd ed., 2009, pp. 3159–3176.
[2] S. Inghelbrecht, J.P. Remon, Roller compaction and tabletting of microcrystalline cellulose/drug mixtures, Int. J. Pharm. 161 (1998) 215–224.
[3] A.K. Samanta, A.D. Karande, K.Y. Ng, P.W. Heng, Application of near-infrared spectroscopy in real-time monitoring of product attributes of ribbed roller compacted flakes, AAPS PharmSciTech 14 (2013) 86–100.
[4] A.M. Falzone, G.E. Peck, G.P. Mccabe, Effects of changes in roller compactor parameters on granulations produced by compaction, Drug Dev. Ind. Pharm. 18 (1992) 469–489.
[5] P. Guigon, O. Simon, Roll press design – influence of force feed system on compaction, Powder Technol. 130 (2003) 41–48.
[6] C. Bacher, P.M. Olsen, P. Bertelsen, J. Kristensen, J.M. Sonnergaard, Improving the compaction properties of roller compacted calcium carbonate, Int. J. Pharm. 342 (2007) 115–123.
[7] F. Freitag, K. Reincke, J. Runge, W. Grellmann, P. Kleinebudde, How do roll compaction/dry granulation affect the tableting behaviour of inorganic materials? Microhardness of ribbons and mercury porosimetry measurements of tablets, Eur. J. Pharm. Sci. 22 (2004) 325–333.
[8] H. Lim, V.S. Dave, L. Kidder, E. Neil Lewis, R. Fahmy, S.W. Hoag, Assessment of the critical factors affecting the porosity of roller compacted ribbons and the feasibility of using NIR chemical imaging to evaluate the porosity distribution, Int. J. Pharm. 410 (2011) 1–8.
[9] A. Gupta, G.E. Peck, R.W. Miller, K.R. Morris, Real-time near-infrared monitoring of content uniformity, moisture content, compact density, tensile strength, and Young's modulus of roller compacted powder blends, J. Pharm. Sci. 94 (2005) 1589–1597.
[10] D. Acevedo, A. Muliadi, A. Giridhar, J.D. Litster, R.J. Romanach, Evaluation of three approaches for real-time monitoring of roller compaction with near-infrared spectroscopy, AAPS PharmSciTech 13 (2012) 1005–1012.
[11] J. Vercruysse, M. Toiviainen, M. Fonteyne, N. Helkimo, J. Ketolainen, M. Juuti, U. Delaet, I. Van Assche, J.P. Remon, C. Vervaet, T. De Beer, Visualization and understanding of the granulation liquid mixing and distribution during continuous twin screw granulation using NIR chemical imaging, Eur. J. Pharm. Biopharm. 86 (2014) 383–392.
[12] H. Trnka, A. Palou, P.E. Panouillot, A. Kauppinen, M. Toiviainen, H. Grohganz, M. Alcala, M. Juuti, J. Ketolainen, J. Rantanen, Near-infrared imaging for high-throughput screening of moisture-induced changes in freeze-dried formulations, J. Pharm. Sci. 103 (2014) 2839–2846.
[13] R.K. May, K. Su, L. Han, S. Zhong, J.A. Elliott, L.F. Gladden, M. Evans, Y. Shen, J.A. Zeitler, Hardness and density distributions of pharmaceutical tablets measured by terahertz pulsed imaging, J. Pharm. Sci. 102 (2013) 2179–2186.
[14] L. Maurer, H. Leuenberger, Terahertz pulsed imaging and near infrared imaging to monitor the coating process of pharmaceutical tablets, Int. J. Pharm. 370 (2009) 8–16.
[15] J. Rantanen, H. Wikstrom, R. Turner, L. Taylor, Use of in line near infrared spectroscopy in combination with chemometrics for improved understanding of pharmaceutical processes, Anal. Chem. 77 (2005) 556–563.
[16] P. Geladi, H. Isaksson, L. Lindquist, S. Wold, K. Esbensen, Principal component analysis of multivariate image, Chemom. Intell. Lab. Syst. 5 (1989) 209–220.
[17] S. Sasic, An in-depth analysis of Raman and near-infrared chemical images of common pharmaceutical tablets, Appl. Spectrosc. 61 (2007) 239–250.
[18] J. Cruz, M. Blanco, Content uniformity studies in tablets by NIR-CI, J. Pharm. Biomed. Anal. 56 (2011) 408–412.
[19] J.M. Amigo, J. Cruz, M. Bautista, S. Maspoch, J. Coello, M. Blanco, Study of pharmaceutical samples by NIR chemical-image and multivariate analysis, Trends Anal. Chem. 27 (2008) 696–713.
[20] J.M. Amigo, C. Ravn, Direct quantification and distribution assessment of major and minor components in pharmaceutical tablets by NIR-chemical imaging, Eur. J. Pharm. Sci. 37 (2009) 76–82.
[21] R. Bro, Multivariate calibration. What is in chemometrics for the analytical chemist? Anal. Chim. Acta 500 (2003) 185–194.
[22] D. Clark, S. Sasic, Chemical images: technical approaches and issues, Cytometry Part A 69 (2006) 815–824.

[23] F. Freitag, P. Kleinebudde, How do roll compaction/dry granulation affect the tableting behaviour of inorganic materials? Comparison of four magnesium carbonates, Eur. J. Pharm. Sci. 19 (2003) 281–289.
[24] S.M. Short, R.P. Cogdill, P.L. Wildfong, J.K. Drennen III, C.A. Anderson, A near-infrared spectroscopic investigation of relative density and crushing strength in four-component compacts, J. Pharm. Sci. 98 (2009) 1095–1109.
[25] M. Donoso, D.O. Kildsig, E.S. Ghaly, Prediction of tablet hardness and porosity using near-infrared diffuse reflectance spectroscopy as a nondestructive method, Pharm. Dev. Technol. 8 (2003) 357–366.
[26] J.D. Kirsch, J.K. Drennen, Near-infrared spectroscopy applications in the analysis of tablets and solid pharmaceutical dosage forms, Appl. Spectrosc. Rev. 30 (1995) 139–174.
[27] A. Watanabe, M. Morita, Y. Ozaki, A study on water adsorption onto microcrystalline cellulose by near-infrared spectroscopy with two-dimensional correlation spectroscopy and principal component analysis, Appl. Spectrosc. 60 (2006) 1054–1061.

III

European Journal of Pharmaceutics and Biopharmaceutics 93 (2015) 293–302

Contents lists available at ScienceDirect

European Journal of Pharmaceutics and Biopharmaceutics

journal homepage: www.elsevier.com/locate/ejpb

Research Paper

Near-infrared chemical imaging (NIR-CI) as a process monitoring solution for a production line of roll compaction and tableting

Milad Khorasani [a], José M. Amigo [b], Changquan Calvin Sun [c], Poul Bertelsen [d], Jukka Rantanen [a,*]

[a] Department of Pharmacy, Faculty of Health and Medical Sciences, University of Copenhagen, Denmark
[b] Department of Food Science, Faculty of Science, University of Copenhagen, Denmark
[c] Department of Pharmaceutic, College of Pharmacy, University of Minnesota, USA
[d] Takeda Pharma A/S, Roskilde, Denmark

ARTICLE INFO

Article history:
Received 11 February 2015
Revised 15 April 2015
Accepted in revised form 17 April 2015
Available online 25 April 2015

Keywords:
Near-infrared chemical imaging
Principal component analysis
Partial least squares
Roll compaction/dry granulation
Ribbon porosity map
Ribbon chemical map
Tablet chemical map

ABSTRACT

In the present study the application of near-infrared chemical imaging (NIR-CI) supported by chemometric modeling as non-destructive tool for monitoring and assessing the roller compaction and tableting processes was investigated. Based on preliminary risk-assessment, discussion with experts and current work from the literature the critical process parameter (roll pressure and roll speed) and critical quality attributes (ribbon porosity, granule size, amount of fines, tablet tensile strength) were identified and a design space was established. Five experimental runs with different process settings were carried out which revealed intermediates (ribbons, granules) and final products (tablets) with different properties. Principal component analysis (PCA) based model of NIR images was applied to map the ribbon porosity distribution. The ribbon porosity distribution gained from the PCA based NIR-CI was used to develop predictive models for granule size fractions. Predictive methods with acceptable R^2 values could be used to predict the granule particle size. Partial least squares regression (PLS-R) based model of the NIR-CI was used to map and predict the chemical distribution and content of active compound for both roller compacted ribbons and corresponding tablets. In order to select the optimal process, setting the standard deviation of tablet tensile strength and tablet weight for each tablet batch was considered. Strong linear correlation between tablet tensile strength and amount of fines and granule size was established, respectively. These approaches are considered to have a potentially large impact on quality monitoring and control of continuously operating manufacturing lines, such as roller compaction and tableting processes.

1. Introduction

Roller compaction (RC) is an important process for dry granulation in the pharmaceutical industry. RC is continuous and it is suitable for processing moisture and heat-sensitive compounds. This results in various economic advantages [1]. During RC, the powder is compacted between two rolls to form ribbons, milled into granules and compacted into tablets. Ribbon porosity is known to have an enormous impact on the granule critical quality attributes (CQAs), such as granule size, size distribution, and amount of fines [2–4]. These important granule CQAs may affect the final product quality (e.g. tablet) [4–6].

Previous studies [4,7,8] have shown that the critical process parameters (CPPs), roll pressure (RP), roll speed (RS), roll morphology and gap size, have an important influence on the ribbon porosity and hence on the granule and tablet characteristics. However, the RP and RS are the most critical CPPs for the ribbon porosity [4,8]. RP controls the compaction pressure applied to the powder material, while the RS controls the dwell time of the powder under pressure in the compaction region and eventually the throughput of the RC. As an example higher RP results in ribbons with lower porosity and larger granules [9]. Larger granules have better flow properties. Nevertheless, larger granules prepared by roll compaction often result in tablets with unacceptable surfaces and inferior tensile strength compared to direct compression [5,10,11]. This phenomenon of inferior tablet tensile strength has been attributed to different effects: (1) The increased granule size reduces surface area for particle to particle bonding, during tableting [13]; (2) Work-hardening of materials leads to higher resistance toward further permanent plastic deformation [11–13]. Materials with plastic deformation properties such as microcrystalline cellulose (MCC) are more sensitive to this phenomenon

* Corresponding author at: Department of Pharmacy, Faculty of Health and Medical Sciences, University of Copenhagen, Universitetsparken 2, 2100 Copenhagen, Denmark. Tel.: +45 35336585.
E-mail address: jukka.rantanen@sund.ku.dk (J. Rantanen).

http://dx.doi.org/10.1016/j.ejpb.2015.04.008
0939-6411/

[13] while brittle materials are not [14]. Fines generated during RC, are undesirable as it often leads to material loss and reduced granule flow properties [15].

On industrial scale, fines are often regranulated to improve the yield. However, a negative influence of recycling on API-conformity was reported [16]. The study by Jones et al. suggested that fines can either promote or inhibit the granule flow, since granule flow is dependent on the amount of fines, size of fines and the characteristics of the bulk solid [17]. Therefore, a balance between the proportion of large and small sized granules in a granule population is needed to improve overall granules flowability.

The maintenance of constant roll parameters throughout the entire roller compaction process does not necessarily guarantee homogeneous quality of ribbons, for example, when powder feeding is inconsistent [Guigon and Simon (2003)] or when material properties have changed [18]. Therefore, a deeper understanding of the process is required in order to consistently produce and maintain the desired product quality. Meanwhile, utilizing the process analytical technology (PAT) tools is possible to closely monitor the ribbon quality through measuring the chemical and physical attributes of the material and the process during operation. Several non-destructive techniques for monitoring the roller compaction and tableting processes have been developed and implemented. These include acoustic relaxation emissions from compacted powder [19,20], terahertz [21–23], near-infrared spectroscopy (NIRS) [4,24–26] and near-infrared chemical imagining (NIR-CI) spectroscopy [8,27,28]. Especially, NIRS and NIR-CI spectroscopy have gained the most interest due to their many advantages, and do not usually directly reflect fast measuring time. Nevertheless, NIRS is a single point spectroscopic technique that does not usually directly reflect distribution of physical or chemical properties, because a bulk near-infrared (NIR) spectrum represents an average composition of the sampled area. Implementation of NIR-CI together with chemometric methods as process monitoring solution provides the information necessary to develop a fast and accurate approach for both qualitative and quantitative characterization of physical and chemical properties of measured samples. The pixel information of NIR-CI makes it possible to assess the distribution of the physical and chemical properties in a sample, which is valuable for guiding the development of formulation, manufacturing process, monitoring finished products, and identifying root cause of manufacturing problems [29,30].

Exploring both chemical and physical properties of roller compacted products has been reported [31,32].

The first part of this study focuses on establishing a design space and understanding the impact of process parameters RP and RS on ribbon and granule properties through a full factorial Design of Experiments (DoE). Based on risk-assessment, literature, and our prior knowledge on RC process, we identified these process parameters as the most important.

The second part of this study focuses on the development and implementation of NIR-CI spectroscopy supported by chemometric methods in order to map the pixel distribution of both porosity and the distribution of the active pharmaceutical ingredient (API) in the ribbons prepared at different process settings. Quantitative models were also developed to predict the granule size diameters (10%, 50% and 90%) by correlating the pixel porosity distribution of ribbons with the corresponding granule size distribution measured by laser diffraction.

The final part of this study concerns the optimization of the optimal process setting based on tensile strength and tablet weight of the tablets produced from several batches. The pixel API distribution map was determined for individual tablets using NIR-CI.

2. Experimental

2.1. Materials

The formulation used was a binary mixture of 60% (w/w) microcrystalline cellulose (MCC), Comprecel® PH 101 USP grade, (MINGTAY Chemical, Taoyan city, Taiwan) and 40% (w/w) acetylsalicylic acid (ASA), Rhodine® 3080 USP grade (Rhodia, Saint-Fons, France) as the model API. The binary mixture was blended in a Bohle bin blender (LM 40, L.B. Bohle Maschinen & Verfahren GmbH, Ennigerloh, Haan, Germany). Blend homogeneity was reached after 3.5 min mixing at 23 rpm.

2.2. Roll compaction and design of experiment

2.2.1. Roller compaction

Roller compacted ribbons and granules were produced using a pilot-scale roller compactor (WP120 Pharma, Alexanderwerk GmbH, Remscheid, Germany) equipped with two counter rotating smooth surface rolls (12 cm diameter and 4 cm width) and a single horizontal feed screw. The gap between the rolls was kept constant at 2.5 mm. The roller compactor was set at the automatic mode, whereas the speed of the feed screw was automatically adjusted through a control circuit to keep the gap constant. Ribbons were collected after the roller compactor had reached a steady state (3 min). Prior to investigations the materials were stored at 25 °C and 45% relative humidity (RH).

2.2.2. Design of experiments

Experiments based on a two-factor two-level full factorial design (Table 1), were used to probe the influences of two key RC process parameters, roll pressure (RP) and roll speed (RS), on the properties of ribbons after roll compaction and granules after milling. The full factorial design consists of five triplicated experiments, which results in 15 different samples. The critical quality attributes (CQAs) of the RC ribbons and granules were determined by six responses, termed as characteristics, including ribbon porosity, amount of fines (measured by sieve analysis and laser diffraction) and the 10%, 50% and 90% fractions of the granule size distribution. The results were analyzed with the DoE software, MODDE 10.1 (Umetrics AB, Umeå, Sweden) using Multilinear models (MLR).

The acceptance criteria for a good DoE model were (a) the difference between R^2–$Q^2 < 0.3$, (b) $Q^2 > 0.5$, (c) model validity > 0.25, and (d) reproducibility > 0.5 [33]. The characteristics are described in more detail below.

2.2.3. Ribbon characterization

For each experimental run, three ribbon samples with a length of ~14 cm were collected for porosity measurements. Ribbon porosity was determined by the oil absorption method. The ribbons were weighed and subsequently placed in a Petri dish containing liquid paraffin oil, Ph. Eur. grade (Sigma–Aldrich, St. Louis, Missouri, USA). The Petri dish was transferred into a desiccator and the vacuum was applied for 15 min. The vacuum was released and the samples were allowed to absorb oil into their internal pores for

Table 1
Experimental design table.

Run	Roll pressure [MPa]	Roll speed [rpm]
R1	2.5	10
R4	2.5	6
R2	3.5	8
R3	4.5	10
R5	4.5	6

30 min. The excess of oil was removed by wiping the ribbons cautiously with a soft paper. The oil saturated ribbons were weighed and the weight gain (volume of oil) of ribbons was used to estimate the pore volume using the oil density.

Optimal experimental time conditions and selection of oil were determined based on results from a design of experiment study (data not shown). The ribbon porosity for the oil absorption method is calculated by Eq. (1) as follows:

$$\varepsilon_{OA}\% = [V_{oil}/(V_{oil} + V_{solid})] \times 100 \quad (1)$$

where ε_{OA}% is the ribbon porosity measured by oil absorption method, V_{oil}, is the volume of oil absorbed and V_{solid}, is the volume of the solid, calculated by dividing the weight of neat ribbon by the true density. True density was measured by fully automatic helium displacement pycnometer (AccuPyc 1330, Micromeritics Instruments Inc., Norcross, Georgia, USA).

2.2.4. Dry granulation/milling

After roll compaction the ribbons were subsequently milled into granules, by the integrated mill, using a 1.4 mm wire primary granulator screen and a 1.0 mm wire secondary granulator screen. ~3.5 kg granules from each experimental run were collected for further characterization.

2.2.5. Granule characterization

2.2.5.1. Sieve analysis. Sieve analysis was performed on 200 g of granule sample from each experimental run using a series of five sieve sizes (1000, 800, 425, 250, and 125 μm). Sieving was carried out using a sieve shaker (KS1, Retsch, GmbH & Co., Düsseldorf, Germany). The sieving time was 5 min with the amplitude of 4 mm. The sieve analyses were performed in triplicate. The percentage of weight of granule fines was determined by Eq. (2). Fines were defined as granules with particle size ⩽125 μm.

$$\text{Fines}_{\text{Sieve}}\ (\%) = (\text{Amount of granules}\ (\leqslant 125\ \mu\text{m})/\text{Total amount of granules}\ (\text{g})) \times 100 \quad (2)$$

Samples measured by sieve analysis get added the suffix (sieve).

2.2.5.2. Laser diffraction. Particle size distribution of the milled granules was measured using a 10 g sample from each experimental run using Mastersizer 2000 equipped with a dry powder feed system, Scirocco 2000, (Malvern Instruments, Worcestershire, United Kingdom). The particle size distribution diameters ($d_{0.1}$, $d_{0.5}$ and $d_{0.9}$) of the granules together with the span values were automatically determined. The percentage volume of fines, defined as particles ⩽138 μm, was determined. The particle size distribution measurements were performed in triplicate. Samples measured by laser diffraction get added the suffix (LD).

2.3. Tablet compression

Granules from each experimental run were tableted at 358 ± 8.5 MPa using a rotary tablet press (Fette 102i, Fette Compacting GmbH, Schwarzenbek, Germany) and 8 mm round flat-faced punch aiming for 320 mg tablets. Magnesium stearate was added as an external lubricant during the tableting process with a PKB2 magnesium stearate spraying system (Fette Compacting GmbH, Schwarzenbek, Germany). Tablets were collected after the tablet machine had reached a steady state (4.5 min).

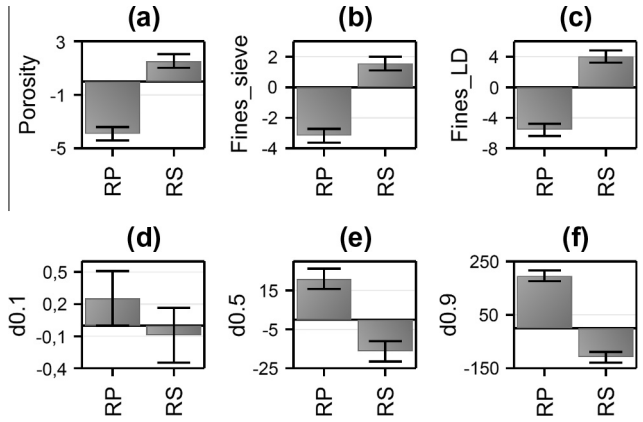

Fig. 1. Coefficient plot for the significant responses based on the full factorial design with RP and RS as process variables.

2.3.1. Tablet characterization

Tablet diametrical breaking strength (F), thickness (h), and diameter (D) of twenty tablets were determined using an automatic tablet tester (HS8, Dr. Schleuniger, Pharmatron, Aesch, Switzerland). Tablet tensile strength (σ_t) was calculated using Eq. (3) as follows:

$$\sigma_t = 2F/(\pi Dh) \quad (3)$$

2.4. Instrumentation, data acquisition and data analysis

Off-line NIR-chemical images of roller compacted ribbons and tablets were obtained with a spectrometer (Headwall Photonics model 1002A-00371, FOSS A/S, Hillerod, Denmark). NIR-chemical images were recorded in the wavelength range of 1100–1700 nm and spectral resolution of 7 nm (total of 142 variables per spectrum). The spectrometer was adapted to a line mapping configuration with a line of 320 pixels and pixel dimensions of 312 × 50 μm^2. Spectra were recorded in the diffuse reflectance mode.

2.4.1. Spectral correction

NIR-CI data processing was performed by using MATLAB 7.1 (The Math-Works, Natick, Massachusetts, USA) software and in-house routines under the name of HYPER-Tools (freely available on demand) together with PLS Toolbox (Eigenvector Research Inc., Wenatchee, USA). The high reflectance standard Spectralon TM (Labsphere, Inc., North Sutton, New Hampshire, USA) was used as background reference.

Table 2
Summary of the design experiments (means, ±SD, n = 3).

Run ID	Porosity [%]	$\text{Fines}_{\text{sieve}}$ (⩽125 μm) [%]	Fines_{LD} (⩽138 μm) [%]	$d_{0.1\ \text{LD}}$ [μm]	$d_{0.5\ \text{LD}}$ [μm]	$d_{0.9\ \text{LD}}$ [μm]
R1	25.9 ± 0.7	23.4 ± 0.5	63.5 ± 0.6	8.6 ± 0.3	96.5 ± 2.2	293.8 ± 20.2
R4	22.2 ± 0.9	20.8 ± 0.6	56.8 ± 0.6	8.1 ± 0.3	115.6 ± 1.8	518.5 ± 33.8
R2	18.9 ± 0.7	18.9 ± 1.0	54.1 ± 1.6	8.7 ± 0.3	125.6 ± 2.4	613.3 ± 32.1
R3	17.1 ± 1.1	17.3 ± 0.3	53.5 ± 0.5	8.5 ± 0.2	127.0 ± 1.2	706.8 ± 34.0
R5	14.1 ± 0.7	13.2 ± 0.7	42.8 ± 1.2	9.3 ± 0.5	177.1 ± 7.3	951.0 ± 14.5

Table 3
Assessment of the responses (models) according to the acceptance criteria.

Model	R^2–Q^2 < [0.2–0.3]	Q^2 > 0.5	Model validity > 0.25	Reproducibility > 0.5	Description
Porosity	0.03	0.94	0.51	0.96	Accepted
$Fines_{sieve}$	0.02	0.95	0.93	0.96	Accepted
$Fines_{LD}$	0.02	0.96	0.98	0.98	Accepted
$d_{0.1\ LD}$	0.3	0.38	0.94	0.57	Rejected
$d_{0.5\ LD}$	0.02	0.96	0.64	0.98	Accepted
$d_{0.9\ LD}$	0.06	0.92	0.96	0.97	Accepted

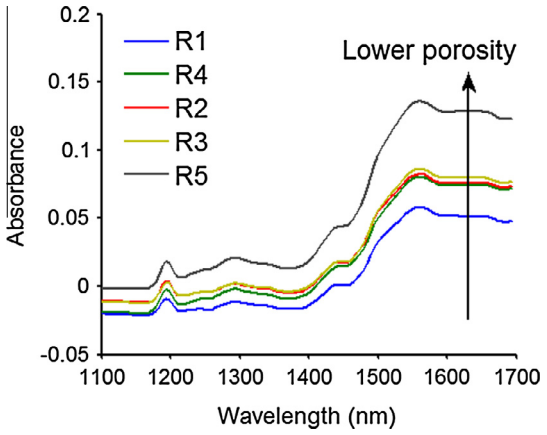

Fig. 2. Mean NIR spectra of each ribbon setting. A spectral baseline shift toward higher absorbance is seen as ribbon porosity decreases.

2.4.2. Data analysis

NIR chemical image is a three-dimensional (3D) hyperspectral data cube, where the X and Y axes represent spatial (pixel) information and the λ axis corresponds to the wavelength. Once all 3D hyperspectral cubes of samples are processed an overall chemical image can be created by merging individual images. Prior to data processing, it is necessary to unfold the 3D hyperspectral data cube to two-dimensional (2D) data matrix in which each row is a spectrum (sample) related to one of the pixels, D ($XY \times \lambda$). After pre-processing and data analysis the 2D data matrix is refolded to the 3D hyperspectral cube, to obtain a treated chemical image.

2.4.3. Chemometric methods

A surrogate method based on NIR-CI-and a principal component analysis (PCA) model was developed to map the porosity distribution for each ribbon. The PCA model reduced the variables (spectral wavelengths) into few principal components (PCs). Each PC consists of a loading and score surface. Each score vector can be re-folded to a score surface image in order to illustrate the relative distribution map for each principal PC. By including the loading vectors and corresponding score surface image, it is possible to relate each PC with any variability source (chemical or physical) in the sample. Mean centering was used as the only pre-processing technique for the PCA model.

NIR-CI and partial least squares (PLS) regression model were developed to map and predict the pixel distribution and content of API in ribbons and tablets. A calibration-set consisting of seven homogenous powder mixtures of ASA and MCC (25%, 30%, 35%, 40%, 45%, 50%, 55% w/w, of ASA) was used. NIR-CIs were recorded for ~10 g each powder mixture. Standard Normal Variate (SNV), Savitzky-Golay smoothing (SGS) with window size of 13 and second order polynomial together with mean centering were applied as pre-processing techniques.

2.4.4. Pixel homogeneity determination of PLS-R treated chemical images

In order to determine the pixel homogeneity of the distribution of a component in a sample, histograms and standard statistical values (mean, standard deviation, skewness and kurtosis) were used [27,34–37]. In a histogram, the pixel-to-pixel variation in chemical image is plotted on the x-axis and the number of pixels that have a particular range of values (bins) is plotted on the y-axis.

It is interesting to note that the pixel location information of the individual spectra is ignored. That is, the histogram is 'blind' to see where the spectra come from on the sample. This representation enables reproducible and objective analysis of chemical images. The mean value of the distribution is calculated by averaging all data points into a single concentration value. The standard deviation (SD), skewness and kurtosis described the shape of the histogram (distribution). The SD describes the spread about the mean value, and highly heterogeneous samples would be expected to have high standard deviations. Skewness and kurtosis describe deviation from a standard normal distribution, and can give insight into the characteristics of relatively small pixel populations at the extremes of the distribution. Skewness measures asymmetrical tailing, a positive skewness indicating tailing toward higher values and a negative skewness tailing toward lower values. The skewness for a normal distribution is zero, and any symmetric data should have skewness close to zero. Kurtosis gives information about the shape of the histogram peak. As the kurtosis of a normal distribution is three, then kurtosis less than three indicates flatter peaks with a smaller tail, whereas kurtosis larger than three describes sharper peaks with a long tail [34,37].

3. Results and discussion

3.1. Design of experiment

The measured characteristics of the ribbons and milled granules from the full factorial design are presented in Table 2. The effects of each process variable, RS and RP, on each response (model) are shown in the coefficient plots in Fig. 1. These will be discussed in turn in the following sections.

3.1.1. Ribbon characteristics

Ribbon porosity ranged from 14.1% to 25.9% for the five batches of ribbon (Table 2). The regression model had a high coefficient of correlation, $R^2 = 0.97$ and $Q^2 = 0.94$. The ribbon porosity is used as an indicator of the RC quality. The coefficient plot (Fig. 1a) indicates that RP affects the ribbon porosity, where higher RP leads to lower porosity (p-value = 5×10^{-9}), and higher RS leads to higher ribbon porosity with p-value = 5×10^{-5}. The interaction between RP and RS was insignificant. The conditions for producing ribbons with lowest (14.1%) and highest (25.9%) mean porosity were RP/RS = 4.5 MPa/6 rpm and 2.5 MPa/10 rpm, respectively. The mean porosity decreases as the RP increases from 2.5 to 4.5 MPa and RS decreases from 10 to 6 rpm. Higher RP leads to more powder consolidation and thereby lower ribbons porosity. Under a constant powder feeding rate and roll gap, faster RS

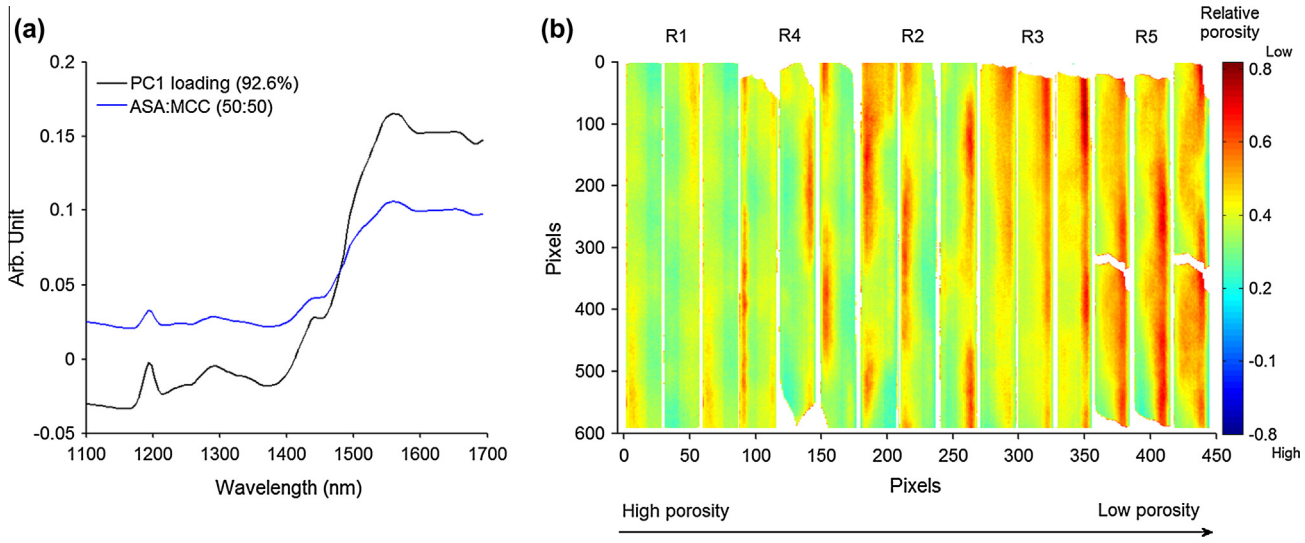

Fig. 3. (a) Loading plot of PC1 and the average NIR spectrum of 50:50 ASA:MCC powder mixture. (b) The PC1 score surface image of roller compacted ribbons ($n = 3$) with varying porosity. Replicated samples are placed side by side. Dark red color indicates higher score values (lower relative porosity), where dark blue color indicates low score values (higher relative porosity). Width and length of the ribbons approx. 40 and 140 mm, respectively. (For interpretation of the references to color in this figure legend, the reader is referred to the web version of this article.)

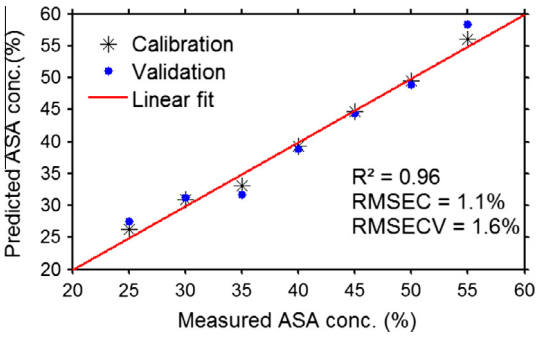

Fig. 4. PLS-model for prediction of API content.

produces mechanically weaker ribbons with higher mean porosity. These findings are in accordance with the literature [4,8,10,24].

3.1.2. Granule characteristics

The amounts of fines were determined based on results from sieve analysis and laser diffraction. The amount of fines ranged respectively from 13.2% to 23.4% by weight and from 42.8% to 63.5% by volume. The effect of RP on the amount of fines measured by sieve analysis is significantly negative (Fig. 1b) while that of RS is positive (Fig. 1b), with p-values 4×10^{-9} and 5×10^{-5}, respectively. The regression models had high R^2 (0.97) and Q^2 (0.95). Similar effects were observed based on fines % measured by laser diffraction (Fig. 1c) with high R^2 (0.98) and Q^2 (0.96). The interaction between RP and RS was insignificant for both responses. A high R^2 (0.96) was found between sieve analysis and laser diffraction results. The particle size diameters measured by laser diffraction ranged from 8.1 to 9.3 μm for $d_{0.1}$, 95.6 to 177.3 μm for $d_{0.5}$ and 293.8 to 951.0 μm for $d_{0.9}$. The coefficient plot (Fig. 1d) indicates that RP had significant ($p = 0.009$) positive effect on $d_{0.1}$. The regression model had R^2 (0.69) and Q^2 (0.38). RP and RS had a significant ($p = 6 \times 10^{-10}$, 4×10^{-10}) positive and significant ($p = 10 \times 10^{-9}$, 2×10^{-7}) negative effect on respectively, $d_{0.5}$, and $d_{0.9}$ (Fig. 1e–f). The regression models for all the three responses had $R^2 > 0.92$ and $Q^2 > 0.85$. Based on the DoE results it is clear that RP and RS had a huge influence on the ribbon and granule characteristics. The combination of higher RP and lower RS leads to stronger ribbons with lower porosity, larger granule size, less fines and broader granule size distribution. These findings are in accordance with the literature [6,38,39]. All models except $d_{0.1}$ could be considered as good models as they meet all acceptance criteria (Table 3).

3.2. Ribbon porosity map based on NIR chemical imaging and principal component analysis

Near infrared reflectance spectroscopy contains both chemical and physical information of measured material [25,40]. Both types of information were utilized in this study. Average NIR spectra of each ribbon setting are shown in Fig. 2. The NIR spectra are sensitive to porosity variation, with lower porosity (higher density) ribbons having a higher apparent slope and more baseline shift [26,40]. This phenomenon has been used earlier to develop separate NIR methods to determine tablet hardness, tablet and ribbon density [25,26,40]. A NIR-CI together with a univariate method was also developed and used to predict ribbon porosity of single ingredient ribbons [8]. However, such a method is not appropriate for samples containing more than one ingredient because the

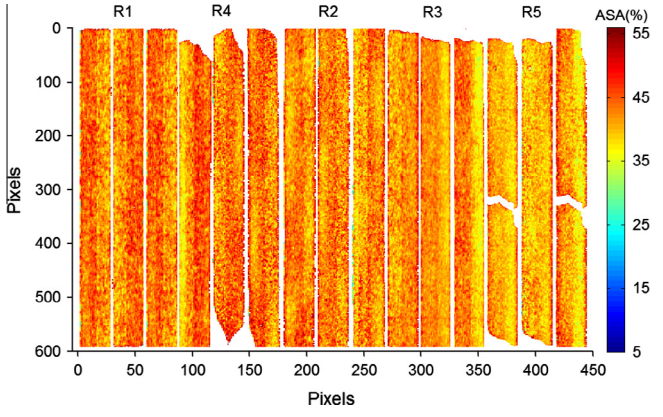

Fig. 5. Predicted API concentration distribution map for ribbons ($n = 3$) by the PLS-R model. Width and length of the ribbons approx. 40 and 140 mm, respectively.

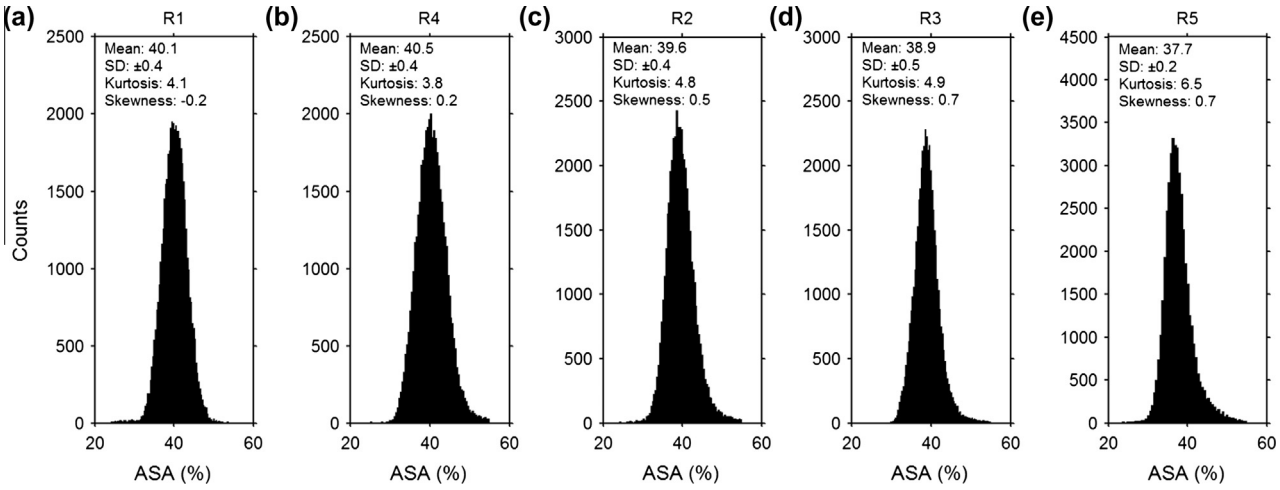

Fig. 6. (a–e) Mean API concentration histograms of the different ribbon settings ($n = 3$).

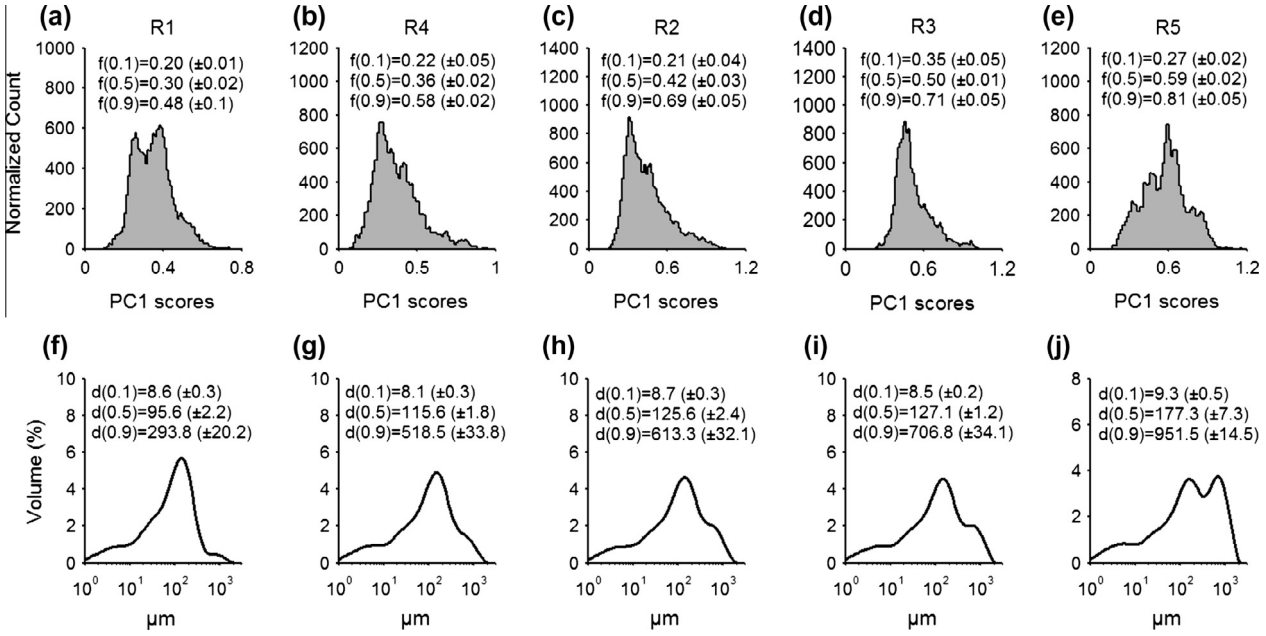

Fig. 7. (a–e) represents, respectively, PC1 score distribution of each ribbon setting and (f–i), granule size distribution of corresponding ribbon settings.

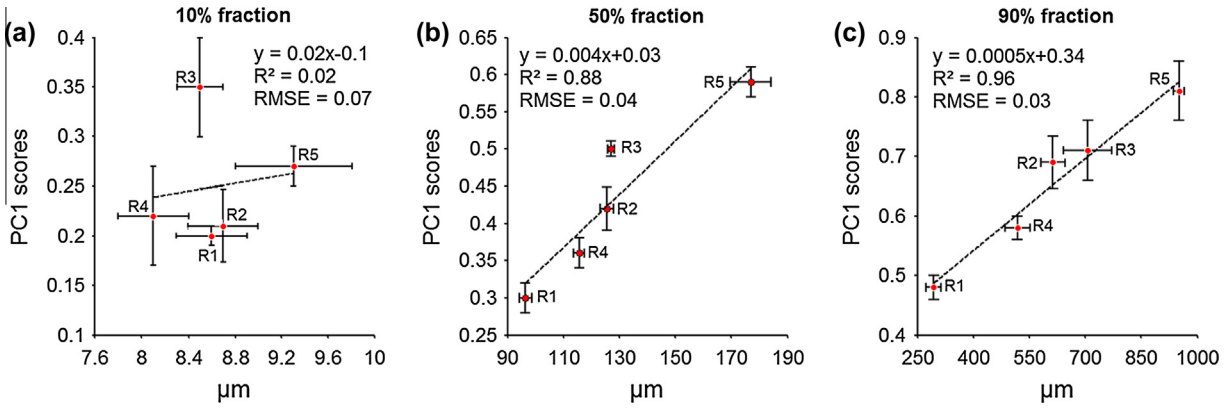

Fig. 8. (a–c) represents, respectively, the correlation between the 10%, 50% and 90% fraction of the PC1 score values of ribbons with the corresponding granule size distribution.

Table 4
Tablet tensile strength (TTS) and tablet weight (TW) made from granules (means, ±SD, $n = 20$).

Run	TTS [MPa]	TW [mg]
TR1	1.3 ± 0.06	319.3 ± 2.9
TR4	1.2 ± 0.03	319.4 ± 1.2
TR2	1.1 ± 0.04	318.1 ± 1.9
TR3	1.1 ± 0.04	318.8 ± 2.1
TR5	0.9 ± 0.05	318.4 ± 2.2

composition of broad and highly overlapped bands in NIR spectra makes it difficult to find distinct and selective absorption bands for each of the ingredients in the sample. This limitation is overcome by applying chemometric approaches capable of extracting the relevant information from the whole data matrix.

PCA was used for identifying the main variation within NIR-CIs of the ribbons in the spectral range of 1100–1700 nm. The first PC loading explained 92.5% of the variation. The pattern of this loading plot was similar to the averaged spectrum of the ASA:MCC (50:50) mixture (Fig. 3a). This indicates that the main variation captured could be attributed to intensity (absorbance) of the spectra, which in turn was affected by the porosity variation. Therefore, the established PCA model can be used as surrogate method for estimation of porosity distribution. From Fig. 3b, it is evident that ribbons with lower porosity (measured by oil method) have higher score values. Fig. 3b also shows heterogeneous score value distribution (porosity distribution) within each roller compacted ribbon, an effect that is more pronounced for ribbons with lower porosity. Simon and Guigon (2003) found that non-continuous feeding process by a feed screw results in heterogeneous porosity distribution along the roller-compacted ribbons [7]. Recently, Souihi et al. [31] published a study wherein they used NIR-CI together with a partial least squares regression (PLS-R) model to predict the ribbon density. To access the feasibility of NIR-CI to predict the reference measured ribbon density, a PLS-R model was used to predict the ribbon density from the average NIR spectra extracted from the ribbon NIR-CIs. Subsequently, the PLS-R model was used to predict the full hyperspectral images at the pixel-level to obtain the ribbon density distribution map. The PLS-R predicted NIR-CIs of the ribbons exhibits sinusoidal density variation, where the ribbon density is lower at the edges and higher at the center. These findings are in consistent with other researchers [32,7,18]. Using the average NIR spectra of each ribbon to predict its hyperspectral image in order to achieve the ribbon density distribution map may be a biased approach, since the sinusoidal density variation is excluded by averaging. However, Souihi et al. [31] did not consider the sinusoidal density variation of the ribbons in their PLS-R model, although they describe and illustrate this phenomenon in their study. An alternative approach could be the development of a PLS-R model with a calibration-set comprised of, e.g., compacts or tablets with uniform density distribution. This PLS-R model could then be used to predict roller compacted ribbons with heterogeneous density distribution.

3.3. Ribbon chemical map based on NIR chemical imaging and partial least squares regression

Spectra extracted from NIR-CIs of ribbons were used as the X matrix and the nominal API concentration of the powder mixtures (calibration-set) was used as the y vector. The correct number of latent variables (LVs) of the PLS model was assessed by The Root Mean Square Error of Calibration (RMSEC) and The Root Mean Square Error of cross-validation (RMSECV), indicating the fit between NIR spectra and API concentration values. Cross-validation was done by full cross-validation. The PLS-R model resulted in two latent variables (Lvs), explaining 98.3% of the variation. The calibration and cross-validation error for this model were relatively small (RMSEC = 1.1%, RMSECV = 1.6%), (Fig. 4).

The API quantification was performed by applying the quantitative PLS-R model to the complete NIR-CI of the ribbons. The pixel distribution map (API distribution map) of all ribbons in the image is shown in Fig. 5. The concentration values for individual ribbon settings shown in Fig. 6 yielded mean API concentration ranging from 37.7 to 40.5 relative API (%) concentrations, which suggests the mean predicted API concentration values of the five ribbon settings are close to the nominal 40% (w/w) API concentration in the initial powder blend. However, the predicted API concentration is seen to decrease with decreasing mean ribbon porosity. The homogeneity of the distribution of API in the ribbons was assessed from the chemical images histogram. The histogram of all ribbon settings spans over a narrow range of API concentration values with relatively small standard variation values, ranging from 0.2 to 0.5 (Fig. 6). The kurtosis and skewness values ranged from 3.8 to 6.5 and −0.2 to 0.7, respectively. Kurtosis > 3 indicates peak broadening and non-uniform API distribution. Skewness > 0 describes tailing toward higher API content. For ribbon setting R4, kurtosis and skewness values are very close to normal distribution. The small kurtosis and skewness value means that the API is homogenously distributed, at the ribbon surfaces. This is in contrast to the relatively non-homogeneous porosity distribution in these ribbons.

3.4. Relationship between ribbon NIR-CI porosity distribution and granule size distribution

Each pixel in the score image contains a score value, which can be related to a porosity value per the PCA model. Again, histograms were used to study the NIR-CI score value distribution (surrogate

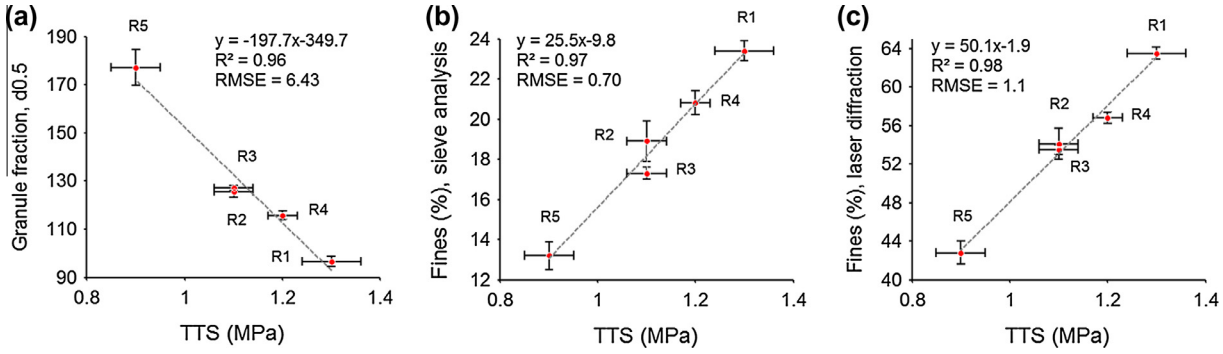

Fig. 9. Linear correlation between tablet tensile strength and respectively median granule size (a), fines measured by sieve analysis (b) and fines measured by laser diffraction (c) ($n = 3$).

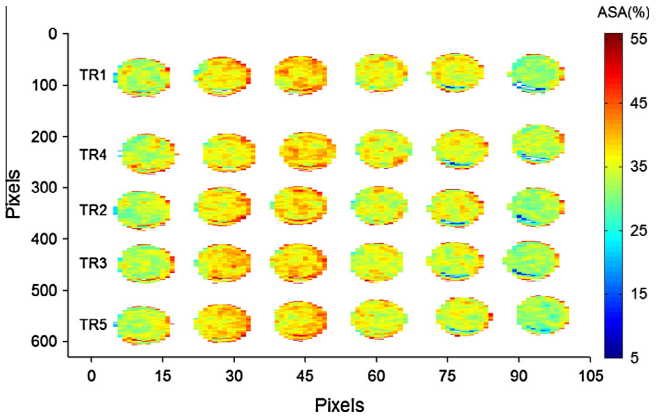

Fig. 10. API distribution map of tablets ($n = 6$) predicted by PLS-R model.

estimation of porosity distribution), of each ribbon setting. Further, the 10%, 50% and 90% fractions' ($f_{0.1}$, $f_{0.5}$, $f_{0.9}$) PC1 score distribution was calculated for each distribution. The NIR-CI score value distribution of each ribbon setting was compared to its corresponding average granule size distribution measured by laser diffraction (Fig. 7). As the ribbon porosity decreases, $f_{0.1}$ (0.2–0.27), $f_{0.5}$ (0.30–0.59) and $f_{0.9}$ (0.48–0.89) all increased (Fig. 8). A nearly linear trend is also seen for $d_{0.5}$ (increasing from 95.6 to 177.3 μm) and $d_{0.9}$ (increasing from 293.8 to 951.5 μm). The correlation values (R^2) of the linear fitting are 0.02, 0.88 and 0.96 respectively for $d_{0.1}$, $d_{0.5}$ and $d_{0.9}$. This trend is consistent with the observed relationship that lower ribbon porosity leads to larger granules in Section 3.1.2. However, the trend with the $d_{0.1}$ fraction is not clear, which indicates a limitation of the NIR-CI prediction.

3.5. Tablet characteristics

Tablets produced based on these different granule batches (R1–R5) were named "tablet run" (TR) followed by the run setting number. The tablet tensile strength (TTS) for compacted tablets varied from 0.9 to 1.3 MPa (Table 4). Fig. 9a shows a strong correlation ($R^2 = 0.97$) between TSS and granule median size. Granules with larger median size revealed tablets with lower TTS, due to work-hardening and reduced surface area for bonding. These findings are in accordance with the literature [11–13]. Additionally, strong correlations $R^2_{\text{sieve analysis}} = 0.97$ and $R^2_{\text{laser diffraction}} = 0.98$ were also obtained between TTS and amount of fines measured by two different methods, shown in respectively (Fig. 9b and c). The weight of tablets varied between 318.1 and 319.4 mg (Table 4) and all measured tablets complied with the mass uniformity requirement of single-dose preparation test from European Pharmacopoeia [41]. Previous studies have shown that tablet weight uniformity is mainly affected by several factors, such as tableting speed, tooling size, level of powder in the hopper (head pressure), particle size, density (porosity), and powder flow on the tablet press [42].

3.6. Tablet chemical map based on NIR chemical imaging and partial least squares regression

API quantification of tablets of each process setting was predicted using NIR-CI and the quantitative PLS-R model, described in Section 3.3. The pixel distribution map (API distribution map) of all tablets in the image is shown in Fig. 9. The predicted API content of these tablets varied between 39.2% and 39.6% (Fig. 10), which is close to the nominal API content of 40%. Based on an analysis of variance (ANOVA) no significant ($p = 0.91$) differences were obtained between the different tablet batches. The kurtosis and skewness values ranged from 5.9 to 8.0 and −0.1 to 0.3, respectively (Fig. 11). Higher kurtosis and skewness values, indicate broadening of the peaks and tailing toward higher API concentration values, respectively. Since Run 4 with the process settings of RP (2.5 MPa) and RS (6 rpm) is the optimum because it results in tablets (TR4) with lowest SD for tensile strength and tablet weight, this setting is chosen as the optimal process setting despite it yields the second highest amount of fines and second smallest granule.

3.7. Suggested process monitoring solution

In the current work a design space was established wherein the process parameters were changed in a controlled way and the effects on the process outputs, in this case the CQAs of measured samples (ribbon, granules and tablets), were measured. The critical process parameters (CPPs) and interactions were identified, experimental knowledge was maximized, and statistical predictive cause–effect relationships between CPPs and CQAs were developed. Subsequently off-line NIR-CI supported by chemometrics methods was developed to archive useful information of the physical and chemical CQAs of the samples (ribbon, tablets). Implementation of these approaches enables selection of the most appropriate sample (model product) for further processing. Fig. 12 is an overview of the overall processes. The next step will be to use

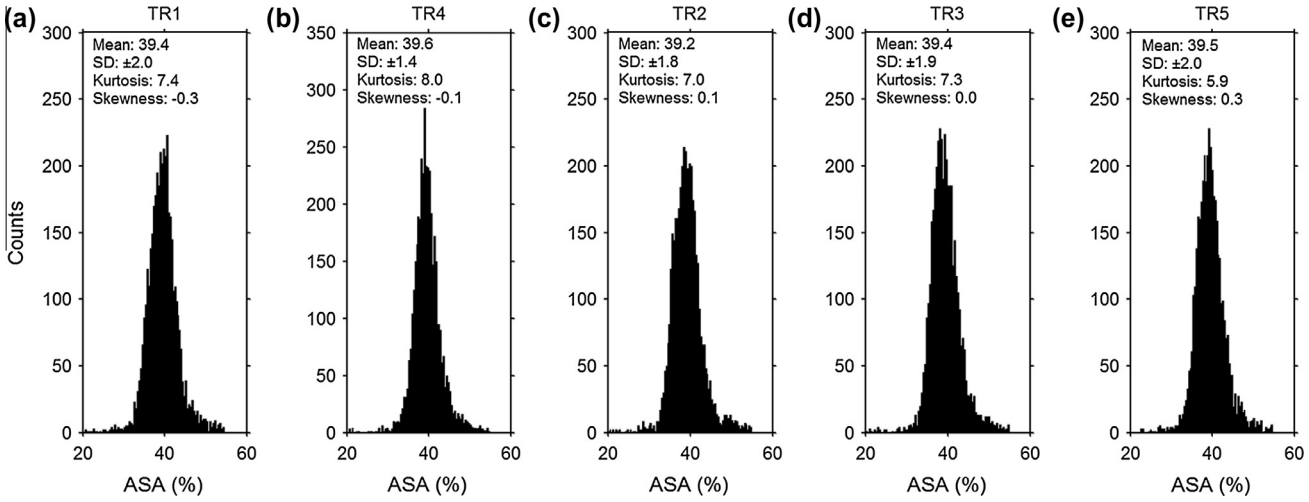

Fig. 11. Mean API concentration histograms of the different tablets ($n = 6$). For each histogram mean concentration, standard deviation, kurtosis and skewness are presented.

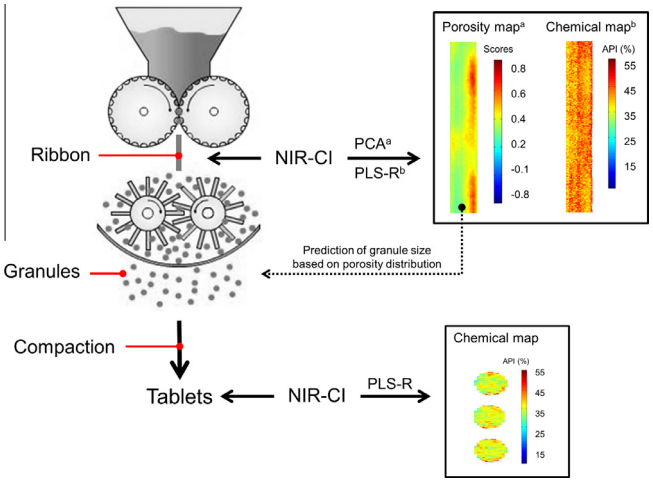

Fig. 12. An overview of the overall process monitoring of roll compaction and tableting; the implementation of NIR-CI to gain information related to the physical or chemical properties of intermediate or final product.

a faster NIR-CI camera for in-line process monitoring. Utilizing the statistical predictive cause–effect relationship models developed from the DoE, it is possible to implement control and feed-back-loops in order to archive an automatized process. Additionally, other multivariate approaches such as O2PLS can be used to provide an overview of the interrelationships between the textural features obtained from the NIR-CI and the DoE parameters as well as the material properties [31].

4. Conclusions

In this study, we have investigated the effects of roll pressure (RP) and roll speed (RS) on the ribbon porosity, granule properties, and tableting performance. A surrogate method based on near-infrared chemical imaging (NIR-CI) spectroscopy and principal component analysis (PCA) was used to map the ribbon porosity distribution. The ribbon porosity distribution gained from the PCA based NIR-CI was used to develop quantitative/predictive models for granule size fractions. Partial least squares (PLS) regression was used to visualize and predict the API distribution and content for both roller compacted ribbons and corresponding tablets. Higher RP and lower RS led to ribbons with lower porosity, larger granules with lower amount of fines, and tablets with lower tensile strengths. We have demonstrated that NIR-CI spectroscopy together with chemometric models can be utilized, as a non-destructive tool, to monitor roller compaction to deliver granules exhibiting robust tableting performance. This method has the potential to be implemented as a quality control tool for the continuously operating manufacturing lines, involving roller compaction.

Acknowledgments

Milad Khorasani, is acknowledging the Drug Research Academy (University of Copenhagen) and Takeda Pharma A/S for financing of the Ph.D. studies. The authors also acknowledge the funding from The Danish Council for Independent Research (DFF), Technology and Production Sciences (FTP), Project 12-126515/0602-02670B.

References

[1] P.J. Sheskey, R.W. Miller, Roller compaction technology for the pharmaceutical industry, in: Encyclopedia of Pharmaceutical Technology, third ed., 2006, pp. 3159–3176.
[2] A.M. Miguelez-Moran, C.Y. Wu, H. Dong, J.P. Seville, Characterisation of density distributions in roller-compacted ribbons using micro-indentation and X-ray micro-computed tomography, Eur. J. Pharm. Biopharm. 72 (2009) 173–182.
[3] C.Y. Wu, S.M. Best, A.C. Bentham, B.C. Hancock, W. Bonfield, Predicting the tensile strength of compacted multi-component mixtures of pharmaceutical powders, Pharm. Res. 23 (2006) 1898–1905.
[4] A.K. Samanta, A.D. Karande, K.Y. Ng, P.W. Heng, Application of near-infrared spectroscopy in real-time monitoring of product attributes of ribbed roller compacted flakes, AAPS PharmSciTech 14 (2013) 86–100.
[5] A.M. Falzone, G.E. Peck, G.P. Mccabe, Effects of changes in roller compactor parameters on granulations produced by compaction, Drug Dev. Ind. Pharm. 18 (1992) 469–489.
[6] C. Bacher, P.M. Olsen, P. Bertelsen, J. Kristensen, J.M. Sonnergaard, Improving the compaction properties of roller compacted calcium carbonate, Int. J. Pharm. 342 (2007) 115–123.
[7] P. Guigon, O. Simon, Roll press design – influence of force feed system on compaction, Powder Technol. 130 (2003) 41–48.
[8] H. Lim, V.S. Dave, L. Kidder, E.N. Lewis, R. Fahmy, S.W. Hoag, Assessment of the critical factors affecting the porosity of roller compacted ribbons and the feasibility of using NIR chemical imaging to evaluate the porosity distribution, Int. J. Pharm. 410 (2011) 1–8.
[9] J.F. Gamble, M. Tobyn, A.B. Dennis, T. Shah, Roller compaction: application of an in-gap ribbon porosity calculation for the optimization of downstream granule flow and compactability characteristics, Pharm. Dev. Technol. 15 (2010) 223–229.
[10] P. Kleinebudde, Roll compaction/dry granulation: pharmaceutical applications, Eur. J. Pharm. Biopharm. 58 (2004) 317–326.
[11] S. Malkowska, K.A. Khan, Effect of recompression on the properties of tablets prepared by dry granulation, Drug Dev. Ind. Pharm. 9 (1983) 331–347.
[12] M.G. Herting, P. Kleinebudde, Studies on the reduction of tensile strength of tablets after roll compaction/dry granulation, Eur. J. Pharm. Biopharm. 70 (2008) 372–379.
[13] C.C. Sun, M.W. Himmelspach, Reduced tabletability of roller compacted granules as a result of granule size enlargement, J. Pharm. Sci. 95 (2006) 200–206.
[14] S.J. Wu, C. Sun, Insensitivity of compaction properties of brittle granules to size enlargement by roller compaction, J. Pharm. Sci. 96 (2007) 1445–1450.
[15] R.J. Lantz, J.B. Schwartz, Tablets, in: Pharmaceutical Dosage Forms: Tablets, third ed., 2005, pp. 15–20.
[16] P.J. Sheskey, T.D. Cabelka, R.T. Robb, B.M. Boyce, Use of roller compaction in the preparation of controlled-release hydrophilic matrix tablets containing methylcellulose and hydroxypropyl methylcellulose polymers, Pharm. Technol. 18 (1994) 132–150.
[17] T.M. Jones, N. PilPel, The flow of granular magnesia, J. Pharm. Pharmacol. 18 (1966) 429–442.
[18] O. Simon, P. Guigon, Correlation between powder-packing properties and roll press compact heterogeneity, Powder Technol. 130 (2003) 257–264.
[19] A. Hakanen, E. Laine, Drug Dev. Ind. Pharm. 21 (1995) 1573–1582.
[20] A. Hakanen, E. Laine, H. Jalonen, K. Linsaari, J. Jokinen, Acoustic emission during powder compaction and its frequency spectral analysis, Drug Dev. Ind. Pharm. 19 (1993) 2539–2560.
[21] P. Bawuah, A. Pierotic Mendia, P. Silfsten, P. Paakkonen, T. Ervasti, J. Ketolainen, J.A. Zeitler, K.E. Peiponen, Detection of porosity of pharmaceutical compacts by terahertz radiation transmission and light reflection measurement techniques, Int. J. Pharm. 465 (2014) 70–76.
[22] L. Maurer, H. Leuenberger, Terahertz pulsed imaging and near infrared imaging to monitor the coating process of pharmaceutical tablets, Int. J. Pharm. 370 (2009) 8–16.
[23] R.K. May, K. Su, L. Han, S. Zhong, J.A. Elliott, L.F. Gladden, M. Evans, Y. Shen, J.A. Zeitler, Hardness and density distributions of pharmaceutical tablets measured by terahertz pulsed imaging, J. Pharm. Sci. 102 (2013) 2179–2186.
[24] D. Acevedo, A. Muliadi, A. Giridhar, J.D. Litster, R.J. Romanach, Evaluation of three approaches for real-time monitoring of roller compaction with near-infrared spectroscopy, AAPS PharmSciTech 13 (2012) 1005–1012.
[25] A. Gupta, G.E. Peck, R.W. Miller, K.R. Morris, Real-time near-infrared monitoring of content uniformity, moisture content, compact density, tensile strength, and Young's modulus of roller compacted powder blends, J. Pharm. Sci. 94 (2005) 1589–1597.
[26] M. Donoso, D.O. Kildsig, E.S. Ghaly, Prediction of tablet hardness and porosity using near-infrared diffuse reflectance spectroscopy as a nondestructive method, Pharm. Dev. Technol. 8 (2003) 357–366.
[27] J.M. Amigo, J. Cruz, M. Bautista, S. Maspoch, J. Coello, M. Blanco, Study of pharmaceutical samples by NIR chemical-image and multivariate analysis, Trends Anal. Chem. 27 (2008) 696–713.
[28] J.M. Amigo, C. Ravn, Direct quantification and distribution assessment of major and minor components in pharmaceutical tablets by NIR-chemical imaging, Eur. J. Pharm. Sci. 37 (2009) 76–82.
[29] J.M. Amigo, Practical issues of hyperspectral imaging analysis of solid dosage forms, Anal. Bioanal. Chem. 398 (2010) 93–109.
[30] G. Reich, Near-infrared spectroscopy and imaging: basic principles and pharmaceutical applications, Adv. Drug Deliv. Rev. 57 (2005) 1109–1143.
[31] N. Souihi, D. Nilsson, M. Josefson, J. Trygg, Near-infrared chemical imaging (NIR-CI) on roll compacted ribbons and tablets – multivariate mapping of physical and chemical properties, Int. J. Pharm. 483 (2015) 200–211.
[32] M. Khorasani, J.M. Amigo, J. Sonnergaard, P. Olsen, P. Bertelsen, J. Rantanen, Visualization and prediction of porosity in roller compacted ribbons with

near-infrared chemical imaging (NIR-CI), J. Pharm. Biomed. Anal. 109 (2015) 11–17.
[33] L. Eriksson, E. Johansson, N. Kettaneh-Wold, C. Wikström, S. Wold, Design of Experiments: Principles and Applications, third ed., 2008, pp. 149–159.
[34] E.N. Lewis, J.W. Schoppelrei, L. Makein, L.H. Kidder, E. Lee, Near-infrared chemical imaging for product and process understanding, in: Process Analytical Technology: Spectroscopic Tools and Implementation Strategies for the Chemical and Pharmaceutical Industries, second ed., 2010, pp. 245–276.
[35] A. Palou, J. Cruz, M. Blanco, J. Tomàs, J. de los Ríos, M. Alcalà, Determination of drug, excipients and coating distribution in pharmaceutical tablets using NIR-CI, J. Pharm. Anal. 2 (2012) 90–97.
[36] A.A. Gowen, C.P. O'Donnell, P.J. Cullen, S.E. Bell, Recent applications of Chemical Imaging to pharmaceutical process monitoring and quality control, Eur. J. Pharm. Biopharm. 69 (2008) 10–22.
[37] R.C. Lyon, D.S. Lester, E.N. Lewis, E. Lee, L.X. Yu, E.H. Jefferson, A.S. Hussain, Near-infrared spectral imaging for quality assurance of pharmaceutical products: analysis of tablets to assess powder blend homogeneity, AAPS PharmSciTech 19 (2002) 1–15.
[38] F. Freitag, P. Kleinebudde, How do roll compaction/dry granulation affect the tableting behaviour of inorganic materials? Comparison of four magnesium carbonates, Eur. J. Pharm. Sci. 19 (2003) 281–289.
[39] S. Inghelbrecht, J.P. Remon, Roller compaction and tableting of microcrystalline cellulose/drug mixtures, Int. J. Pharm. 161 (1998) 215–224.
[40] J.D. Kirsch, J.K. Drennen, Near-infrared spectroscopy: applications in the analysis of tablets and solid pharmaceutical dosage forms, Appl. Spectrosc. Rev. 30 (1995) 139–174.
[41] European Pharmacopoeia, 2.9.5, Uniformity of Mass of Single-dose Preparations Units, eighth ed., 2014, pp. 297–298.
[42] N. Souihi, M. Josefson, P. Tajarobi, B. Gururajan, J. Trygg, Design space estimation of the roller compaction process, Ind. Eng. Chem. Res. 52 (2013) 12408–12419.